Meereswissenschaftliche Berichte
MARINE SCIENCE REPORTS

No. 50

The general circulation and water masses characteristcs in the Gulf of Aqaba and northern Red Sea

by

Riyad Manasreh

Institut für Ostseeforschung
Warnemünde
2002

Contents

Zusammenfassung

Die F/S Meteor Forschungsreise M44/2 erstreckte sich im Frühjahr 1999 vom nördlichen Rand des Golf von Aqaba über die Straße von Tiran bis in das nördliche Rote Meer. Auf 12 hydrographischen Stationen, von denen 6 im Golf von Aqaba und 6 im nördlichen Roten Meer lagen, wurden insgesamt 72 Vertikalprofile von Temperatur und Salzgehalt mit einer CTD aufgenommen. Kontinuierliche Stromprofile wurden während der Fahrt und auf den Stationen mit einem schiffsgebundenen 150 kHz NB ADCP bis zu einer Tiefe von 350 m gemessen.

Die im nördlichen Golf von Aqaba registrierten Zeitreihen des Wasserstandes und meteorologischer Parameter standen für die Untersuchungen zur Verfügung. Auf der Station S2, im nördlichen Teil des Golfs, wurden von Mai 1997 bis August 2001 alle zwei Wochen Vertikalprofile der Temperatur und des Salzgehalts bis zu einer Tiefe von 400 m genommen. Zeitreihen der Strömung wurden mit verankerten Workhorse ADCP an zwei küstennahen Stationen im nördlichen Teil des Golfs registriert.

Der Wind weht im nördlichen Golf von Aqaba überwiegend schwach aus Nordwest bis Nordost. Er ist während des Sommerhalbjahres durch eine Tagesgang überlagert, der nachts den Wind abschwächt und ihn während des Tages verstärkt. Der Wasserstand im nördlichen Golf von Aqaba weist einen ausgeprägten Jahresgang mit einem Minimum im Sommer und einem Maximum während des Winters auf. Weiterhin weist der Wasserstand Schwankungen mit der diurnalen (23.72 ± 0.82 h), der semidiurnalen (12.39 ± 0.22 h) Gezeitenperiode und der 1. barotropen Eigenschwingung des Golfs von Aqaba mit einer Periode von 1.13 h auf. Darüber hinaus oszilliert der Wasserstand des Golfs mit einer Periode von 8.38 h, die aller Wahrscheinlichkeit nach durch die 1. barotropen Eigenschwingung des Roten Meeres angeregt wird.

Die Wassertemperatur in den oberen 400 m des nördlichen Golf von Aqaba variierte zwischen 20.84 und 28.04 °C und weist neben einem ausgeprägten Jahresgang auch zwischenjährliche Variationen auf. Der Salzgehalt variierte zwischen 40.20 und 40.75 und hat somit einen weit geringeren Einfluß auf die Dichtevariationen als die Temperatur. Die Tiefenwasserbildung des Golfs von Aqaba erfolgt im nördlichen Teil des Golfs zwischen Februar und April. Es lagert sich unterhalb der Schwellentiefe der Straße von Tiran ein und hat somit keinen Einfluß auf die Tiefenwasserbildung des Roten Meeres.

Das Oberflächenwasser des nördlichen und das Zwischenwasser des mittleren und südlichen Teils des Golfs von Aquaba fließen durch die Straße von Tiran in das nördliche Rote Meer ab und tragen dort zur Bildung des Tiefenwassers bei. In der Straße von Tiran wurde Einstrom von Wasser aus dem Roten Meer in den oberen 70 m beobachtet. Unterhalb von 70 m Tiefe strömte Wasser aus dem Golf in das Rote Meer. Die Strömungsgeschwindigkeit nahm in der Tiefenschicht linear mit der Tiefe zu und erreichte Strömungsgeschwindigkeiten von 100 cms^{-1} in 200 m Tiefe.

Das dynamische Regime im nördlichen Roten Meer war durch einen zyklonischen Wirbel mit einem Durchmesser 50-60 km gekennzeichnet. Die maximale Strömungsgeschwindigkeit am Rande des Wirbels erreichte 40 cms^{-1}. Die mit dem Wirbel verbundene Aufwölbung der Dichteschichtung kann die Bildung von Zwischenwasser im nördlichen Roten Meer unterstützen.

Im südlichen Golf von Aqaba wurde auf der Station VI im Bereich der Tiran-Front eine barokline Zirkulation beobachtet, die in der Deckschicht nach Osten und zwischen 120-280 m Tiefe nach Nordwest setzte. Diese Zirkulation war von einer baroklinen halbtägigen Gezeitenschwingung überlagert. Das Verschwinden der halbtägigen Gezeitenperiode in den Strömungsfluktuationen im nördlichen Golf während der Konvektionsphase im Frühjahr, deutet

darauf hin, dass die baroklinen Gezeiten in der Straße von Tiran angeregt und von dort in den nördlichen Teil des Golfs propagieren soweit es die Schichtung in der Deckschicht ermöglicht.

Das dominante Signal in den Strömungsmessungen entlang der Achse des Golfs von Aqaba war eine Kette von subinertialen zyklonisch-antizyklonischer Wirbelpaare mit einem Durchmesser vom doppelten Rossbyradius ($R \approx 10$ km). Ein einzelner antizyklonischer Wirbel mit einem Durchmesser von 5-8 km wurde an der nördlichen Spitze des Golfs in den oberen 300 m beobachtet.

Die küstennahe Strömung im nordöstlichen Teil des Golfs beträgt im Mittel 6.4 cms^{-1}. Die Schwankungen im Periodenbereich kleiner 2 Tage betragen dagegen 3.1 cms^{-1}. Während der Sommersaison ist die Strömung weitgehend parallel zur Topographie ausgerichtet und folgt den Windschwankungen mit einer Verzögerung von annähernd drei Tagen.

Die wesentlichen Faktoren, die die beträchtliche zeitliche Variabilität der Strömung im nördlichen Golf von Aqaba bestimmen sind: (1) der Wind, (2) die thermohaline Zirkulation, (3) die Gezeiten und (4) die Topographie.

Summary

Meteor cruise 44/2 scanned the Gulf of Aqaba and northern Red Sea during spring 1999. 72 salinity and temperature profiles were measured at 12 stations; 6 in the northern Red Sea, and other 6 stations in the Gulf of Aqaba. The shipboard NB ADCP 150 kHz recorded continuously current profiles down to 350 m en route.

Time series of sea level and meteorological parameters, which recorded in the northern gulf, were used. More than four years (May 1997-August 2001) of temperature and salinity profiles were taken biweekly at station S2 in the northern tip of the gulf. Multi-surveys by the ADCP 150 kHz were carried out along an offshore track parallel to the gulf axis, and other zigzag surveys were worked in the northernmost gulf. Time series of current measurements near the northeastern shore of the gulf by Workhorses 300 kHz were used.

The wind during summer nights in the northern Gulf of Aqaba is calmer than during the day, resulting in the diurnal peak (24.04 ± 0.85 hr), and relatively calm conditions prevail during the rest of the year. The sea level anomalies depict a yearly cycle at the northern tip of the Gulf of Aaqba. The minimum and maximum of the anomalies were observed in the summer and winter-spring season, respectively. The spectral analysis revealed the semidiurnal (12.39 ± 0.22 hr) and diurnal (23.72.05 ± 0.82 hr) barotropic tides. Shorter periods (1.05 and 8.03) were detected, which are related to the seiches that are generated in the Gulf of Aqaba and the Red Sea, respectively. The theoretical values of the fundamental period (1.13 and 8.38 hr), using Merian's formula, with agreement with observed periods, respectively.

The deep-water formation of the northern Red Sea is contributed by the Gulf of Aqaba. The deep-water in the gulf (<450 m) seems to be rather passive and plays no specific role in the water mass formation of the northern Red Sea. The circulation in the upper 200 m in the northern Red Sea characterizes of finding a well developed cyclonic gyre with a diameter of about 50-60 km and maximum velocity of about 40 cms^{-1}, which it may contributes to the preconditioning for the intermediate water formation in the northern Red Sea. The winter regime of water exchange between the Gulf of Aqaba and the Red Sea was obvious during spring. Inflow (NNW) into the

Gulf of Aqaba occurred in the upper 70 m over the sill, while outflow (SSW) into the Red Sea was below 70 m. The strength of the outflow to the Red Sea generally increased linearly with depth and reached up to about 100 cms^{-1} at 200 m depth.

The current in the southern gulf at station VI was vertically separated into an easterly flow with clockwise rotation (12.3 hr period) in the upper 100 m, and a north westerly current carried by an internal tidal wave with the same period in the 120-280 m of the water column. Chains of cyclonic-anti-cyclonic eddy pairs are the dominant signal along the gulf axis. The total diameter for each pair is twice the baroclinic Rossby radius ($R \approx 10$ km). A single anti-cyclonic eddy was observed in the upper 300 m in the northern tip of the Gulf of Aqaba with a diameter ranged between 5-8 km.

The temperature variations in the northern tip of the Gulf of Aqaba -during more than four years- appear pure seasonal signal. The temporal variation of the salinity and temperature ranged between 40.20-40.75 and 20.84-28.04 °C, respectively, in the upper 400 m. The real effects on the thermodynamics process on the seawater of the Gulf of Aqaba are dominated by the temperature variations, while the salinity plays a minor role.

The seasonal differences in the current were detected near the northeastern shore of the gulf. A semidiurnal (12.19 ± 0.58 hr) signal was obvious during summer and winter, while no signals appeared during spring. The coastal current mainly is parallel to the wind direction (SSE-SSW) during summer, while it fluctuates (SE-SW ←→ NW) rest of the year, mostly with regular frequency. The coherence between the filtered north component of the wind and the current at 20 m depth appeared well compatibility with respect to the time in spring-summer seasons, but with a delay of north current relative to north wind components. The transition period of the direction was nearly 3.5 days.

The key factors of the substantial temporal variability of the current in the northern tip of the gulf are: (1) the winds, (2) thermohaline inflow, (3) the variation of the phase of the tidal signals, (4) the diurnal and semidiurnal currents, and (5) the topographical feature.

1 Introduction

1.1 Aims of the work

The Red Sea can be considered as a miniature world ocean. It presents a unique combination; it is relatively small and has a fairly geometry, yet it presents several issues as the global ocean such as the role of convective and subductive water mass formation in maintaining meridional thermohaline overturning, air-sea interactions leading to formation events, interactions with adjacent semi-enclosed basins, and the significance of small scale mixing processes. (ESHEL et al. 1994; ESHEL & NAIK 1996). The Red Sea water is one of the most important intermediate water masses in the Indian Ocean, being a major source of warm and highly saline waters in the interior of the ocean (PLAEHN et al. 2001).

The physical properties of the Red Sea were studied by several authors to describe and understand the dynamics and thermodynamics of the water masses. However, more studies are needed to understand better the circulation in response to the driving forces of the Red Sea.

The present study focuses in particular on the Gulf of Aqaba that is a semi-enclosed water basin attached to the northern part of the Red Sea. The gulf is a poorly studied area, which is important for the water mass formation of the Red Sea. Moreover, the ecosystem of the Gulf of Aqaba with its great variety of coral reefs and biological diversity is of great environmental value. A multidisciplinary and international research program, the Red Sea Program (RSP), was developed under the leadership of the Center for Tropical Marine Ecology (ZMT) in Bremen. It was funded by the German Ministry of Education and Research (BMBF) 1995-1998 (RSP I) and in its second phase 1999-2000 (RSP II).

This investigation is a contribution to the RSP and was planed to study the physical part, i.e., the general circulation and the water masses characteristics in the Gulf of Aqaba and the northern Red Sea.

The results of this investigation are important for a better understanding of the ecosystem stability of the under water life, coral reef ecology, and for a scientific rationale for possible planning and limitation of the industrial zones at the coast, which may affect some lively places along the coast of one of the richest coral bands.

In contrast to the Red Sea and the Gulf of Suez only a few oceanographic studies have been performed in the Gulf of Aqaba hitherto. Hence, many questions with respect to the water mass formation, the circulation, and the water exchange of the Gulf of Aqaba with the Red Sea require research.

This study is based on two years of fieldwork and previous investigations made through my M.Sc. study and aims at:

- To achieve a general description of the deep-water formation of the Gulf of Aqaba, and its contribution to the water budget of the Red Sea.
- To achieve a general circulation pattern of the Gulf of Aqaba, and the propagation and transportation of the inflow and outflow waters between the Red Sea and the Gulf of Aqaba through the Strait of Tiran.

- To understand the coastal flow with the relation of the external forces; wind driven and remotely forces.
- To obtain a scientific bases for sustain able use and management which preserves the quantity of the under water live, coral reefs, and gives scientifically advice for a possible impact of fish farms in the Gulf of Aqaba.

This thesis is structured in four chapters. Chapter one gives a general overview on the oceanography of the Red Sea and Gulf of Aqaba. Chapter two describes measurements and data processing of the large-scale survey and the local scale fieldwork of the investigations. Results and discussions are presented in the third chapter. The last chapter summarizes the work and gives some conclusions and recommendations.

This work was done in the frame of the RSP on Marine Science in the Gulf of Aqaba and northern Red Sea. The RSP secretariat at the ZMT in Bremen coordinated the program activities. The RSP was launched in the second half of 1995. The Marine Science Station (MSS) joined the research activities on a bilateral basis in 1997.

1.2 General overview on the Red Sea

To understand the dynamical process in the Gulf of Aqaba, it is important to look at the dynamics of the Red Sea, because of the close interaction between the two systems. Therefore, we start with general overview of the Red Sea.

1.2.1 Topography and geology history of the Red Sea and the Gulf of Aqaba

The Red Sea forms a long and narrow trench, roughly NNW-SSE oriented, which is about 1930 km long and 270 km wide and is located between 12° N and 28° N. The sea splits north 28° N into the shallow Gulf of Suez to the west and into the deep Gulf of Aqaba on the eastern side. The continental shelf (water depth less than 50 m) is widely extended in the southern half of the Red Sea. The central trough more than 1000 m deep is found north of 16° N; its width is about 50 km and deepest parts reach a depth of 2700 m. The sills region, which separates the Red Sea from the Indian Ocean, stretches over a rather long distance. The sill at the southern entrance of the Red Sea lies 140 km inside of the narrow Strait of Bab el Mandeb off Hanish Island, where the greatest depth is about 100 m. The shallower sill lies in the north of the Hanish archipelago at 13°44′ N and its depth is 137 m (MAILLARD & SOLIMAN 1986; WERNER & LANGE 1975). The Strait of Bab el Mandeb is the narrowest area where the main channel, west of the Perim Island (12°34′ N) is about 300 m deep (THOMPSON 1939b; SVERDRUP et al. 1961); see Figure 1.1and Figure 1.2.

The Gulf of Aqaba is the eastern segment of the V-shaped northern extension of the Red Sea. It is located in the sub tropical arid area between 28°-29°30′ N and 34°30′-35° E, it is about 180 km long and has a maximum width of 25 km. The width decreases at the northern tip to about 5 km. The interior of the Gulf of Aqaba is occupied by three deep elongated basins (HALL & BEN-AVRAHAM 1978; BEN-AVRAHAM et al. 1978; BEN-AVRAHAM et al. 1979a; BEN-AVRAHAM et al. 1979b; HULINGS 1989). The basins are separated by relatively low sills. Table 1-1 describes names of the main deeps with its size in the Gulf of Aqaba. The maximum depth of the Gulf is 1830 m, which is nearly equal to that of the Red Sea, and the depth mean is about 800 m. It is the only ocean basin with such a depth to width ratio (HULINGS 1989; POR & LERNER-SEGGEV 1966; MORCOS 1970). The Gulf is considered to be a semi-enclosed water body. It is connected with the Red Sea by the Strait of Tiran, which has a sill depth of about 265 m (HALL 1975), see Figure 1.3.

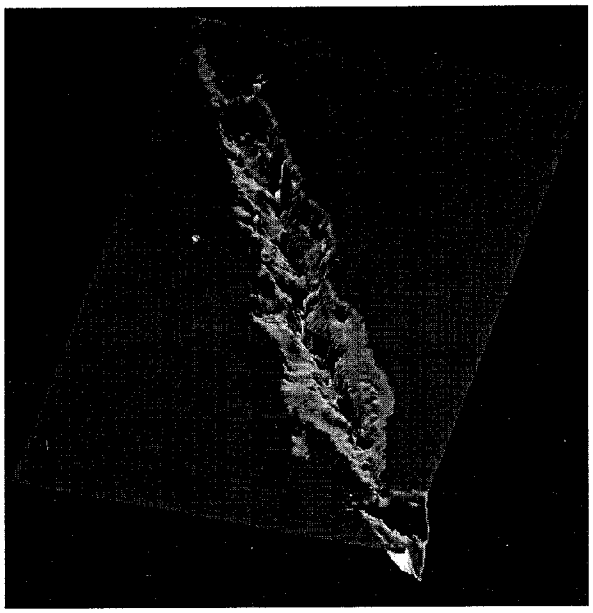

Figure 1.1: Three dimensional rendering bathymetry of the Red Sea (Photo courtesy: http://gom.csi.lsu.edu/~swelsh/redsea/redsea.html).

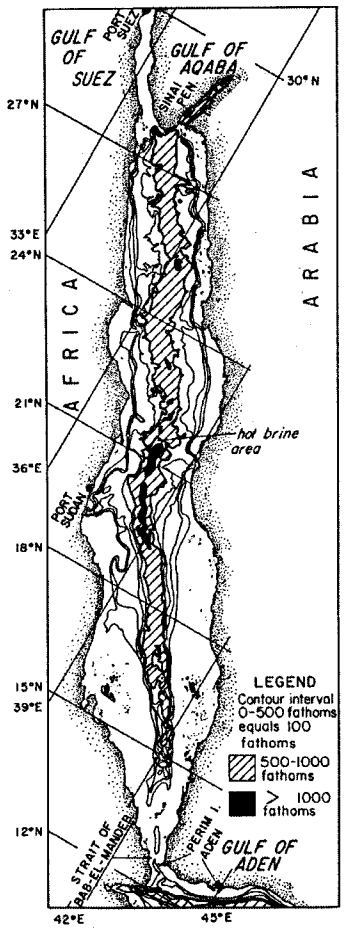

Figure 1.2: Bathymetric chart of the Red Sea (after ALLAN 1966).

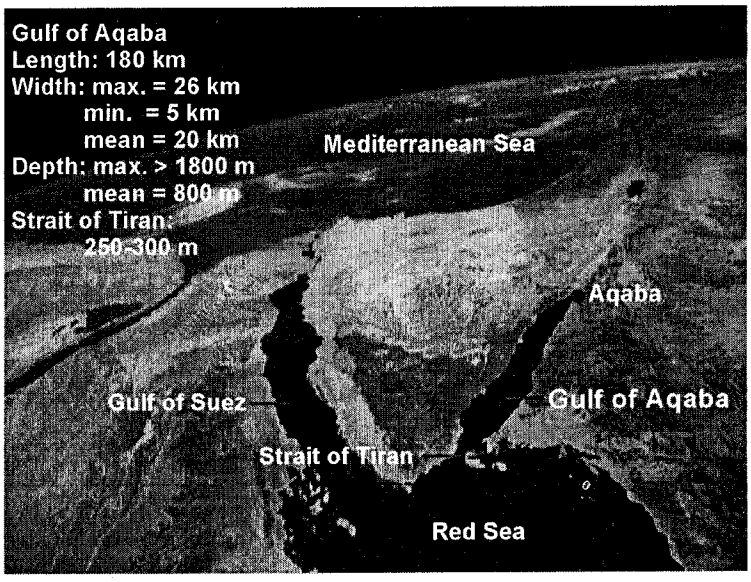

Figure 1.3: Satellite image of the northern Red Sea, Gulf of Suez, and the Gulf of Aqaba.

Table 1-1: The main deep basins in the Gulf of Aqaba.

Location	Deep name	Depth (m)	Long (km)	Wide (km)
Northern basin	Aqaba Deep	900	50	3-8
Central basin	Aragonese Deep	1850	6-8	2
	Arnona Deep	1550	4-5	1
Southern basin	Dakar Deep	1400	18	4
	Tiran Deep	1300	18	3

The shape, bathymetry, and structure of the gulf resulted from the Cenozoic break up of the Arabian-African plate and left lateral strike-slip movement along the Dead Sea rift. The Gulf of Aqaba is a part of the Jordan Rift-Dead Sea-Araba Valley-Gulf of Aqaba graben. This graben extends from the Zagros-Taurus mountains in Turkey through the Red Sea into East Africa (GREGORY 1929). This rift divides the western Gulf of Suez and the eastern Gulf of Aqaba.

This rift is also called Afro–Arabian Rift Valley. It is one of the most extensive rifts on the earth's surface, extending from Jordan in south-western Asia southward through eastern Africa to Mozambique. The system is some 6400 km long and 48-64 km wide in average. It consists of two branches. The main branch, the Eastern Rift Valley (often called the Great Rift Valley, or Rift Valley), extends along the entire length of the system. In the north the rift is occupied by the Jordan River, the Dead Sea and the Gulf of Aqaba. It continues southward along the Red Sea and into eastern Africa. The rift was formed 30 million years ago (as Africa and the Arabian Peninsula

separated) and produced such massifs as Kilimanjaro and Mount Kenya (ENCYCLOPEDIA BRITANNICA 2001).

The Red Sea is considered as a relatively young sea, whose development probably resembles that of the Atlantic Ocean in its early stages. The Red Sea's trough apparently formed in the least two complex phases of land motion. The movement of Africa away from Arabia began about 55 million years ago. The Gulf of Suez opened up about 30 million years ago, and the northern Red Sea about 20 million years ago. The second phase began about 3 to 4 million years ago, creating the trough in the Gulf of Aqaba and also in the southern half of the Red Sea valley. This motion, estimated as amounting to 15.0 to 15.7 millimeters per year, is still proceeding, as indicated by the extensive volcanism of the past 10000 years, by seismic activity, and by the flow of hot brines in the trough (ENCYCLOPEDIA BRITANNICA 2001).

1.2.2 Yearly cycle of the climate of the Red Sea and Gulf of Aqaba

The Red Sea is located in the arid climate belt of the northern hemisphere, a region that is characterized by an excess of evaporation from the water surface over the small precipitation. There is no runoff because no rivers enter the Red Sea. Along the entire length prevailing winds blow consistently from the north-northwest during half of the year, from May to September, but during the other half of the year, October to April, the north-northwest wind extends as far south as lat. 22° or 21° N, and south of 20° N the wind direction is reversed, and south-southeast winds are dominating (SVERDRUP et al. 1961), see Figure 1.4.

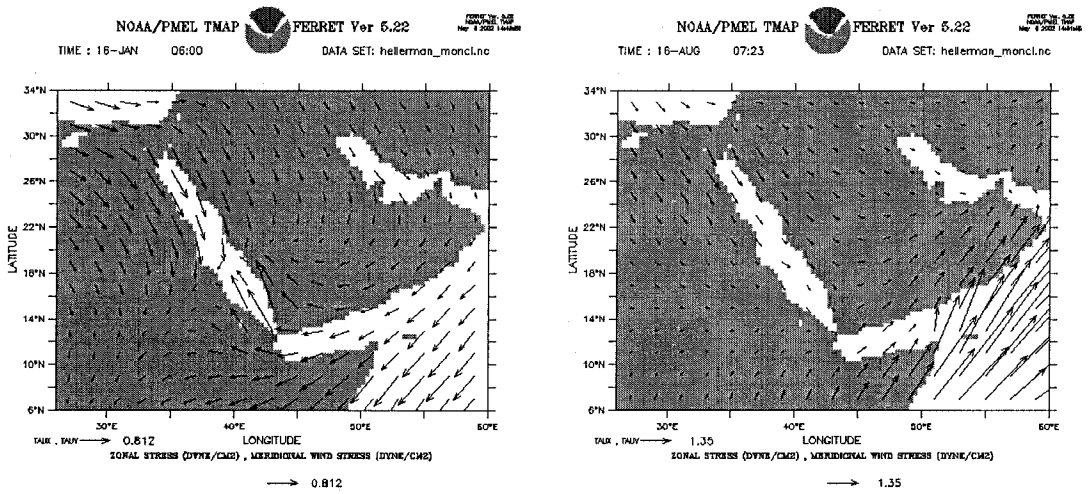

Figure 1.4: Wind stress vectors (dyne/cm^2) in the area of the Red Sea during winter (January) and during summer (August) (Photo courtesy: ferret.wrc.noaa.gov).

Evaporation is very high with an estimated value of 2 m/yr that results in a loss of 0.03 Sv (1 Sverdrup = 10^6 m^{3}s^{-1}) over whole area of the Red Sea (450×10^3 km^2). The seasonal variation of the evaporation is a much debated question and does not exceed the accuracy of the estimation. Precipitation is negligible (MAILLARD & SOLIMAN 1986), see Figure 1.5.

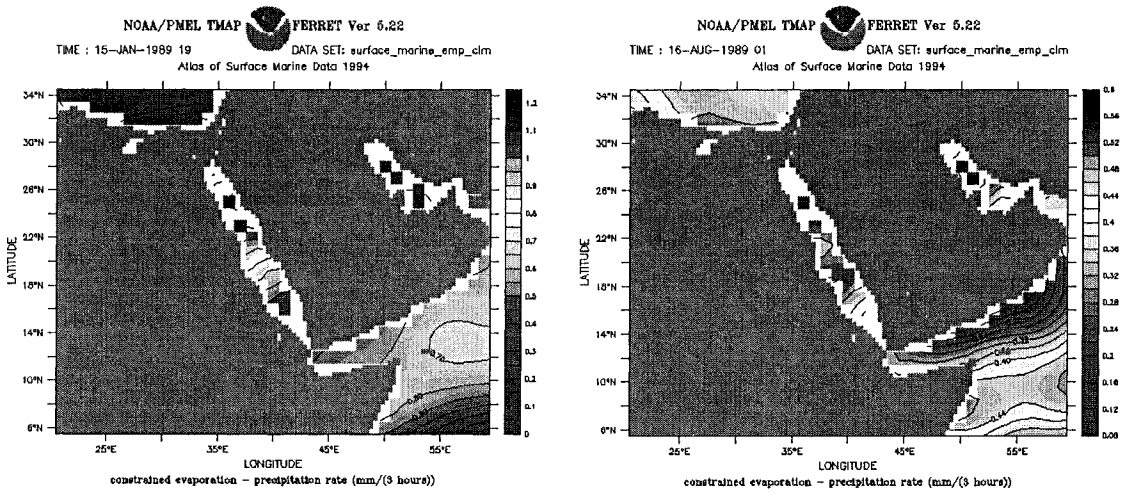

Figure 1.5: Constrained evaporation minus precipitation (mm/3h) in the area of the Red Sea during January and August (Photo courtesy: ferret.wrc.noaa.gov).

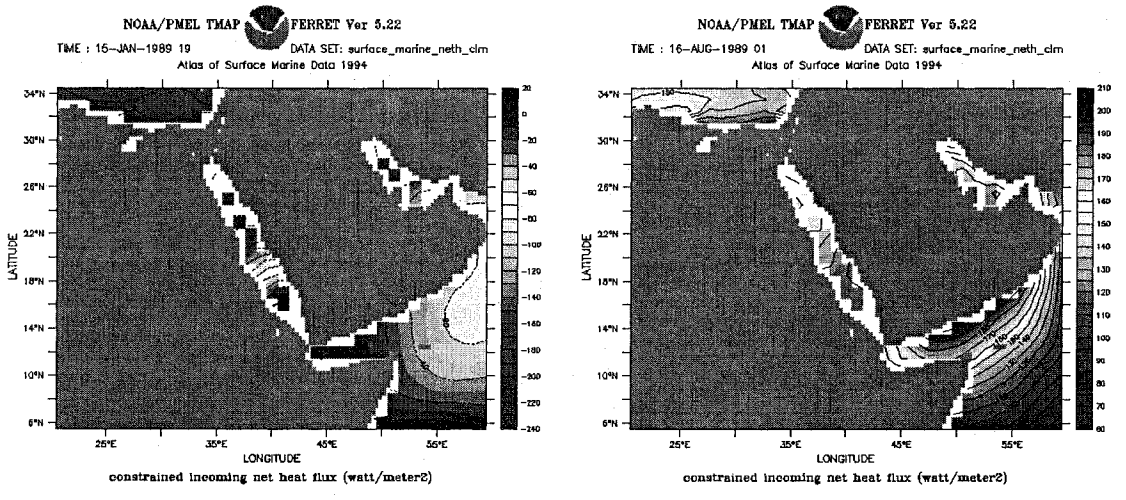

Figure 1.6: Constrained incoming net heat flux (watt m^{-2}) in the area of the Red Sea during January and August 1989 (Photo courtesy: ferret.wrc.noaa.gov).

The heat flux into the Red Sea is positive in summer and negative in winter. On January 1989 the net heat flux between 14°-28° N was ranging from 20 to –240 watt m^{-2}. In summer, August 1989, the net heat flux in the Red Sea was ranging between 120-160 watt m^{-2}. In summer, as well as in winter, the heat flux was increasing towards the south, see Figure 1.6.

The heat flux into the Gulf of Aqaba was estimated of about 50 to 210 watt m^{-2} (ANATI 1974).

The Gulf of Aqaba is affected by both the climate of the northern Red Sea and the very warm portion of the Saharan bio-climatic zone. The climate is arid with high temperature and is affected by airflow from the Indian monsoon trough and the Mediterranean low pressure system (HULINGS 1989). Mean values of 15 years (1966-1980) meteorological data measured at the very northern edge of the gulf by the Jordanian Meteorological Department are summarized in Table 1-2.

Table 1-2: Meteorological parameters at Aqaba, 1966-1980. M.M=Monthly mean, M.D.ma=mean daily maximum, M.D.mi=Mean daily minimum, R.hu=Monthly mean of the Relative humidity, W.sp=Monthly mean of the Wind speed, R.fl=Monthly total of the Rainfall.

Month	Air temperature °C			%	Kn	mm/month
	M.M	$M.D._{ma}$	$MD._{mi}$	R.hu	W.sp	R.fl
January	16.0	20.4	11.6	54	7.5	6.6
February	17.6	22.2	13.1	53	7.2	9.0
March	20.0	25.1	15.4	50	7.8	4.6
April	24.1	29.3	18.8	45	8.0	3.4
May	27.8	33.4	22.3	40	9.0	2.1
June	30.2	36.2	24.6	40	9.9	0.0
July	31.5	37.2	25.9	43	8.8	0.0
August	31.6	36.9	26.2	46	9.5	0.0
September	29.5	34.5	24.4	47	10.5	0.0
October	26.6	31.4	21.9	49	9.1	0.2
November	22.0	26.3	17.7	51	8.4	4.0
December	17.2	21.5	12.9	57	7.9	6.0

The wind vector over the Gulf of Aqaba is fairly constant, see Table 1-2, for both mean wind speed; (7.5-10.5 kn) and wind direction. The wind is blowing 85% of the time from northern to north-eastern, along the main axis of the Gulf. The wind vector in the Gulf of Aqaba is directed to the south (northern winds) as in the northern Red Sea during almost all of the year (see Figure 1.4). The remaining 15% of wind directions are variable. The most frequent of them are the southerly winds. Eastern and western winds are extremely rare. When they occur they last only for some hours, most often during the transition from northerly to southerly winds.

1.2.3 Water budget of the Red Sea

The water inflow and outflow of the Red Sea is controlled by both the sea level and density differences between the Red Sea and the Indian Ocean. The sea level changes of the Red Sea are determined by the water balance of the Red Sea. Therefore to obtain the characteristic of the seasonal water exchange variation the monthly values of evaporation and the sea level difference between Aden-Perim and Aden-Sudan were accounted for. The level differences between the Red Sea and Gulf of Aden depends on the following factors: on a real decrease of water volume due to intensive evaporation from sea surface, on the variation of a positive component of water exchange through Bab el Mandeb and Suez Canal and on the water redistribution in the sea due to the wind (BOGDANOVA 1974).

The monthly sea level and level differences between the northern and southern parts of the sea regions as well as its central part, between Aden and Perim, are summarized in Table 1-3. The longitudinal profile of level surface according to the yearly mean of the sea level (Figure 1.7)

indicates a lowering from south to north during the warm season. However, in the middle of the sea (Sudan) the level is somewhat lower than the northern one (Suez). The level decrease over the whole Red Sea during the warm season is related to the evaporation loss excess over the Aden inflow, i.e. over the positive water exchange component through Bab el Mandeb. The mean sea level increase begins from September and continues to January pointing to a dominance of the water inflow over evaporation. Some sea level increase is also observed from March to April. A convex form of the level surface in the central part of the sea is the most distinct in November and a concave one in June (BOGDANOVA 1974).

The evaporation is very high in the Red Sea as mentioned in section 1.2.2. The most important effects of evaporation are the loss of water and the increase of the salinity, and consequently the density, of the water. The resulting pressure gradient creates an upper inflow of water from the Indian Ocean towards the Red Sea and outflow of deep and dense Red Sea water in the opposite direction. Both of these flows are by far higher than the volume of evaporated water per unit of time.

Indirect estimates of the transport of Red Sea water through the Bab el Mandeb Strait suggest an annual mean transport of 0.33 Sv (SIEDLER 1969), varying from approximately 0.6 Sv in winter to nearly zero in late summer (PATZERT 1974a). The winter period (November-May) is characterized by a classical two-layer exchange flow (SIEDLER 1969). However, in summer the north westerly winds apparently drive a three-layer exchange, consisting of a thin surface outflow from the Red Sea, an inflowing intermediate layer of Gulf of Aden thermocline water, and a weak outflowing deep layer (MAILLARD & SOLIMAN 1986).

Table 1-3: The annual sea level (cm) variation of the Red relative to the long time mean value and level difference between central sea part, its northern, and southern sea parts.

Point of observa-tions	Set of* Obser-vations	I	II	III	IV	V	VI	VII	VIII	IX	X	XI	XII	Amp.
Suez(1)	12	10	9	9	12	6	0	-12	-21	-18	-12	3	12	33
Sudan(2)	37	13	9	6	7	5	-5	-16	-22	-14	4	11	11	35
Perim(3)	6	6	6	5	3	9	3	-6	-12	-15	9	-3	3	21
Aden(4)	25	5	7	7	10	10	4	-6	-14	-12	-10	-3	1	25
	Level differ (cm)													
(2)-(1)		3	0	-3	-5	-1	-5	-4	-1	4	8	8	1	13
(2)-(4)		8	2	-1	-2	-5	-9	-10	-8	-2	6	14	10	24
(2)-(3)		7	3	1	4	-4	-8	-10	-10	1	5	14	8	24
(3)-(4)		-1	-1	-2	-7	-1	-1	0	2	-3	1	0	2	9

*: The numbers of observations on these stations are the length of the results in years, i.e. monthly and yearly sea level were of a different accuracy.

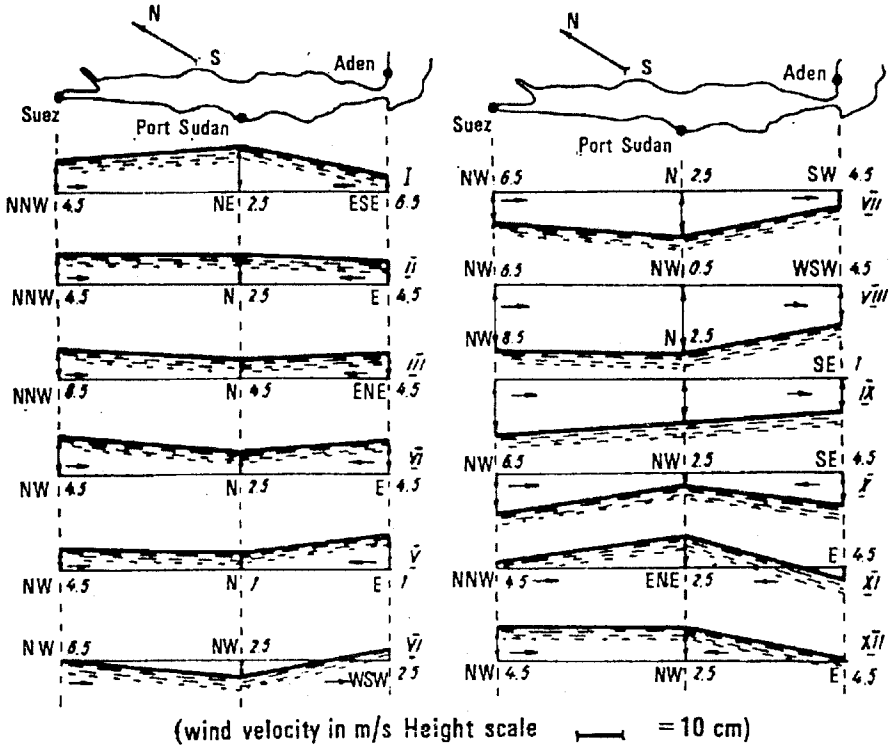

Figure 1.7: Annual variation of the longitudinal profile of the Red Sea surface height, relative to its mean value. (after BOGDANOVA 1974).

JOHNS et al. (1974) studied the circulation between the Red Sea and the Gulf of Aden in late summer, they observed the current at three different depths 15, 43 and 127 m using current meters in the Strait of Bab el Mandeb, they found evidence to support a three layered current pattern in Bab el Mandeb at least during late summer. The current speed and direction scatter diagram at 15 and 127 m appeared outflow water to the Gulf of Aden, and at 43 m the opposite direction was detected.

MAILLARD & SOLIMAN (1986) estimated the outflow from the Red Sea of 0.36 Sv during July-August. MAILLARD & JOHNS (1997) described a comprehensive Bab el Mandeb experiment during 1995-1996 involving moored ADCPs and T-S sensors that revealed the annual cycle of the exchange in a detail that had not been available before. The inflow and outflow transports of the exchange flows were well resolved and showed a very repeatable transition between the winter two-layer regime and summer three layer regime over the 17 months of continuous observation (Figure 1.8). The annual mean outflow of Red Sea deep-water through the strait was estimated to be 0.39 Sv, with maximum exchange reaching 0.7 Sv in February and average summer outflow of ~0.05 Sv. The estimated net inflow of 0.036 Sv agrees well with the yearly evaporation flux of 0.03 Sv.

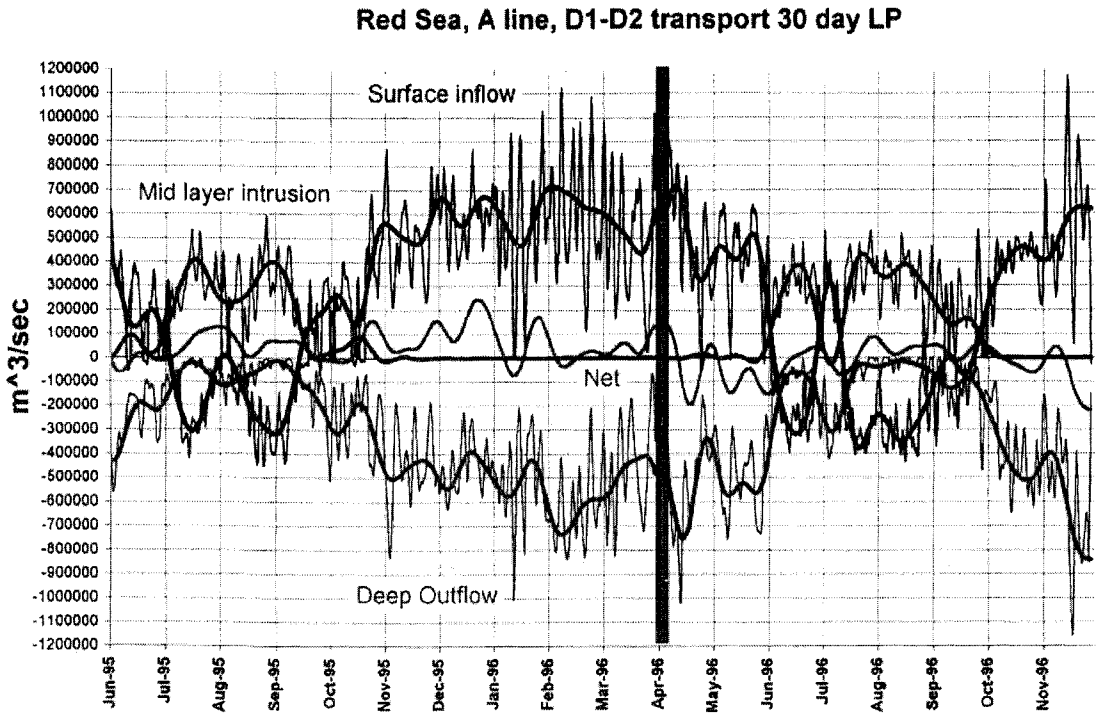

Figure 1.8: Volume transports for the surface layer, the deep outflow layer, and the mid-depth summer intrusion in the Bab el Mandeb. The two-layer exchange in February reaches 0.7 Sv. Deep outflow diminishes to 0.05 Sv in summer. Annual average deep outflow ~0.39 Sv. Net flow into the Red Sea over one year (April 1995-1996) is ~0.036 Sv (Modified after MAILLARD & JOHNS 1997).

The exchange of water between the Red Sea and the adjacent parts of the ocean takes place through the Suez Canal and through the Strait of Bab el Mandeb. The exchange through the Suez Canal is of no importance to the water and salt budget of the Red Sea but shows some interesting details. Any flow of water through the Suez Canal is complicated by the fact that the canal passes through the Bitter Lakes, the bottom of which consist of layers of pure salt which are gradually being dissolved, thus increasing the salinity of the waters in the canal to a concentration above that of the Red Sea or Mediterranean Sea waters. In October-December the salinity at the surface of the canal above the Great Bitter Lake is as high as 50.00 and at the bottom it is above 55.00. The flow through the Suez Canal is mainly determined by three factors: (1) the difference in sea level between the Red Sea and Mediterranean Sea, (2) the prevailing local winds, and (3) the great salinity of the canal waters due to the solution of the salt layers of the Bitter Lake. The sea level is higher in Suez on the Red Sea side than at Port Said on the Mediterranean side, except in July-September, and because the difference in sea level dominates, the surface flow is directed from the Red Sea to the Mediterranean in all seasons except in July-September, when it is reversed (WÜST 1934; SVERDRUP et al. 1961).

1.2.4 Stratification and water mass distribution in the Red Sea

Two main water masses are present in the Red Sea in winter. The surface water originating from the Indian Ocean, about 80 m deep, is warm and fresh, but undergoes strong cooling and concentration between the southern and northern boundaries of the sea. The surface water in the Red Sea during winter has a temperature range ~22 to 26 °C in the southern part, and ~21-22 °C in

the northern part, and has salinity between ~37 to 40 in the southern, and ~40 to 41 in the northern Red Sea. The deep-water is very homogeneous below the sill depth, with T ≈ 21.7 °C and S ≈ 40.57 (MAILLARD & SOLIMAN 1986). The sinking of the surface water in the vicinity of the northern boundary is assumed to be mostly a winter process, where the strong convection in the northern Red Sea occurred down to 500 m water column. The main convective flow is created by the mixing of the dense Gulf of Aqaba and Gulf of Suez water (which is far colder and saltier than the Red Sea deep-water) with the north Red Sea subsurface water (MAILLARD 1974), see Figure 1.9.

Three water masses are present in summer in the Red Sea. The warm and saline surface water mass flows out into the Indian Ocean (T ≈ 32 °C and S ≈ 38). The surface water in the Red Sea has the highest temperature in the southern part (T ≈ 32 °C) and the lowest temperature in the northern part (T ≈ 26 °C). Below the surface water inflow of cool water from the Indian Ocean (T ≈ 20 °C and S = 36) is taking place. Below the inflowing cold Indian Ocean water warm and saline Red Sea water is flowing out at a rather reduced rate. Its temperature is about T ≈ 24 °C and the salinity S ≈ 39. The water mass of the intermediate water in the southern Red Sea has the same characteristics of the water mass of the upper 200 m depth in the northern Red Sea during winter and summer. The properties of the deep-water in the Red Sea, described above, are quite independent of the season. The stratification of the Red Sea during summer becomes gradually weaker from south to north in the upper 200 m. The stratification in the southern part of the Red Sea is ranging between (θ ~22 to 32 °C, and S ~37 to 40), whereas in the northern part the stratification ranges between (θ ~21 to 27 °C, and S ~40 to 41).

A remarkable feature of the Red Sea is the extremely high water temperature and salinity found in various depressions of the sea floor. This is the result of geothermal heating through vents in the ocean crust, which brings minerals contained in the crust and in the sediment into solution. The resulting brine is dense enough to remain at the ocean floor even at very high temperature. Values close to 58 °C have been recorded, together with "salinities" in excess of 300. The Red Sea was the first region where hot brines were discovered at the sea floor (TOMCZAK & GODFREY 2001).

The local investigation of temperature and salinity in the northern part of the Gulf of Aqaba was studied in the Jordanian waters (BADRAN 1996; MANASREH 1998), see Table 1-4. They found that the upper 200 m had different water mass characteristics during summer and winter. During summer, the temperature and salinity ranges in the upper 200 m between 21 to 26 °C and 40.35 to 40.55, respectively. Mixing dominated during winter in the northern tip of the gulf (T ~20-21 °C and S ~40.55-40.65). Below 200 m the water was homogenous during summer and winter and had the same ranges of temperature and salinity in the upper 200 m during winter. The deepening of mixed layer between October to April was calculated of a mean rate of 1.97 $m.day^{-1}$. Salinity inversion was detected by PALDOR & ANATI (1979) in October; waters in the upper 150 m of salinity 40.77 overlay waters of lower salinity (40.67) in the 150-300 m depth interval. The same phenomenon was also reported by WOLF-VECHT et al. (1992) and MANASREH (1998), but they noticed a salinity minimum at 100 m all through summer, which penetrated down to 200 m during November.

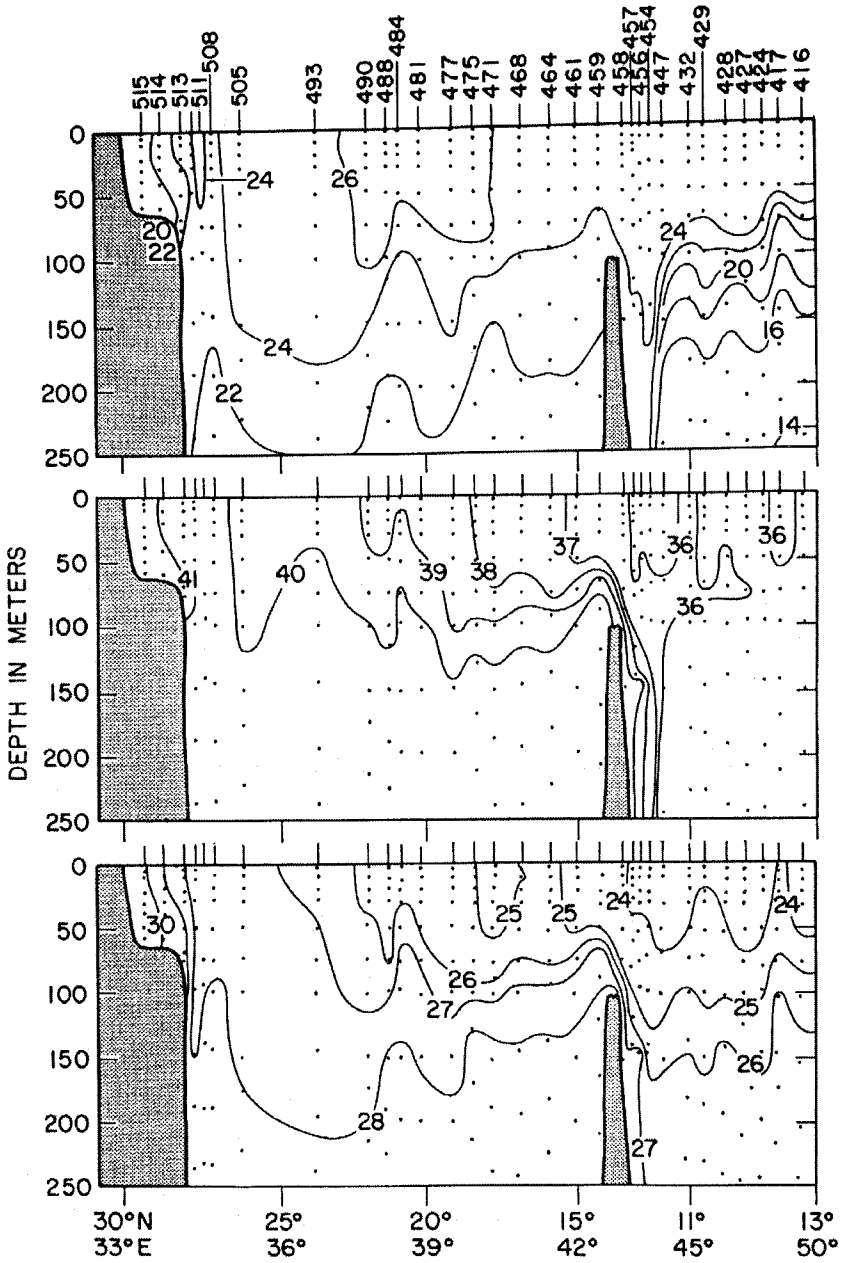

Figure 1.9: Sections of the potential temperature (°C) (upper), salinity (psu) (middle), and potential density (σ_θ) (lower) from the Gulf of Suez to the Gulf of Aden and the ENE toward the Arabian Sea during winter 1963. Data from the COM. R. GIRAUD (station 416-515 from January 1st to February 7th, 1963) were used (after PATZERT 1972b).

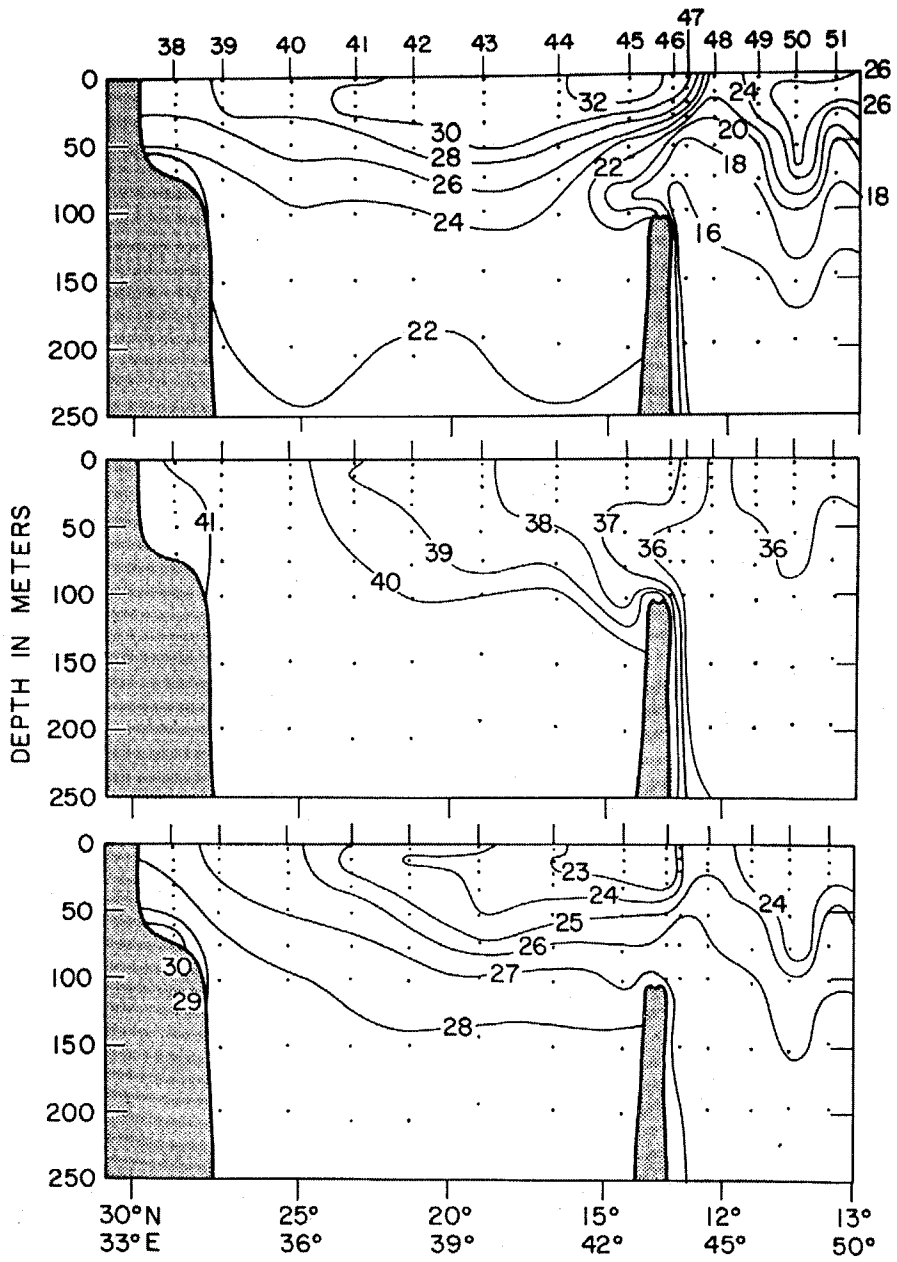

Figure 1.10: Sections of the potential temperature (°C) (upper), salinity (psu (middle)), and potential density (σ_θ) (lower) from the Gulf of Suez to the Gulf of Aden and the ENE toward the Arabian Sea during summer 1963. Data from the R/V ATLANTIS (station 38-51 from July 29th to August 4th, 1963) were used (after PATZERT 1972b).

Table 1-4: Monthly mean of the temperature (°C), salinity (psu) and the sigma-t ($kg.m^{-3}$) at the surface water and in the segments 0-100, 100-200 and 200-300 m of the water column at the southern part of the Jordanian sector of the Gulf of Aqaba between May 1997 to April 1998.

	Temperature (°C)				Salinity (psu)				Sigma-t ($kg.m^{-3}$)			
Month	T_0	T_{0-100}	$T_{100-200}$	$T_{200-300}$	S_0	S_{0-100}	$S_{100-200}$	$S_{200-300}$	σ_0	σ_{0-100}	$\sigma_{100-200}$	$\sigma_{200-300}$
May	21.5	21.3	21.08	21.02	40.6	40.6	40.64	40.65	28.6	28.6	28.77	28.80
Jun.	24.9	23.5	21.69	21.04	40.5	40.5	40.56	40.63	27.5	27.9	28.54	28.78
Jul.	26.1	24.5	21.94	21.04	40.5	40.4	40.51	40.59	27.2	27.6	28.43	28.75
Aug.	25.3	23.9	21.66	21.02	40.4	40.3	40.50	40.57	27.3	27.7	28.50	28.74
Sep.	24.8	23.9	21.84	21.14	40.4	40.3	40.44	40.52	27.5	27.7	28.41	28.66
Oct.	24.6	24.4	21.98	21.06	40.5	40.5	40.43	40.51	27.6	27.6	28.35	28.68
Nov.	25.0	24.9	23.26	21.08	40.5	40.5	40.44	40.49	27.5	27.5	27.99	28.66
Dec.	23.2	23.2	23.29	21.83	40.5	40.5	40.55	40.47	28.0	28.0	28.07	28.43
Jan.	21.9	21.9	21.98	21.93	40.5	40.5	40.56	40.56	28.4	28.4	28.45	28.47
Feb.	21.7	21.7	21.77	21.61	40.4	40.4	40.51	40.52	28.4	28.4	28.48	28.53
Mar.	21.3	21.3	21.37	21.39	40.5	40.5	40.52	40.52	28.5	28.5	28.60	28.60
Apr.	21.2	21.1	21.14	21.16	40.5	40.4	40.49	40.49	28.6	28.6	28.64	28.64

1.2.5 Circulation

The Red Sea is often considered as a channel with flow occurring only in northerly or southerly direction, parallel to its central axis. Utilizing this simple description, the Red Sea circulation may be summarized as follow:

- Winter. The surface flow is moving against the wind direction into the northern Red Sea during winter. Two explanations are possible. During winter, large evaporation and cooling could create a sea-surface slope that cannot be maintained by the weak winds in the north. Also, northerly flow is necessary to compensate for the sinking water in the north forming intermediate deep-waters at this season. Another possibility is that the pile-up of warm water near 20° N by the strong surface wind stresses in the south causes the slope in the north to increase and the surface flow to be directed against the weak winds in the north.
- Summer. During the summer, winds of the southwest monsoon in the Gulf of Aden cause a drop in sea level at the entrance to the Red Sea. The upwelling in the Gulf of Aden lifts the deep-water of higher density towards the sill depths of the Bab el Mandeb. This weakens both the barotropic and the baroclinic pressure gradient between the Red Sea and the Indian Ocean. Since the winds in the southern Red Sea are southward at this time, a wind driven surface outflow and an intermediate inflow must be due primarily to the weakening in sea surface slope through the Strait of Bab el Mandeb. This drop in steric sea level at the entrance to the sea ultimately effects the circulation of the entire Red Sea. The observed summer drop in

monthly mean sea level at Port Sudan and Port Suez are due to the adjustment of the Red Sea level to the sea level in the Indian Ocean, modified by the wind stress distribution between Port Suez and Port Aden.

Figure 1.11 and Figure 1.12 represent the monthly mean longitudinal temperature sections along the central axis of the Red Sea from the Gulf of Suez to the Gulf of Aden for the months from January to August; monthly mean vector winds over the Sea; mixed layer depths; and a schematic representation of the circulation (PATZERT 1972b).

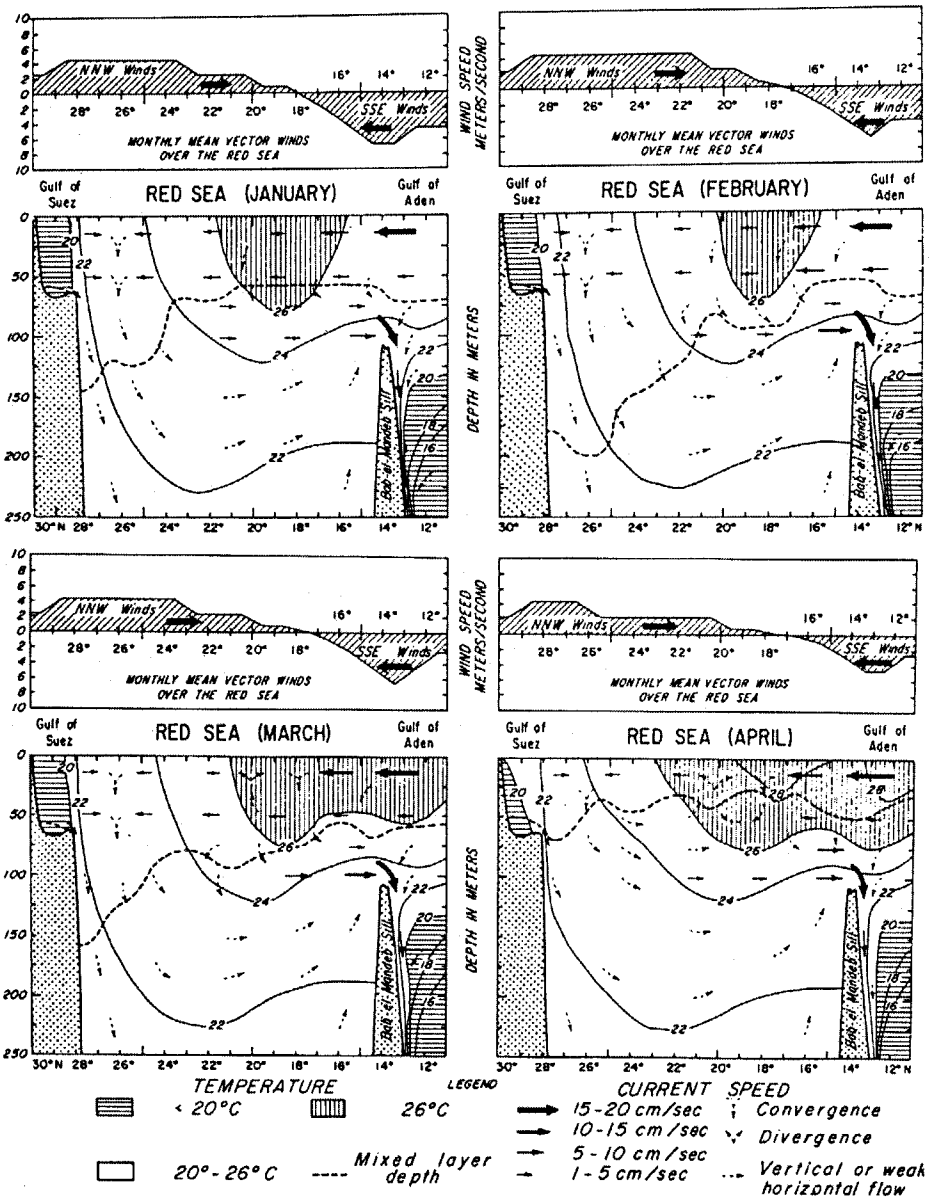

Figure 1.11: Monthly mean longitudinal temperature sections along the central axis of the Red Sea from the Gulf of Suez to the Gulf of Aden for January, February, March, and April; monthly mean vector winds over the Sea; mixed layer depths; and a schematic representation of the circulation (after PATZERT 1972b).

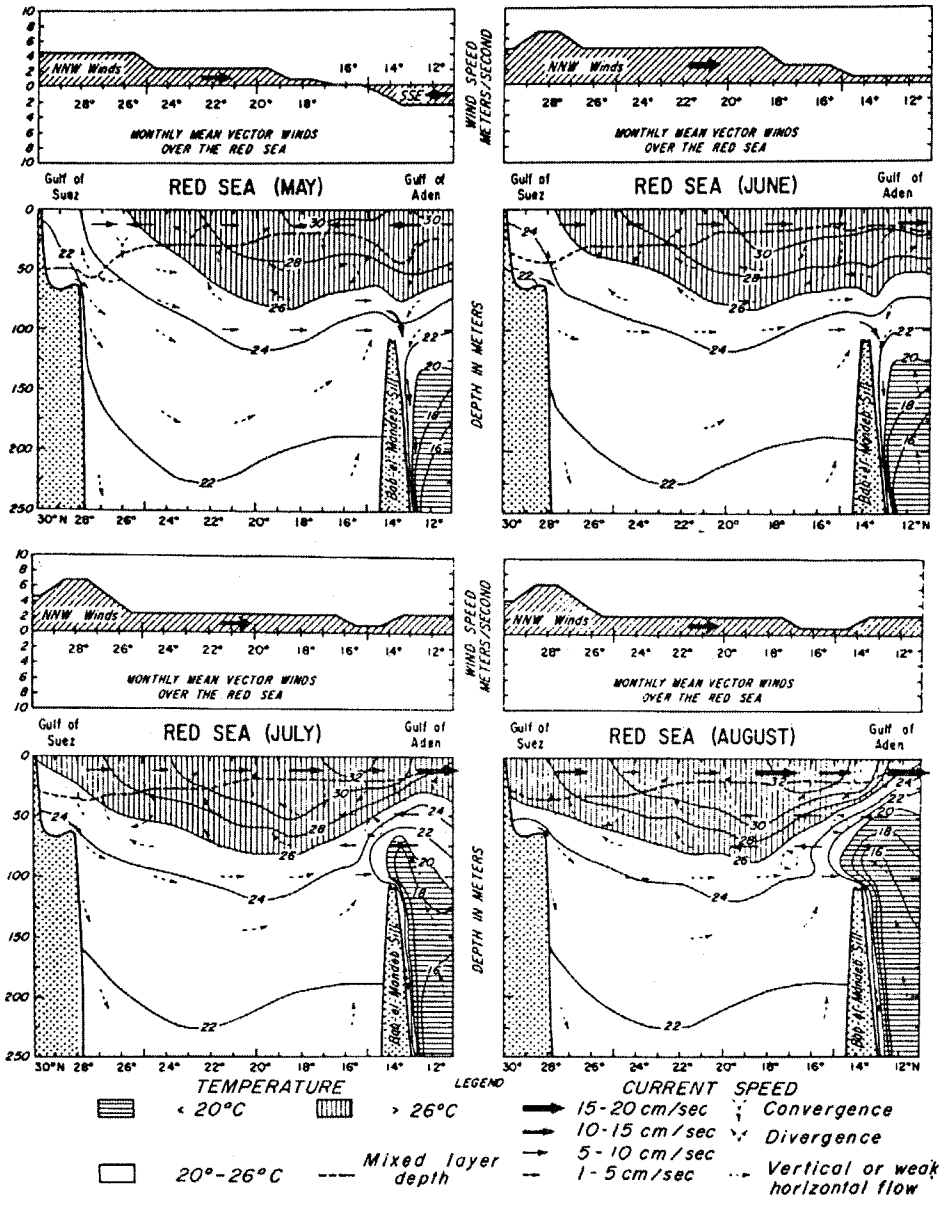

Figure 1.12: Monthly mean longitudinal temperature sections along the central axis of the Red Sea from the Gulf of Suez to the Gulf of Aden for May, June, July, and August; monthly mean vector winds over the Sea; mixed layer depths; and a schematic representation of the circulation (after PATZERT 1972b).

The horizontal circulation of the Red Sea is characterized by a number of gyres or eddies distributed along the axis of the Sea (Figure 1.13), of which some may be semi-permanent (QUADFASEL & BAUDNER 1993). In the northern Red Sea, drifter trajectories point to a cyclonic gyre at least in winter (CLIFFORD et al. 1997). This gyre may be linked to the aforementioned intermediate water formation process in the northern Red Sea, and could possibly cause a preconditioning for the intermediate water formation. In the central Red Sea the circulation appears to be dominated by anti-cyclonic eddies that occur most regularly near 23-24° N and 18-19° N. These locations may be tied to coastline and topography variations (QUADFASEL & BAUDNER

1993). Both cyclonic and anti-cyclonic features are found in the southern Red Sea but no persistent gyre pattern seems to exist there. When present, these gyres usually span most of the width of the Red Sea and can have horizontal velocities of 0.5 m/s or more. Thus they are more energetic than the ~0.1 m/s mean flows in the surface layer associated with the large-scale thermohaline circulation of the Red Sea.

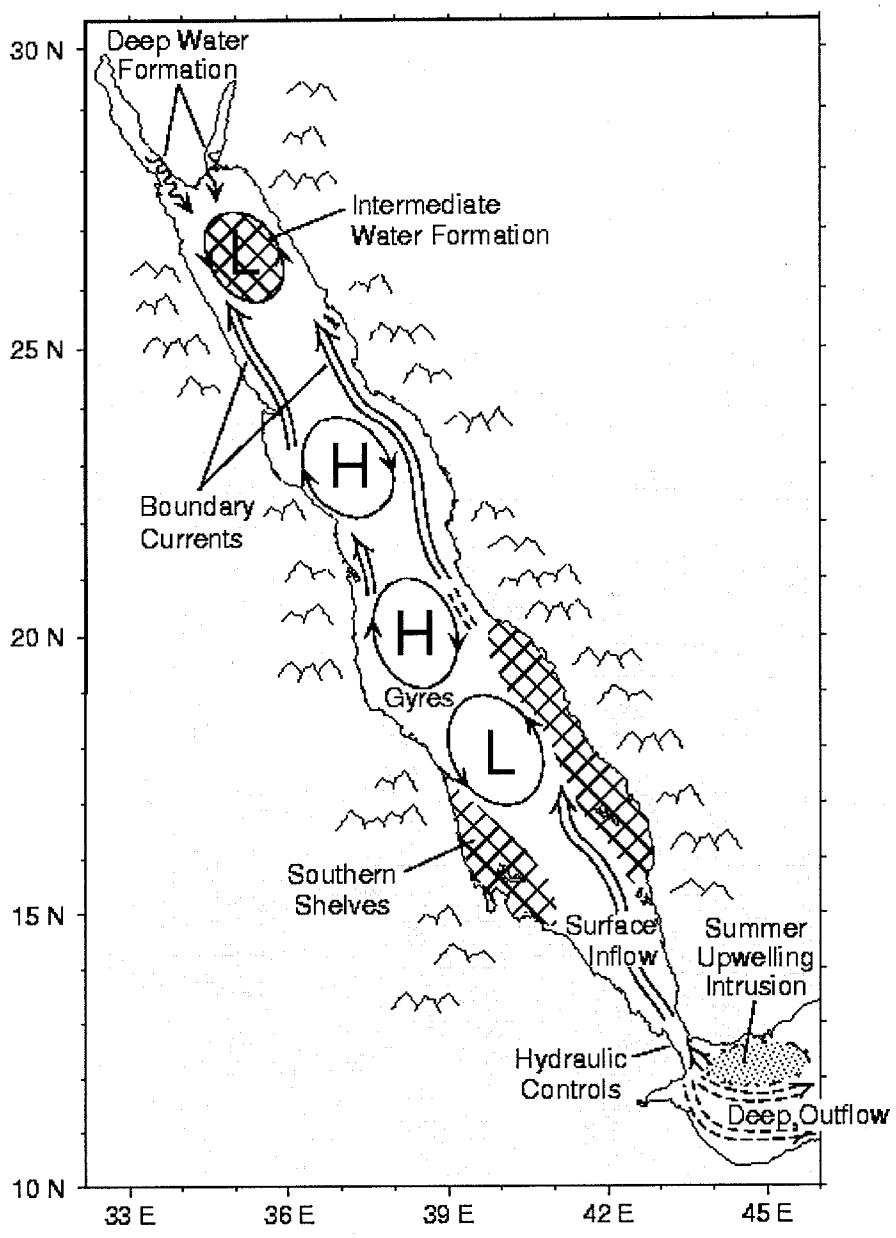

Figure 1.13: Circulation scheme for the Red Sea (After Report of a Workshop Held at Stennis Space Center, Mississippi, May 11-13, 1999)

The circulation in the Straits of Tiran, which controls the water exchange between the Gulf of Aqaba and Red Sea, has been studied by several authors (ANATI 1974; MURRAY et al. 1984; ASSAF & KESSLER 1976; KLINKER et al. 1976; and PALDOR & ANATI 1979). All reports except

the latest were based on calculations of heat flux and mass balance, rather than actual current measurements. The results must be considered as very preliminary so far. Nevertheless all studies agree on the general circulation pattern at the Straits of Tiran. However, they differ considerably in estimating the rate and magnitude of water exchange between the Gulf of Aqaba and the Red Sea.

KLINKER et al. (1976) described different schemes for summer and winter. In summer, they suggested a three layer water exchange system, where water from the Red Sea (q_1) enters the gulf and travels northwards to about mid length of the Gulf. There, when the water has cooled and become more saline it loses buoyancy and starts to sink and travel southward (q_2) beneath the in-flowing water. These two opposite water movements take place in the upper 150 m and have a stationary layer between them below 50 m. In deeper water below 150 m a third water parcel (q_3) moves from the Red Sea into the Gulf of Aqaba. The extent of the northward travel of these waters has not been identified. However, in connection with the findings of the authors themselves and of PALDOR & ANATI (1979), that the deep-water below 150 m was uniform in temperature and salinity in the entire Gulf of Aqaba while the upper water differed significantly from south to north, it can be concluded that the deep-water inflow reported by KLINKER et al. (1976), or a part of it at least, reaches the northern end of the Gulf.

The four quantities q_0, q_1, q_2 and q_3 reported by KLINKER et al. (1976) were estimated by two basic assumption; the conservation of mass and the critical Richardson condition across the Straits of Tiran. This resulted in similar values for q_1 but quite different values for q_3.

The conservation of mass calculation gave:

$q_0 = -280\ m^3\ s^{-1}$ evaporation from ASSAF & KESSLER (1976)

$q_1 = -2.38\times10^4\ m^3\ s^{-1}$ surface inflow

$q_2 = +4.55\times10^4\ m^3\ s^{-1}$ subsurface outflow

$q_3 = -2.20\times10^4\ m^3\ s^{-1}$ deep inflow

Calculations based on critical Richardson conditions across the Straits of Tiran gave:

$q_1 = -2.10\times10^4\ m^3\ s^{-1}$

$q_2 = +3.40\times10^4\ m^3\ s^{-1}$

$q_3 = -1.10\times10^4\ m^3\ s^{-1}$

In winter, the authors suggested a two layer water exchange system in the upper 150 m. Both methods for calculating the water exchange through the Strait gave similar estimates of quantities q_1 (inflow) and q_2 (outflow) of about $7\times10^4\ m^3\ s^{-1}$.

Based on current measurements in the Straits of Tiran of about one month duration (February) MURRAY et al. (1984) also suggested a two layer water exchange system between the Red Sea and the Gulf of Aqaba. According to these authors the water exchange in both directions was the same; $2.9\times10^4\ m^3\ s^{-1}$.

Different estimates have been reported regarding the average residence time of the water in the Gulf of Aqaba. The figure most commonly used by many authors is one year (KLINKER et al. 1976; PALDOR & ANATI 1979; HULINGS 1979).

GENIN & PALDOR (1998) studied the current near the northern end of the Gulf of Aqaba during 1988 to 1991. The study revealed consistence seasonal trends. Southward current along the west coast observed most of the year, with a short period (November-January) of northward flow

and an abrupt reversal in early February. They found, when the water column was vertically mixed, a clear onshore (westward) current was observed near the surface and a return (offshore) current over the bottom. This cross shore pattern was consistent with a wind-driven Ekman circulation.

BERMAN et al. (2000) applied the Princeton Ocean Model (POM) in order to simulate the wind-driven circulation in the Gulf of Aqaba under prevailing wind conditions. Thermohaline circulation and tidal forcing were ignored in the model. The authors concluded that the circulation in the gulf is made up of a series of permanent gyres oriented along its axis. The location and diameter of these gyres can change in accordance with the depth of thermocline. During winter, three gyres in the northern half of the gulf were found; the northernmost gyre is anti-cyclonic with 18 km diameter, and a single cyclonic gyre occupied the southern half of the gulf. During spring and summer, the situation becomes more much complex than in winter, the northernmost gyre is cyclonic with a 10 km diameter. The topography, and depth of the thermocline are the main factors of the circulation pattern in the northern Gulf of Aqaba. As the depth of the thermocline becomes large enough a transition from summer to winter circulation is triggered which, in turn, causes a change in the location of the center of the gyres as well as their diameter. The topography of the shoreline determines the direction of the local current via the boundary condition of tangential flow at the shore. The great effect of the curved coastline in the narrow northern part of the gulf could be a reason for the development of the several gyres there. This can be invoked to explain a peculiar observation noted in GENIN & PALDOR (1998). The study reported a reversal of the current direction along the west coast near the northern end of the gulf.

1.2.6 Deep-water formation

The climatic conditions and prevailing winds determine the character of the deep-water formation in the Red Sea. Owing to the excessive evaporation the surface salinity of the water in the northern Red Sea reaches values between 40 – 41. In summer the temperature of surface water is very high, mostly exceeding 30°, but in winter the temperature decreases, particularly in the northern part, to average values in February as low as 18 °C. The lowering of the temperature in winter, together with intense evaporation in that season, leads to the formation of deep-water that fills the entire basin of the Red Sea below the sill depth. This deep-water has salinity between 40.5 and 41.0 and a temperature between 21.5° and 22°. The formation of this deep-water is further facilitated by the character of the currents, which are modified by the prevailing winds (SVERDRUP et al. 1961).

Estimates of the annually averaged rate of Red Sea deep-water formation range from 0.06 Sv (WYRTKI 1974) to 0.16 Sv (CEMBER 1988). This water forms in the northern Red Sea predominantly during winter, and fills the deep basin below the sill depth (approximately 160 m) of the Bab el Mandeb Strait with a nearly homogeneous water mass of temperature 21.7 °C and salinity 40.6 (NEUMANN & MC GILL 1962). A second source of somewhat less dense Red Sea water, or Red Sea "intermediate" water, is believed to be formed also predominantly in winter by an open sea convection process in the northern Red Sea that remains poorly understood (CEMBER 1988). This process appears to be distinct from the Red Sea deep-water formation process that occurs in the northern gulfs of the Red Sea (Gulf of Suez and Gulf of Aqaba) and that fills most of the deep volume of the Red Sea. Another class of intermediate waters may be formed on shallow shelves in the southern Red Sea (MAILLARD 1974). Volumetrically, the rate of intermediate water formation appears to be greater than the rate of deep-water formation, and is thought to supply the main contribution to the lower layer outflow from the Red Sea through Bab el Mandeb. The deep-water residual time estimates ranged from 200 years (SIEDLER 1969) to 300 years (MANINS 1973).

In general, it is believed that the high evaporation in the northern Red Sea leads to intermediate and/or deep convection. The Gulf of Suez has been identified as one likely location for deep-water mass formation, but the estimated rates are still uncertain.

ESHEL & NAIK (1996) present climatologies of a numerical model of the Red Sea, focusing on the dynamics of winter intermediate water formation. Northward flowing boundary currents are identified as the major dynamical elements. At the northern boundary, the eastern current follows the bathymetry, eventually turning back to the south. At ~26° N and the western shore the two boundary currents collide. At the collision site, the denser eastern current subducts under the western boundary current. The subduction forces the western boundary current eastward into the interior. Convection communicates the surface fluxes to the downwelled plume and intermediate water forms. The estimated rate, 0.11 Sv, agrees with previous estimates.

2 Observations in the Gulf of Aqaba

The fieldwork in the Gulf of Aqaba and the northern Red Sea has been done from February 1999 to March 1999, and from September 1999 to August 2001. It can be divided into two parts: the R/V Meteor cruise Leg 44/2, providing a larg scale description of the oceanographic field of the Gulf of Aqaba and the northern Red Sea; and the long term observations near the MSS in Aqaba-Jordan, providing a detailed describtion of the seasonal variation of water masses and the circulation of the northern part of the gulf.

2.1 Research program of the R/V Meteor cruise Leg 44/2

The area of observation during the R/V Meteor cruise leg 44/2 covered the Gulf of Aqaba and a small region of the northern Red Sea near to the Strait of Tiran, see Figure 2.1 and Figure 2.2. Six stations (Pos. I-VI) were distributed, 25-30 km apart, along the axis of the Gulf of Aqaba. The Red Sea part consisted of further six stations (Pos. VII-XII) aligned mainly along meridian and longitudinal sections.

The Gulf of Aqaba was sampled four times on 21-23 February, 25-27 February, 1-3 March and 5-7 March; the Red Sea was visited three times on 24-25 February, 27-28 February and 3-4 March. Figure 2.3 and Table 2-1 give the positions and bottom depths at the stations.

Figure 2.1: Research vessel Meteor.

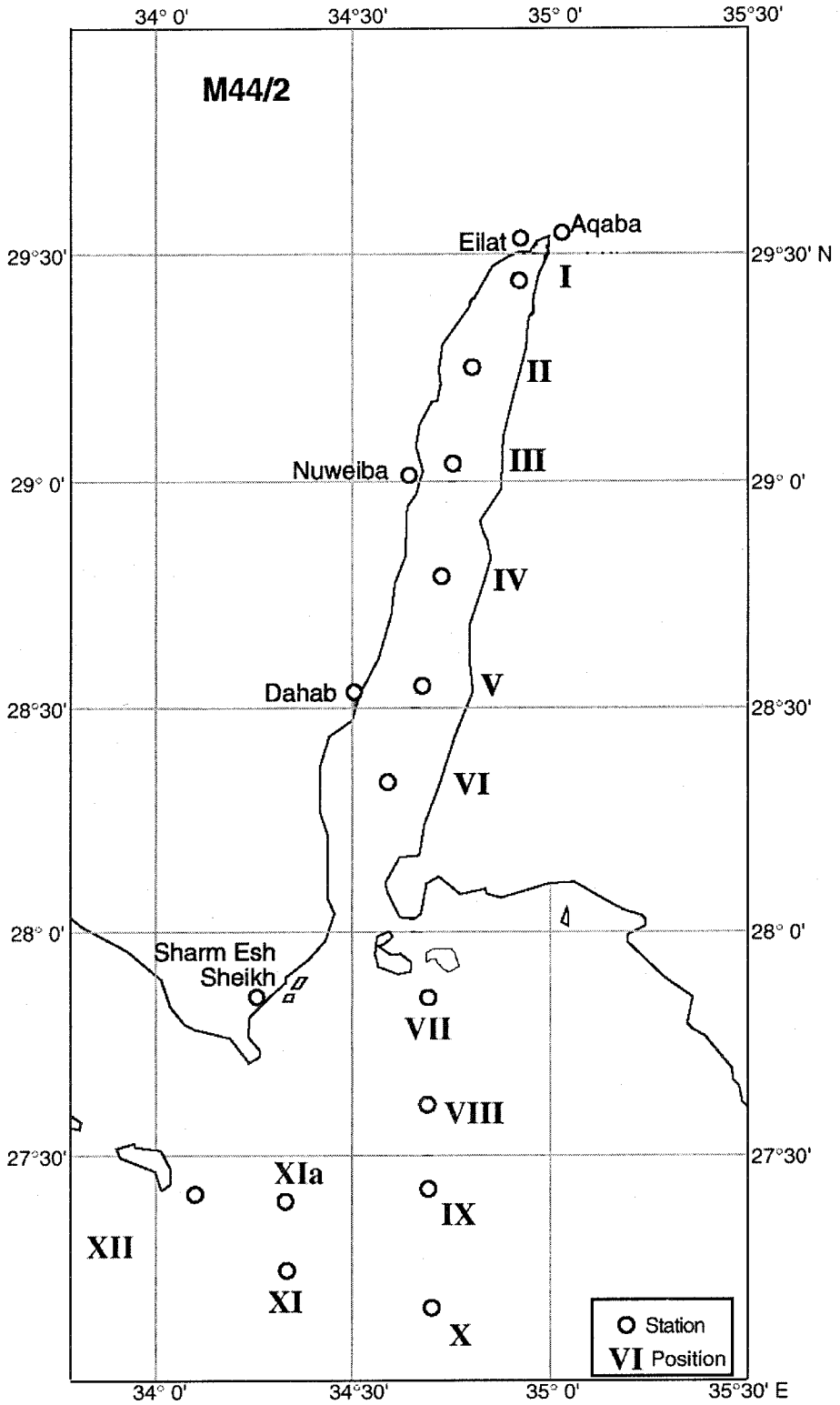

Figure 2.2: Area of observation during the R/V Meteor cruise leg 44/2.

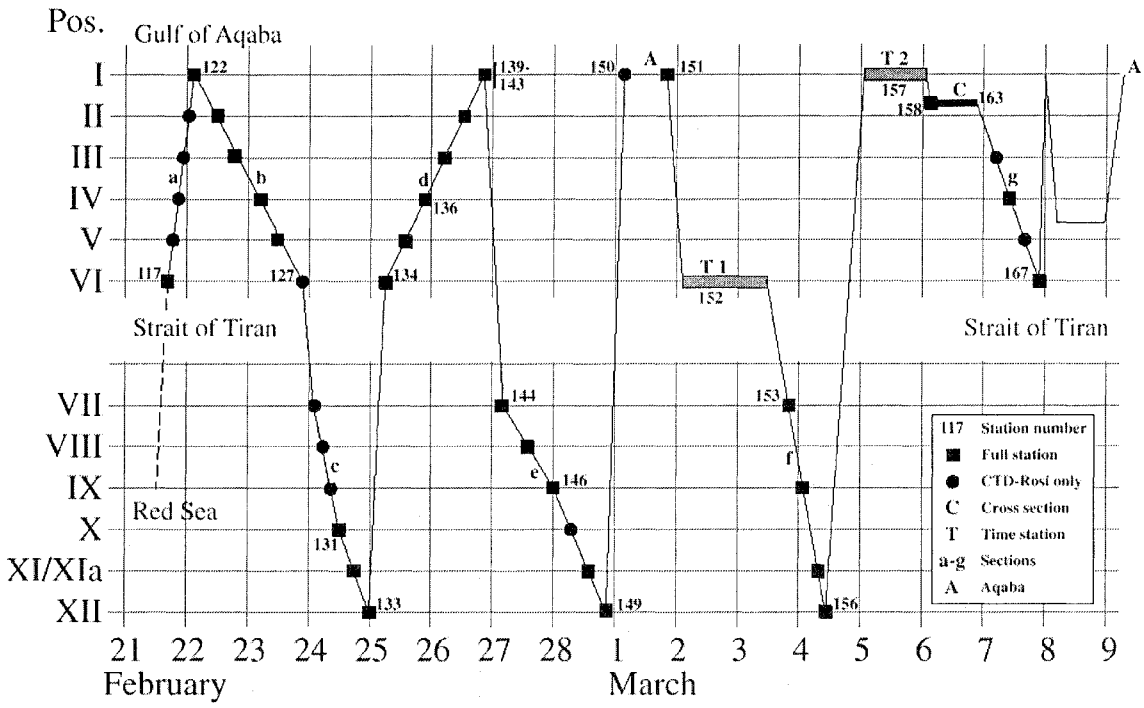

Figure 2.3: Route and position of the stations on the R/V Meteor cruise leg 44/2.

Table 2-1: The position and bottom depth of the stations.

Station	Latitude (N)	Longitude (E)	Bottom depth ±30 m
I	29° 29.52′	34° 57.00′	600
II	29° 16.98′	34° 48.96′	850
III	29° 05.04′	34° 46.08′	840
IV	28° 49.98′	34° 44.04′	1400
V	28° 34.92′	34° 39.06′	1200
VI	28° 20.22′	34° 33.06′	850
VII	27° 53.04′	34° 40.02′	650
VIII	27° 38.94′	34° 40.08′	900
IX	27° 25.08′	34° 40.08′	900
X	27° 11.04′	34° 39.96′	1150
XI	27° 17.88′	34° 22.08′	1320
XIa	27° 23.82′	34° 22.08′	1100
XII	27° 25.02′	34° 04.92′	810

Meteorological data as well as seawater temperature and salinity near the sea surface and current profiles down to 350 m depth were continuously recorded en route. 72 salinity and temperature profiles were measured on 52 stations with a CTD. Additionally, at two 24 hours stations 30 'yoyo'-CTD profiles were carried out. The CTD used was a Neil Brown Mark IIIb. It was attached to a 24 bottle 10 L General Oceanic rosette water sampler. Four of the bottles were equipped with deep-sea reversing electronical thermometer from SIS. When employed, the rosette was lowered and heaved at a speed of 0.5 ms^{-1} in the upper 100 m and at a speed of 1 ms^{-1} thereafter.

Calibration of the pressure and temperature sensors was done prior to the cruise at the IFM Kiel. During the cruise thermometer reading were used to check the laboratory calibration of the temperature sensor. The salinity samples, typically three per profile, have been analyzed after the cruise with an Autosal Salinometer in Kiel.

The shipboard ADCP worked very well during the cruise R/V Meteor 44/2. The range of the 150 kHz ADCP was about 350 m, using a bin length of 8 m and a pulse length of 16 m. The number of bins was 60. The profiles were averaged over 2 minutes. A GLONASS/GPS-receiver was used for the correction of the ship's motion and three dimensional GPS receiver (ADU) was used for highly accurate heading measurements in order to correct the Schuler oscillation of the gyro-compass.

The physical research program was focused on a detailed analysis of the water masses in the Gulf, their vertical stratification, their short term dynamics and their age determination by tracer chemistry. Since station measurements were not permitted in the Strait of Tiran and their surroundings, the exchange with the Red Sea had to be assessed indirectly.

2.2 Long term research in the MSS

2.2.1 Study sites and temporal resolution

The long term research in the MSS (see Figure 2.4) commenced in September 1999 and was finished on August 2001. The study was designed to get a complete set of data combined with R/V Meteor cruise data, to achieve the aims of this study. Figure 2.5 shows the location of the study region and study sites in the Gulf of Aqaba. Biweekly current measurements were carried out along an offshore track L4 parallel to the shore line using ADCP 150 kHz where the maximum depth of the current measurements was 250 m, moreover, several zigzag surveys (ZZ) were performed in the northern tip of the gulf using the same ADCP with the same configuration. Profiles of temperature and salinity (0-400 m depth) were taken biweekly at station S2 and monthly at stations S1 and S3, and all projected to about 3 km offshore, Table 2-2.

Two Workhorses ADCP (300 kHz) were deployed at three positions; w1-a, w1-b and w2, during different periods. At w1-a the current was measured in the 20-50 m depth range, at w1-b in the 4-32 m, and at w2 in the 20-80 m depth range of the water column, see Figure 2.5 and Table 2-2.

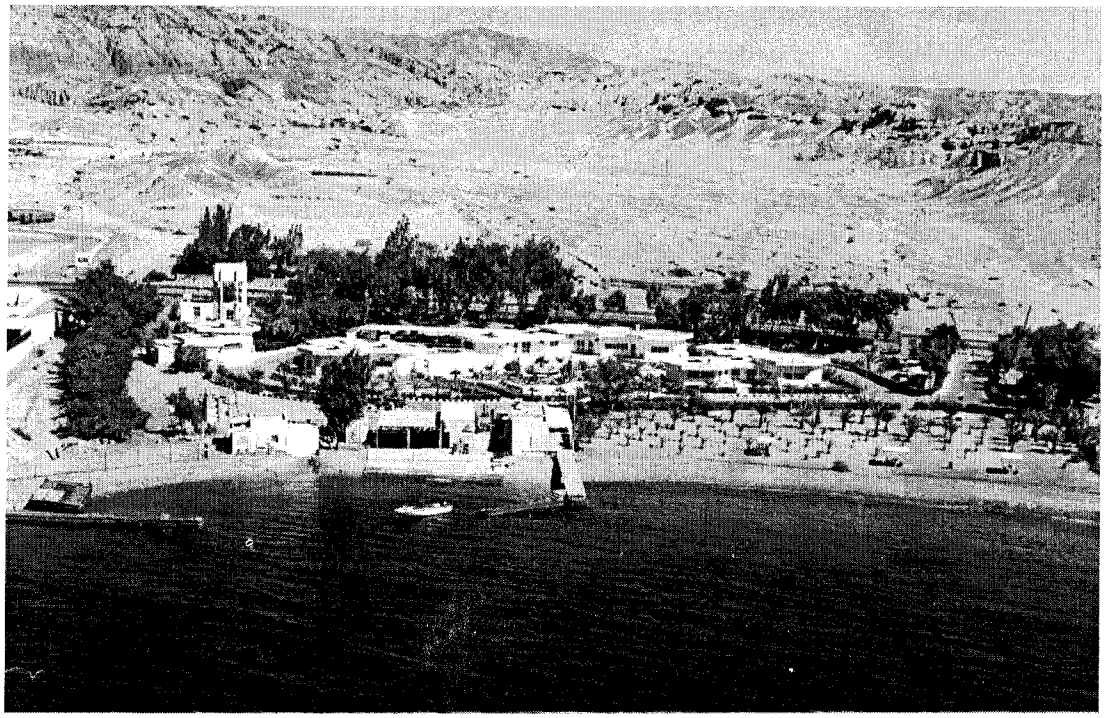

Figure 2.4: Marine Science Station in Aqaba.

2.2.2 Field work's instruments and equipments

All the instruments and equipments which were used during my research in the MSS were provided from the Red Sea Project (RSP I & II), in cooperation between the Center for Tropical Marine Ecology (ZMT) in Bremen-GERMANY and Marine Science Station (MSS) in Aqaba-JORDAN.

All oceanographic equipment necessary for the present investigations were fitted for use on two small vessels, the Boston Whaler (6 m × 2 m) and the Catamaran (8 m × 3 m), both boats are shown in Figure 2.6. The Boston Whaler was equipped with a winch, an electrical generator Model GP 5203 SB, a Global Positioning System (GPS) Model GP-80, a depth finder of the Echo scan series. The Catamaran is equipped with a winch, an electrical generator, and a special frame for fixing the ADCP 150 kHz.

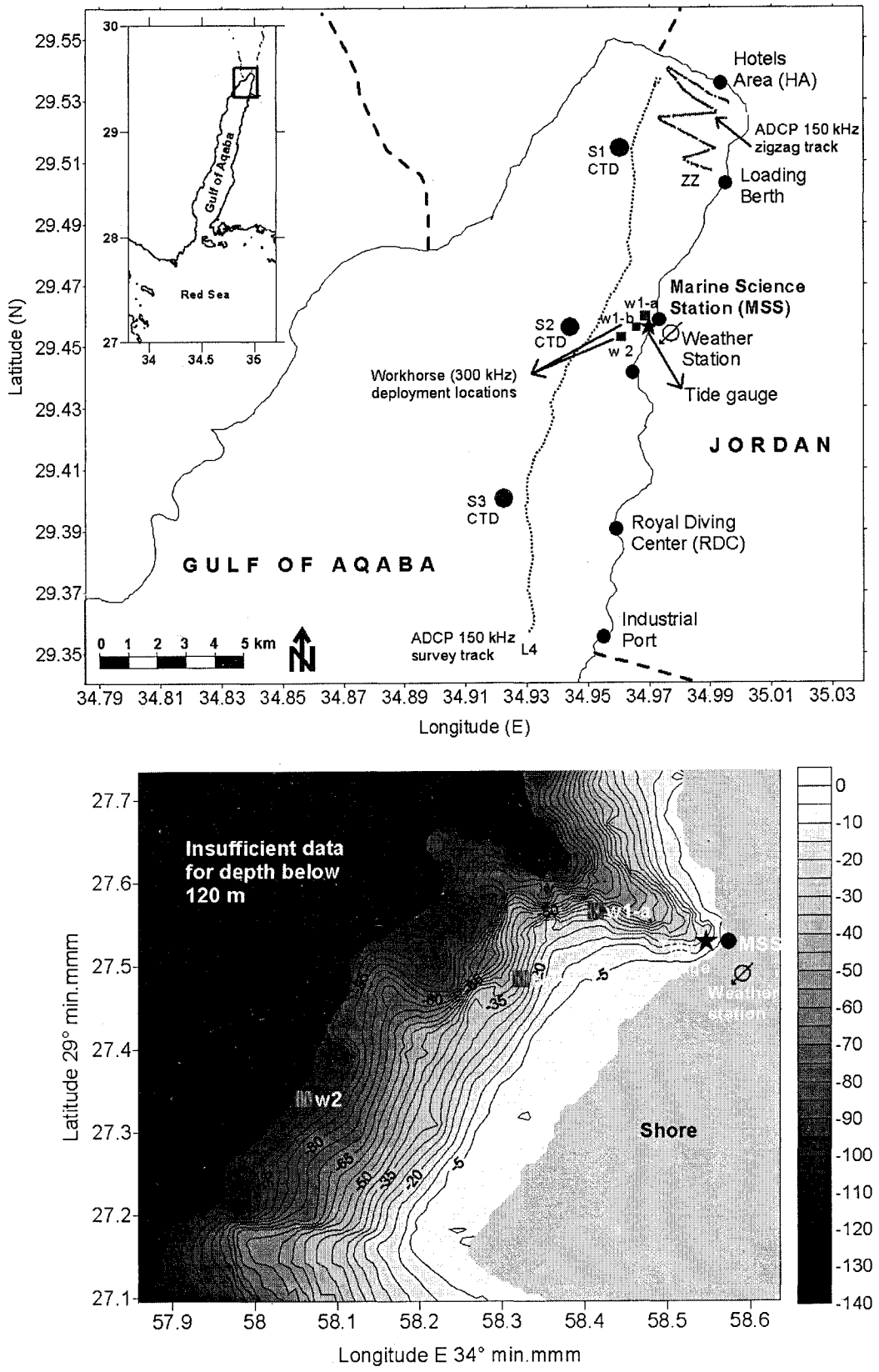

Figure 2.5: Location of the study region and the site locations in the long term observations in the Gulf of Aqaba.

Table 2-2: The station locations of the study region in the Gulf of Aqaba.

Site / Station	Latitude (N)	Longitude (E)	Bottom depth (m)
S1	29° 30.201′	34° 57.876′	430
S2	29° 27.503′	34° 57.225′	570
S3	29° 24.157′	34° 56.559′	640
w1-a	29° 27.563′	34° 58.414′	50
w1-b	29° 27.485′	34° 58.325′	37
w2	29° 27.339′	34° 58.062′	100

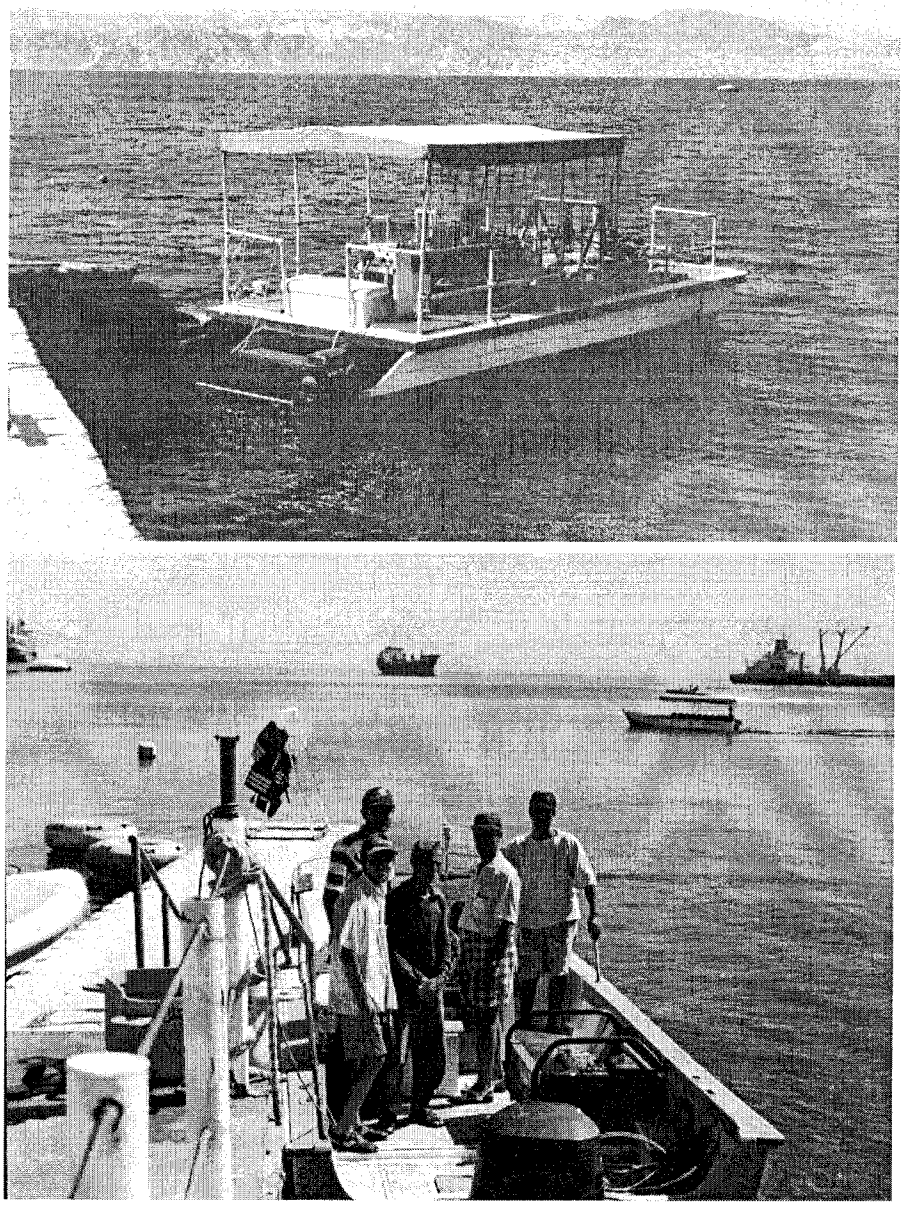

Figure 2.6: Research vessels, the Boston Whaler (lower) and the Catamaran (upper).

The field measurements were performed using the list of the instruments given below:

- Acoustic Doppler Current Profilers (ADCP): Broadband 150 kHz and Workhorse 300 kHz. The 150 kHz ADCP's were fixed on the front of the boats in a vertical position on the water surface. The survey field consisted of longitudinal track parallel to the shoreline and zigzag track in deep-water, using 150 kHz (L4 and ZZ tracks in Figure 2.5). The second ADCP Workhorse (2×300 kHz) were deployed for long time in front of the MSS, Figure 2.7. The ADCP was designed to measure the horizontal and vertical current components at different layers in the water column, the width of this water column depends on the transmitting frequency. The range of the 150 kHz ADCP can reach 250 m for water profiling and 380 m for bottom tracking. The 300 kHz ADCP can measure in a maximum range of 165 m in the water column. The system setup of the ADCPs, which were applied in this work are shown in Table 2-3 and Table 2-4.
- A self contained Conductivity, Temperature and Depth meter (CTD) Model Ocean Sensors OS200 & OS453 (Figure 2.8) was used to measure temperature, salinity and depth (pressure) profiles at the stations S1, S2 and S3, see Figure 2.5. The resolution and precision of the CTD measurements were 0.005 & 0.05 dBars for pressure, 0.0001 & 0.001°C for temperature, and 0.0003 & 0.003 psu for salinity, respectively. The instrument was computer programmed to record temperature, salinity and depth (pressure) measurements continuously every 2 seconds while being lowered at a rate of 1 ms^{-1}.
- Global Positioning System (GPS) was used to determine the latitude and longitude of positions at the sites and the stations. The depth finder of type Echo scan was used to detect the bottom depth for the field work sites, and for providing a fine scale bathymetric chart of the area in front of MSS.
- Weather station (Delta-T) equipped by Dl2e data logger, air temperature sensor, wind direction and speed (cup anemometers and wind vanes), and relative humidity sensor, see Figure 2.9.
- Tide gauge (Hydrotide Recording Tide Gauge), see Figure 2.10. Its resolution is 0.0015% (16 bit conversion accuracy), and storage accuracy is 0.025%.

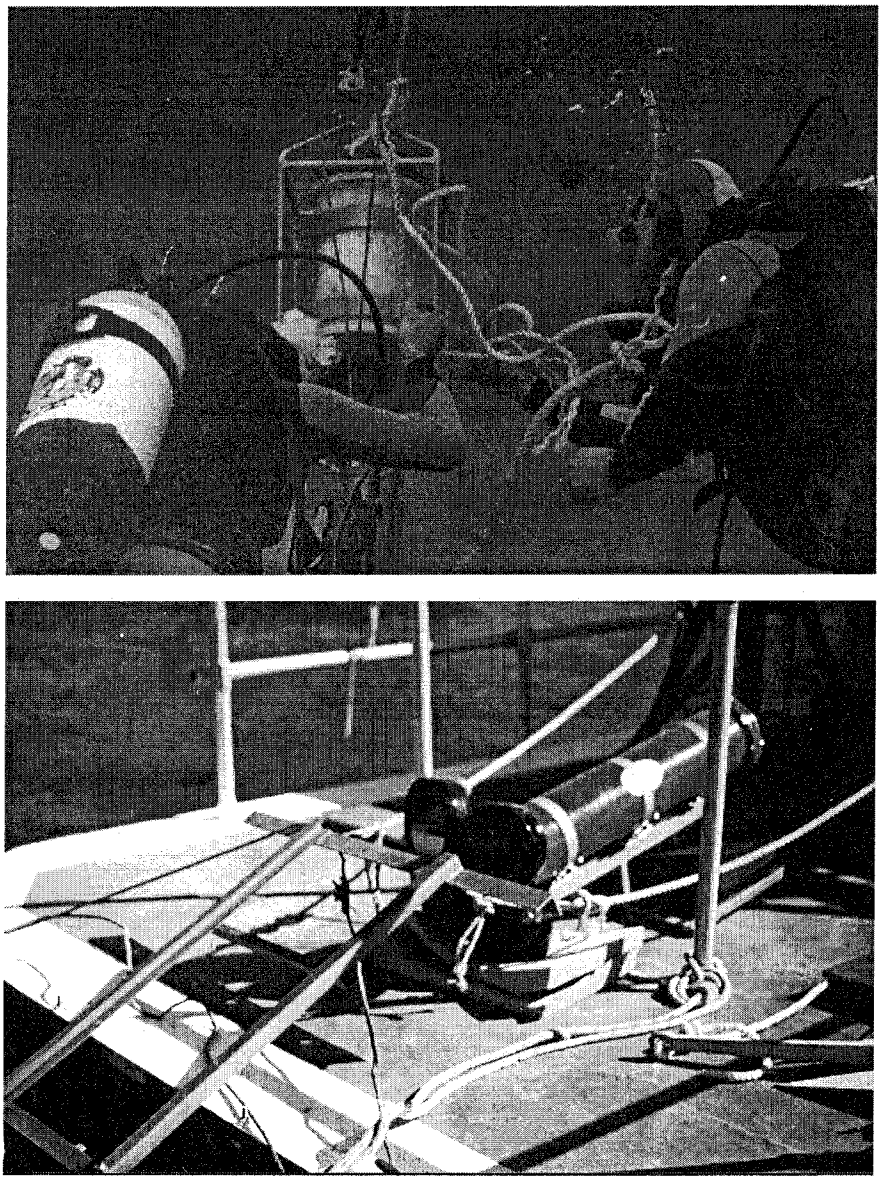

Figure 2.7: Principle of the ADCPs deployment; the Workhorse 300 kHz (upper), and the ADCP 150 kHz (lower).

Table 2-3: The system setup of ADCP 150 kHz.

		ADCP 150 kHz
Water track setup	Pings per ensemble	40
	Depth cell size	6.00 m
	Number of depth cell	40
	Blank after transmit	2.00 m
Bottom track velocity	Pings per ensemble	8
	Maximum tracking depth	370 m
System configuration	Frequency	150 kHz
	Beam angel	20°
Water track prediction	First dept cell	10.64 m
	Last depth cell	244.64 m
	Predicated maximum range	202.94 m
	Minimum ping time	0.94 s
	Velocity standard deviation	0.44 cms^{-1}
Bottom track prediction	Predicated maximum range	364.27 m
	Velocity standard deviation	0.09 cms^{-1}
Data collection predications	Minimum ping time	1.24 s
	Minimum ensemble time	49.12 s
	Time per ensemble	50 s

Table 2-4: The deployment configurations of the workhorse 300 kHz at positions w1-a, w1-b, and w2.

	w1-a	w1-b	w2
Number of depth cells	10	10	20
Depth cell size	4.0 m	2.5 m	4.0 m
Blank after transmit	1.5 m	1.5 m	1.5 m
Pings per ensemble	80	160	80
Time per ping	22.49 s	3.74 s / 15 s	22.49
Time per ensemble	30 min	10 min / 40 min	30 min
Beam angle	20°	20°	20°
Orientation	Down	Up	Down
Transducer depth	18 m	36 m	15 m

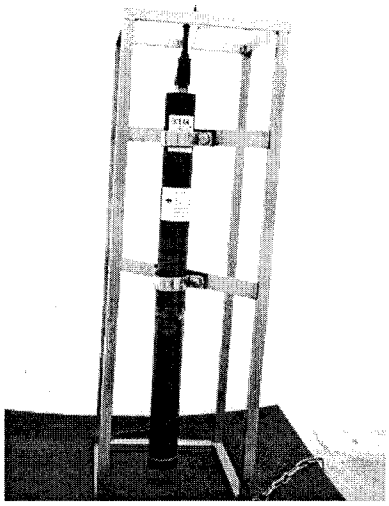

Figure 2.8: Conductivity, temperature and depth meter (OS200).

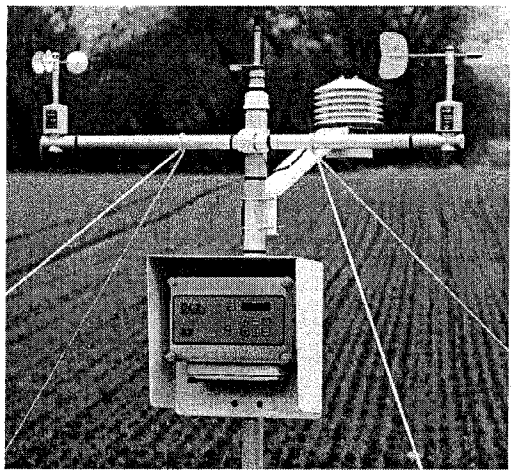

Figure 2.9: Meteorological recorders and sensors for air temperature, wind speed and direction, and relative humidity.

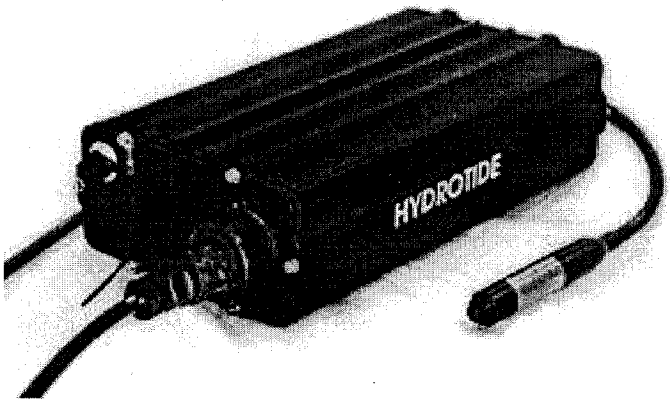

Figure 2.10: Tide gauge (Hydrotide Recording Tide Gauge).

3 Results and discussions

3.1 Bathymetry of the Gulf of Aqaba

The Gulf of Aqaba is characterized by three basins, the northern, central, and southern basin. These basins are separated by sills whose depths exceed the sill depth in the Strait of Tiran (265 m).

The depth measurements in the Gulf of Aqaba were carried out along the sections of the R/V Meteor cruise 44/2 from February 21st to March 7th 1999. A compilation of these data with existing the bathymetric charts of the gulf (DAVID & WALTER 1996; WASSEL & SMITH 1996) is shown in Figure 3.1.

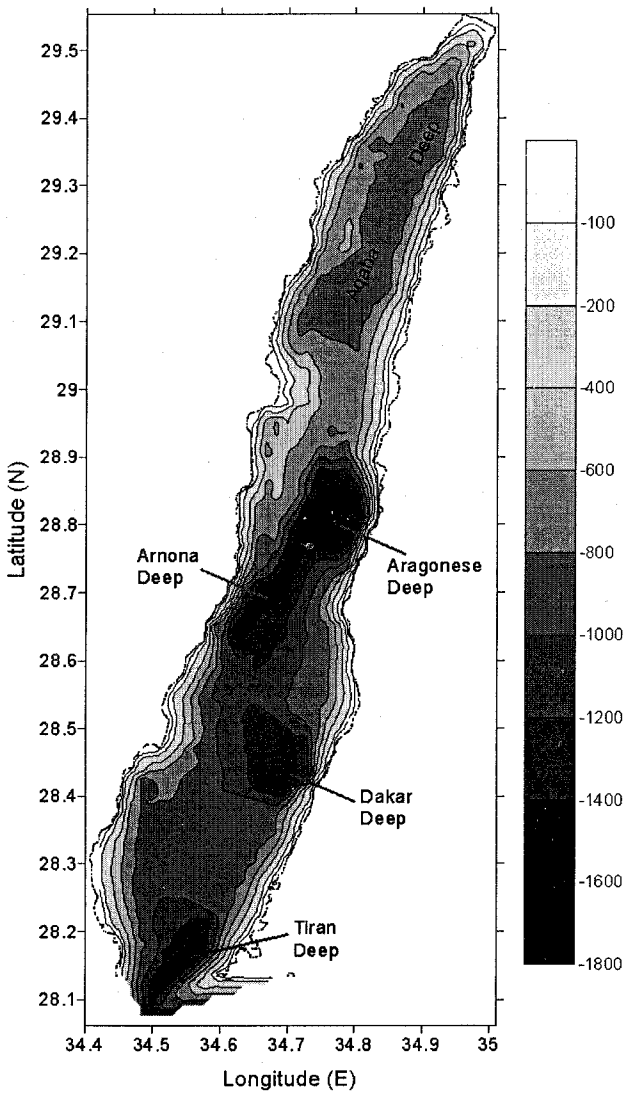

Figure 3.1: Bathymetric chart of the Gulf of Aqaba.

3.2 Meteorology of the Gulf of Aqaba

In order to characterize the meteorologic conditions of the Gulf of Aqaba, we use data from two sources; the Jordanian Meteorological department for the period January 1997 until October 1999, and from a weather station at the MSS from October 1999 to December 2001.

The statistic of meteorological parameters at Aqaba; wind speed (ms^{-1}), wind direction (°), relative humidity (%), and air temperature (°C) is summarized in Table 3-1 from January 1997 to December 2001.

Table 3-1: Monthly Mean value of the meteorological parameters for the whole period from January 1997 to December 2001at Aqaba (W. sp.: wind speed, W. dir.: wind direction, R. hu.: Relative humidity. And Air temp.: Air temperature).

	W. sp. (ms^{-1})			W. dir. (°)	R. hu. (%)			Air Temp. (°C)		
Month	Mean	Min.	Max	Mean	Mean	Min.	Max	Mean	Min.	Max
Jan.	3.24	0.36	9.60	2.79	57.37	23.34	87.27	15.71	8.52	25.50
Feb.	3.93	0.26	10.97	358.59	53.96	22.90	86.52	16.25	9.14	25.90
Mar.	4.09	0.22	10.02	350.72	49.56	18.94	84.25	19.72	12.20	30.13
Apr.	4.44	0.22	10.03	350.90	42.61	13.74	82.71	24.37	14.83	37.10
May.	4.55	0.44	9.83	354.11	40.06	14.14	77.96	28.86	19.35	40.25
Jun.	5.06	0.19	9.33	359.11	39.57	16.63	75.45	31.40	22.98	41.61
Jul.	3.94	0.27	9.89	352.97	40.33	17.70	81.75	33.41	26.01	41.59
Aug.	4.38	0.52	9.83	355.91	50.33	22.59	83.87	32.50	26.67	40.40
Sep.	4.82	0.17	9.72	358.50	52.35	18.78	85.99	30.25	23.72	40.13
Oct.	4.29	0.65	9.96	357.74	54.38	19.37	88.51	26.34	18.07	37.41
Nov.	3.78	0.21	9.28	4.07	54.64	23.85	88.23	22.04	14.88	30.57
Dec.	3.17	0.35	8.88	3.74	59.36	25.12	91.36	16.80	9.69	26.36

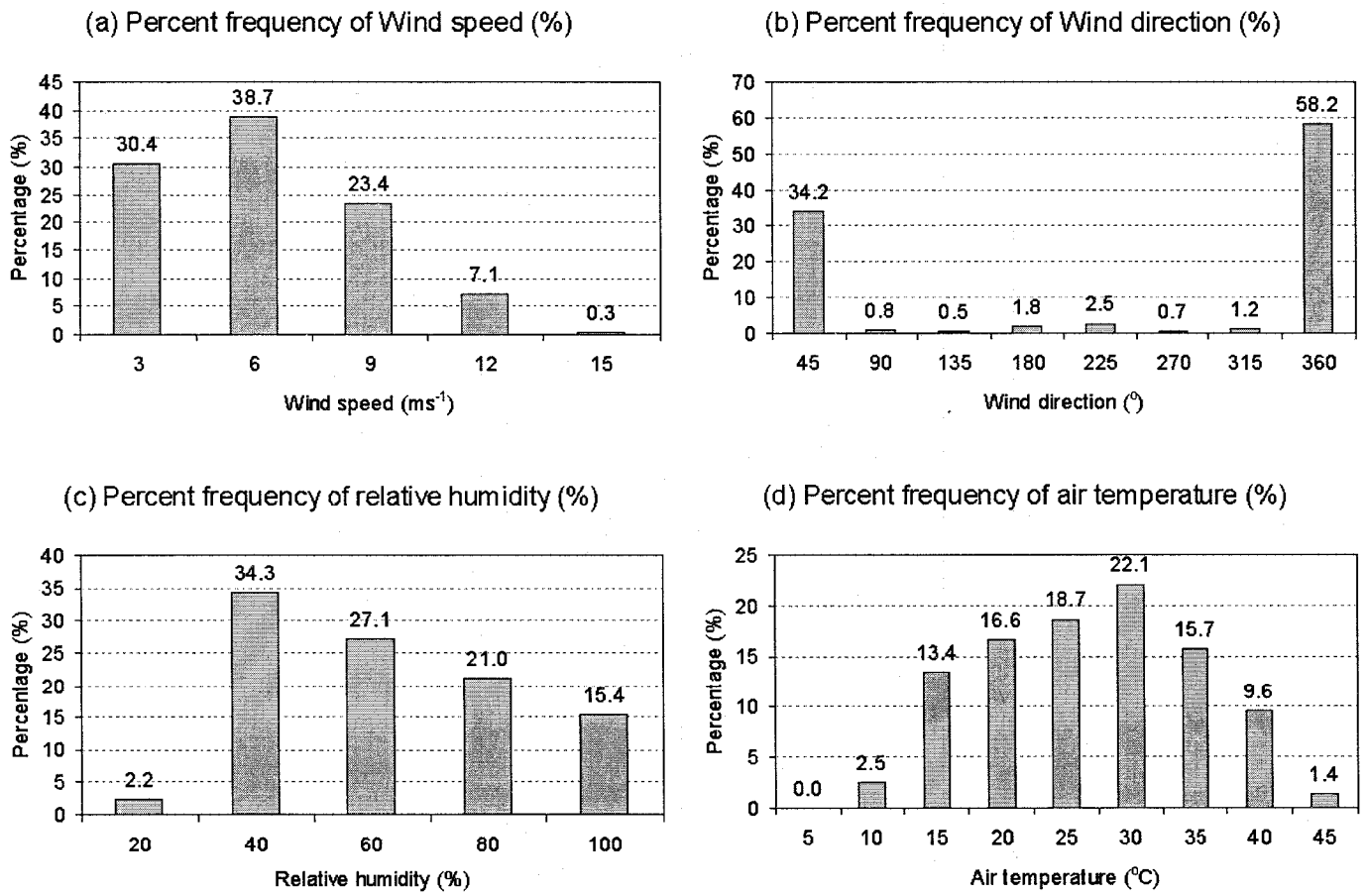

Figure 3.2: Percent frequencies of the wind speed, wind direction, relative humidity, and air temperature (%) through five years 1997-2001 at Aqaba.

Figure 3.2 shows the percent frequency of wind speed, which was 69.1 % for wind speeds below 6 ms^{-1}. This indicates that the wind blowing over Aqaba was relatively calm. The frequency of the wind direction from NNE to NNW was 92.2%. This means that the northern winds dominated as over the northern Red Sea, see section 1.2.2. Occasionally southern winds blew for several hours but are switching again to northern winds. The frequency of those southerly winds was 4.3%. The frequency of relative humidity (%) is inversely distributed to the frequency of the air temperature (°C). This means that the cooler winter temperature is less saturated with water vapor than the warm air temperature during summer. This results in a much greater loss of buoyancy of the surface water during winter than during summer in the Gulf of Aqaba.

The Gulf of Aqaba region is characterized by a calm and dry climate. It is very hot in summer and relatively warm in winter, as shown in, Table 3-1 the mean air temperature during August for the years (1997 – 2001) was 32.50 °C, and during February (1997 – 2001) was 15.71 °C.

In the northern tip of the Gulf of Aqaba the mean wind speed is ~4.2 ms^{-1}. The wind has a clear diurnal peak (24.04 ± 0.85 hr) during summer, see (a) in the power spectra shown in Figure 3.3. During spring and winter seasons, this diurnal peak is not significant. The reason for the diurnal peak is that in summer the wind during nights is weaker than during the day. Spring and winter seasons are relatively calm in comparison to summer.

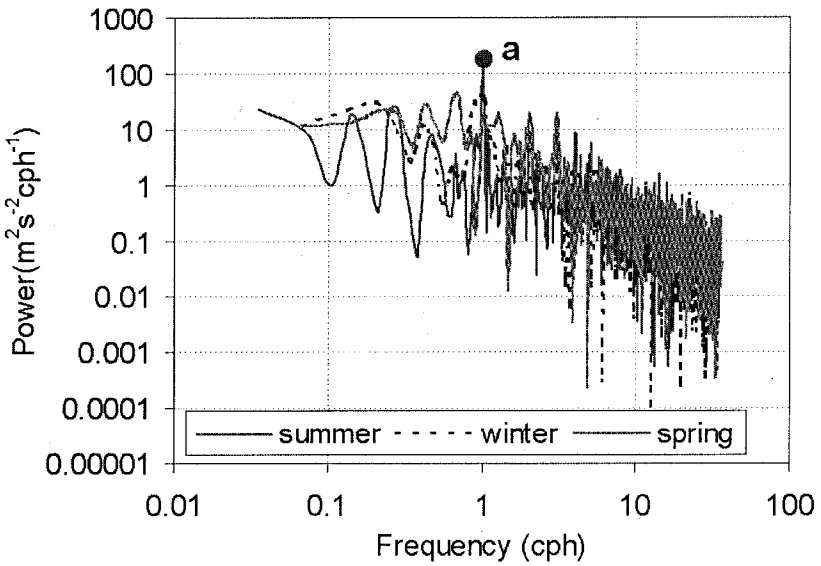

Figure 3.3: Power spectra analysis of the wind in the northern tip of the Gulf of Aqaba.

3.3 Rossby radius, and tide variations of the Gulf of Aqaba

3.3.1 Rossby radius (R_n)

The baroclinic radius is a natural scale in the ocean associated with boundary phenomena such as coastal currents and the geostrophic adjustment to disturbances in the pressure field resulting in fronts and eddies. The first mode baroclinic radius is typically ranging between 10-30 km in the ocean, depending on stratification, depth and latitude.

In a stratified fluid the baroclinic Rossby radius is defined as:

$$R_n = \frac{c_n}{f} \tag{3.1}$$

Where, R_n is Rossby radius (m), c_n (ms^{-1}) is the wave speed of the n^{th} baroclinic mode, f ($rads^{-1}$) is the Coriolis parameter $2\Omega\sin\varphi$, where Ω ($rads^{-1}$) is the angular velocity of the rotation of the earth 7.292×10^{-5} $rads^{-1}$, φ (rad) is the latitude.

The wave speed is the eigenvalue of an eigenvalue problem, defined by a differential equation for the vertical structure of dynamic modes in a flat bottomed stratified ocean, containing the buoyancy frequency $N(z)$, and the corresponding boundary conditions at the sea surface and at the bottom;

$$N^2(z) = -\frac{g}{\rho_o}\frac{\partial \rho_o}{\partial z} \tag{3.2}$$

N^2 (rad^2s^{-2}) is the Brunt Väisälä (or buoyancy) Frequency (BVF), g (ms^{-2}) is the earth gravity, ρ_o (kgm^{-3}) is the density, and z (m) is the depth. As shown in (3.2) the BVF varies with depth depending on the density gradient. High values of N are usually found in the main pycnocline zone, i.e. where the vertical density gradient is strong.

The Rossby radius was calculated for the Gulf of Aqaba based on the R/V Meteor cruise 44/2 CTD measurements at position VI in the southern part of the Gulf of Aqaba, where the wave speeds of the first three modes and corresponding Rossby radii were:

$c_1 = 0.76$ ms^{-1}; $R_1 \approx 10$ km, $c_2 = 0.38$ ms^{-1}; $R_2 \approx 5.5$ km,

$c_3 = 0.25$ ms^{-1}; $R_3 \approx 3.6$ km.

The baroclinic Rossby radius, in agreement with previous citation, was $R = R_1 \approx 10$ km.

The inertia period ($T = \frac{\pi}{\Omega \sin\varphi}$), see e.g. NEUMANN & PIERSON (1966) for the definition, in the Gulf of Aqaba equals 24.7 hr.

3.3.2 Sea level variations and Tides

In order to discuss the sea level variations we use data measured in the northern tip of the Gulf of Aqaba for one year (August 2000-July 2001) referenced to the annual mean value.

The maximum range of the sea level variations during August 2000 to July 2001 was 1.57 m. The highest value of the sea level was 0.82 m observed on March 8th, and the lowest value was -0.75 m recorded on August 29th (Figure 3.4).

The seal level anomalies depict a yearly cycle at the northern tip of the Gulf of Aqaba, see Figure 3.5. The minimum of the sea level anomalies was observed in the summer season with -0.16 m, measured in August. The maximum of the sea level anomaly occurred in the winter-spring seasons. The maximum of 0.19 m was recorded in March. The yearly cycle of the anomalies follows the corresponding sea level variations of the northern Red Sea, see section 1.2.3, Figure 1.7.

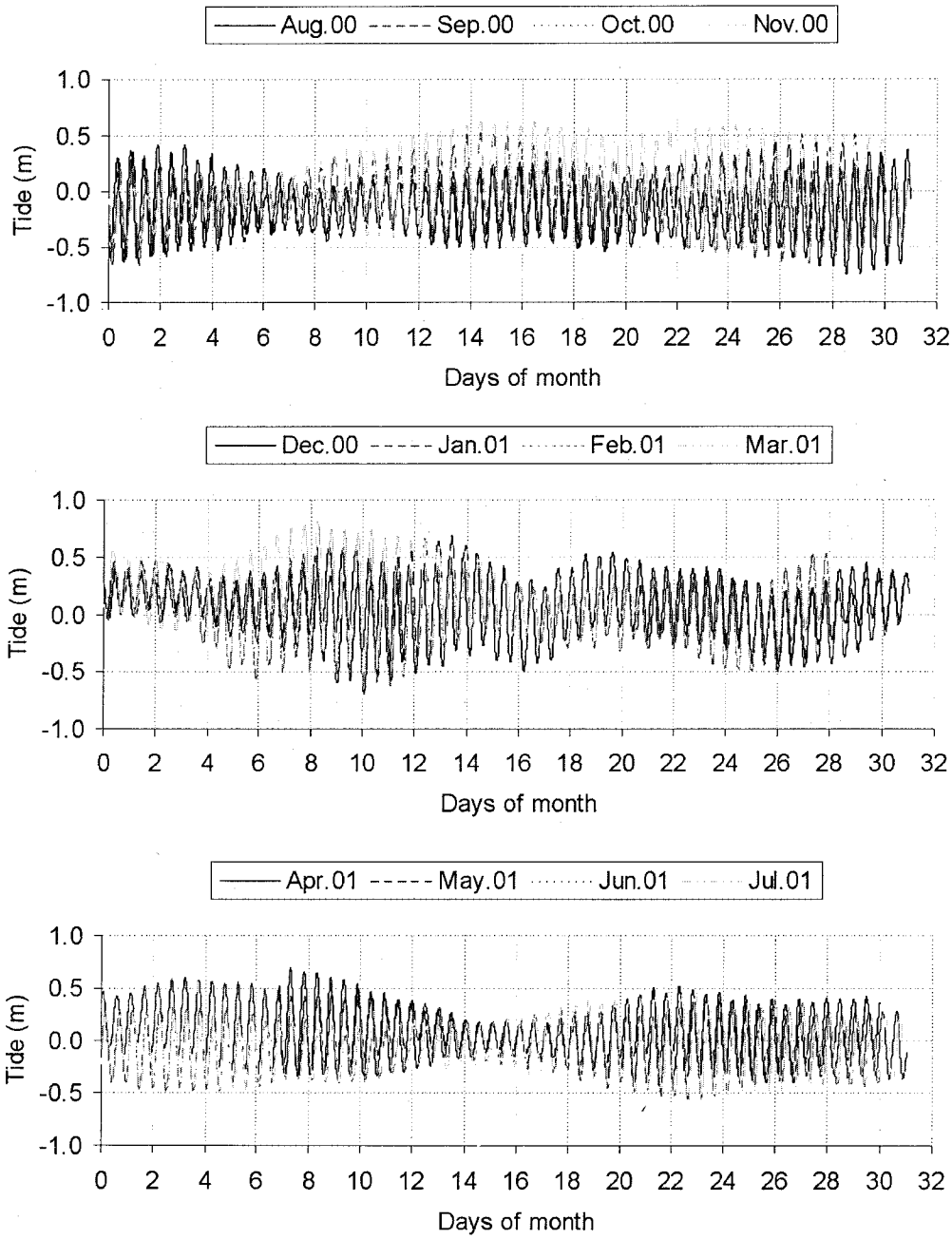

Figure 3.4: Time series records of the tides (m) referenced to the annual mean of the sea level in the northern tip of the Gulf of Aqaba.

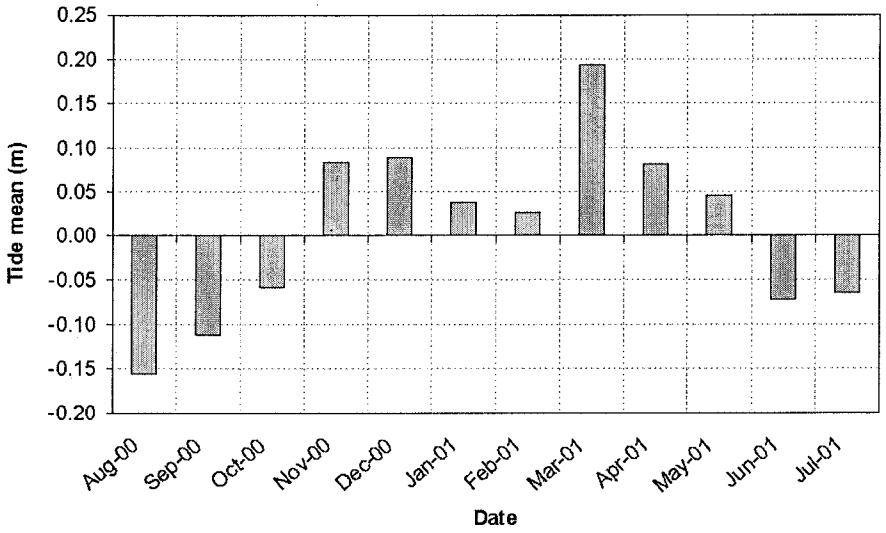

Figure 3.5 Monthly mean sea level anomaly (m) at the northern tip of the Gulf of Aqaba during August 2000 -July 2001.

Besides the yearly cycle of the sea level there are variations with much shorter time scales, forced by the tides of the Red Sea, and seiches of the Red Sea and the Gulf of Aqaba itself. A spectrum analysis of the sea level records in the northern tip of the gulf has been done to determine and evaluate the partial tides and the seiches with their corresponding periods.

Figure 3.6 shows the spectrum of the sea level in the northern Gulf of Aqaba. Four distinguished peaks (a, b, c, and d) were detected. The corresponding periods are:

$T_a = 12.39$ hr $\pm$ 0.22 hr, $T_b = 23.72$ hr $\pm$ 0.82 hr,

$T_c = 1.05$ hr $\pm$ 0.0016 hr, and $T_d = 8.03$ hr $\pm$ 0.094 hr.

Here T_a and T_b represent the semidiurnal and diurnal barotropic tides, respectively. Based on the principle harmonic components and their basic values in Table 3-2 (DEFANT 1961), the semidiurnal signal ($T_a = 12.39$ hr $\pm$ 0.22 hr) might be constituted of the principle lunar (M_2; 12.42 hr), the smaller lunar evectional (λ_2; 12.22 hr), and the smaller lunar elliptic (L_2; 12.19 hr) harmonic component. The diurnal signal ($T_b = 23.72$ hr $\pm$ 0.82 hr) might comprise the luni-solar diurnal (K_1; 23.93 hr), the principal lunar diurnal (P_1; 24.07 hr), and the small lunar elliptic (J_1; 23.10 hr) harmonic component. The short period c (1.05 hr) and the other period d (8.03 hr) are related to the standing waves or so-called seiches that are generated in the Gulf of Aqaba and the Red Sea, respectively. The reason for these seiches is that progressive barotropic waves traveling along the basin are reflected at the far ends and then the two sets of waves traveling in opposite directions can interfere with each other resulting in a standing wave with the resonance period of the basin. Owing to the fast propagation, $C = \sqrt{gH}$, the effect of the inertial frequency can be ignored. Then the period of oscillation (T) of the seiches is given by:

$$T_n = \frac{2L}{nC} = \frac{2L}{n\sqrt{gH}}$$, which is known as Merian's formula (3.3)

Where L is the length of the water body, C is the long wave speed, g is the earth gravity, H is the mean depth of the water body, and n is a positive integer (POND, S., and G. L. PICKARD 1983).

Equation (3.3) was derived for a long water body of uniform width and depth. The problem of seiches in natural formed basins has been the subject of thorough theoretical investigation. The theory apply for long basins, where the horizontal motion perpendicular to the line, which connects the deepest points of the bottom, ("Talweg"), can be ignored, i.e. the water moves only parallel along the Talweg (DEFANT 1961; and NEUMANN & PIERSON 1966).

The fundamental periods of the seiches in both the Gulf of Aqaba and Red Sea have been calculated using Merians formula based on the mean depth H, and the length of the Talweg, L. Due to the complex bathymetry of both the Gulf of Aqaba and the Red Sea we can expect only approximated results.

For the Gulf of Aqaba we take L = 180 km, g = 9.81 ms^{-2}, H = 800 m, and n = 1; and for the Red Sea we use L = 1250 km, g = 9.81 ms^{-2}, H = 700 m, and n = 1. Then the fundamental periods of the first mode seiche are T (Aqaba) = 1.13 hr and T (Red Sea) = 8.38 hr, which agree well with the observed values of T_c (1.05 hr) and T_d (8.03 hr), see Figure 3.6.

In spite the rough approximation in equation (3.3), the results are very close to the observations. Note that, the discrepancy between L (1250 km) and the real length (~1930 km) might be due to the complex topography of the Red Sea. For basins of variable depth and width, the eigenvalue problem should be solved numerically, which is beyond the scope of this work.

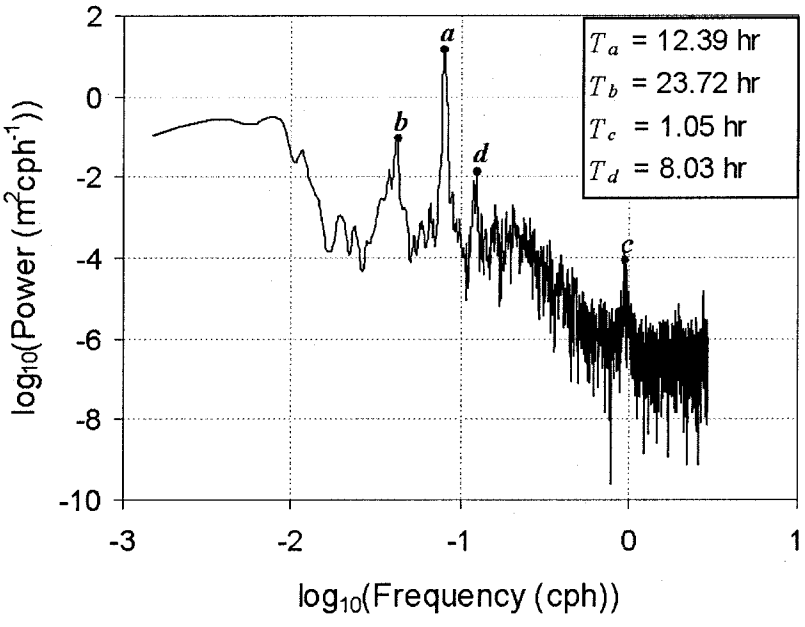

Figure 3.6: Power spectrum of the sea level in the northern tip of the Gulf of Aqaba.

Table 3-2: Principal harmonic components according to DEFANT (1961).

Name of partial tides	Symbol	cos sin	Argument	Speed per mean solar hour	Period in solar hours	Coefficient ratio M_2 : 100
Semi-diurnal components						
Principal lunar	M_2	cos	255·55	28·98410°	12·42	100·0
Principal solar	S_2	cos	273·55	30·00000	12·00	46·6
Larger lunar elliptic	N_2	cos	245·65	28·43973	12·66	19·2
Luni-solar semi-diurnal	K_2	cos	275·55	30·08214	11·97	12·7
Larger solar elliptic	T_2	cos	272·55	29·95893	12·01	2·7
Smaller lunar elliptic	L_2	cos	265·45	29·52848	12·19	2·8
Lunarelliptic second order	$2N_2$	cos	235·75	27·89535	12·91	2·5
Larger lunar evectional	ν_2	cos	247·45	28·51258	12·63	3·6
Smaller lunar evectional	λ_2	cos	263·65	29·45563	12·22	0·7
Variational	μ_2	cos	237·55	27·96821	12·87	3·1
Diurnal components						
Luni-solar diurnal	K_1	sin	165·55	15·04107°	23·93	58·4
Principal lunar diurnal	O_1	sin	145·55	13·94304	25 82	41·5
Principal solar diurnal	P_1	sin	163·55	14·95893	24·07	19·4
Larger lunar elliptic	Q_1	sin	135·65	13·39866	26·87	7·9
Smaller lunar elliptic	M_1	sin	155·65	14·49205	24·84	3·3
Small lunar elliptic	J_1	sin	175·45	15·58544	23·10	3·3
Long-period components						
Lunar fortnightly	Mf	cos	075·55	1·09803°	327·86	17·2 8·6
Lunar monthly	Mm	cos	065·45	0·54437	661·30	9·1 4·6
Solar semi-annual	Ssa	cos	057·55	0·08214	2191·43	8·0 4·0

3.4 Results of the large scale investigation

3.4.1 Water masses and stratifications

3.4.1.1 Spatial distribution of the potential temperature (θ), salinity (S), and density (σ_θ)

Short term investigation of the temperature and salinity during the phase of weak stratification in the Gulf of Aqaba was done during R/V Meteor cruise 44/2 in the Gulf of Aqaba and the northern Red Sea for the period from February 21st to March 7th 1999 at the stations shown in Figure 2.2 and Figure 2.3. The distribution of the (a) potential temperature θ (°C), (b) salinity S (psu), and (c) density σ_θ (kgm^{-3}) are shown on sections along the stations I-X of the Gulf of Aqaba and the northern Red Sea. In Figure 3.7 (a), the θ variation with depth in the Gulf of Aqaba was different to that in the northern Red Sea. The surface water in the northern Red Sea, with temperatures between 21.50-23.47 °C and in salinities between 40.0 and 40.3, was separated from the intermediate water of about 21.5 °C with 40.50 and the bottom water with about 21.3 °C and 40.53 by a thermocline centered at about 100 m depth. The temperature of the surface water of the Red Sea was decreasing gradually from south to north (from station X to I) whereas salinity was increasing. In the Gulf of Aqaba, generally well mixed water was found in the upper 300 m depth, extending slightly deeper than the sill depth of the Strait of Tiran. A weak thermocline between 350-500 m separated the homogeneous deep-water of the Gulf of Aqaba with a potential temperature of about θ ~20.5 °C and a salinity of 40.67 from the surface water. The deep-water of the Gulf of Aqaba, separated from the Red Sea by the sill of the Strait of Tiran, was cooler and saltier than the deep-water body observed in the Red Sea. The surface water of the Gulf of Aqaba, ranging in temperature between 22.0 and 21.30 °C and in salinity between 40.30 and 40.70 from south to north, was cooler and more saline than the surface water of the northern Red Sea. Both

surface water masses are separated by a front slightly north of the Strait of Tiran. We call this " Strait of Tiran front". The surface water in the Gulf of Aqaba just north of the Strait of Tiran front had the same θ-S characteristic as both the intermediate and the deep-water in the northern Red Sea. This suggests that the Gulf of Aqaba is an important source for the deep-water formation of the Red Sea. The surface water S (~40.70) in the northern Gulf of Aqaba was higher than the bottom water S (~40.55) in the northern Red Sea. This indicates that the northern part of the Gulf of Aqaba is the preferred location for the deep-water formation of the gulf. Table 3-3 summarizes the minimum and maximum θ (°C), S (psu), and σ_θ (kgm^{-3}) values at the sea surface at the stations (I-X).

A cross section of CTD casts in the northern tip of the Gulf of Aqaba about 8 km southward station I was done on March 6th 1999 during R/V Meteor cruise 44/2 at five stations (s1, s2, s3, s4, and s5) distributed on the latitude line 29.41° N between the east and west coasts. Figure 3.8 (a) shows the distribution of the θ on the cross section in the northern part of the Gulf of Aqaba. The well mixed surface water was separated from the deep-water by a pycnocline in about 450 m depth. Weak horizontal and vertical gradients were observed. The differences of θ were 0.37 °C horizontally and 0.63 °C vertically. The difference of S was 0.05 vertically and horizontally, see Figure 3.8 (b). This indicates that the water mass in the northern part of the Gulf of Aqaba was rather homogenous during the period of February 21st to March 7th 1999. The σ_θ in Figure 3.8 (c) shows a value range between 28.75-28.91 kgm^{-3}. The pattern observed in θ and σ_θ in the pycnocline suggests upwelling at the eastern coast and downwelling at the western coast. Such a pattern would in general be associated with a southward directed geostrophic circulation trapped at the shores. Moreover, Figure 3.8 (c) shows in the eastern part a downward shape of the density, σ_θ, in the upper 300 m and the upward bent shape near 500 m depth. This suggests a northward current in upper 300 m, and a southward counter current below the surface current. This is consistent with the directly observed current patterns, Figure 3.28, as deep as the ADCP ranges.

3.4.1.2 Water masses properties

Water masses can be classified on the basis on their θ-S characteristics depicted in a θ-S diagram, which was introduced by Helland-Hansen (1916).

All the CTD casts taken during the R/V Meteor cruise 44/2 in the Gulf of Aqaba and the northern Red Sea were plotted in the θ-S diagram shown in Figure 3.9.

The water masses of the Gulf of Aqaba were more saline and colder than the water masses in the northern Red Sea, as shown in Figure 3.9. The deep-water in the Red Sea had the same characteristics as the surface water in the upper 450 m in the Gulf of Aqaba with respect to θ and S. This indicates that the upper and intermediate water layers of the Gulf of Aqaba contribute to the deep-water formation of the northern Red Sea due to the strong cooling and evaporation in the Gulf of Aqaba during February and March. The deep-water of the Gulf of Aqaba below 450 m depth is separated from the water of the Red Sea by the sill of the Strait of Tiran. This water mass seems to be rather passive and plays no specific role in the water mass formation of the northern Red Sea.

Table 3-3: Minimum and maximum values of the sea surface θ (°C), S (psu), and σ_θ (kgm^{-3}) for the positions (I – X) in the Gulf of Aqaba and the northern Red Sea from February 21st to March 7^{tt} 1999 during R/V Meteor cruise 44/2.

	θ (°C)		S (psu)		σ_θ (kgm^{-3})	
Station	Min.	Max.	Min.	Max.	Min.	Max.
I	21.269	21.481	40.648	40.675	28.669	28.763
II	21.393	21.487	40.651	40.691	28.686	28.709
III	21.374	21.519	40.526	40.659	28.573	28.681
IV	21.277	21.620	40.540	40.574	28.545	28.666
V	21.440	21.680	40.458	40.544	28.492	28.583
VI	21.497	22.306	40.175	40.420	28.182	28.443
VII	22.726	23.116	40.144	40.236	27.808	27.993
VIII	22.186	23.208	40.144	40.282	27.781	28.172
IX	22.981	23.202	40.011	40.188	27.805	27.172
X	23.452	23.486	40.013	40.030	27.604	27.622

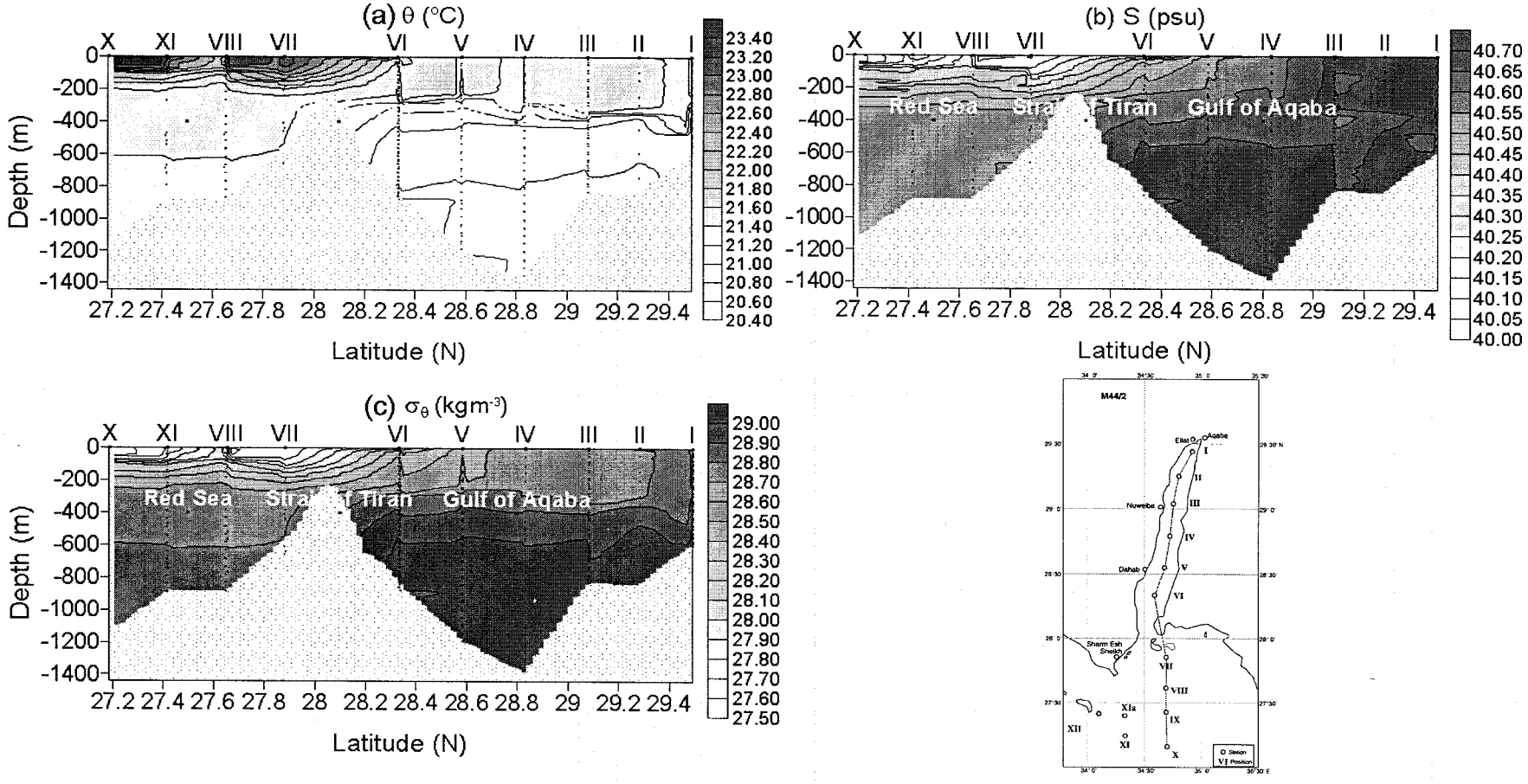

Figure 3.7: Long section distribution of the θ (°C), S (psu) and σ_θ (kgm^{-3}) in the Gulf of Aqaba and the northern Red Sea from February 21st to March 7th 1999, R/V Meteor cruise 44/2.

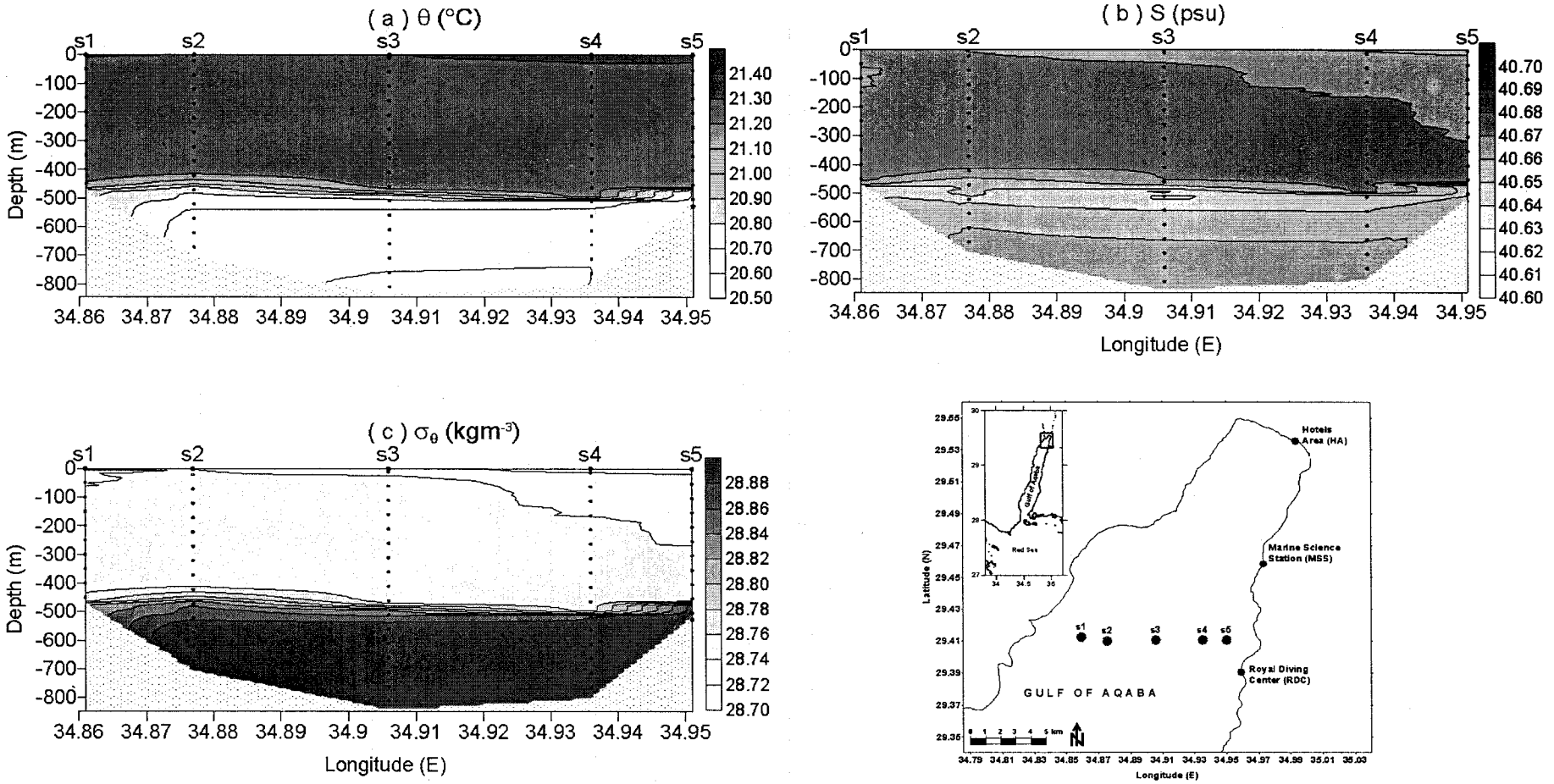

Figure 3.8: Cross section distribution of the θ (°C), S (psu) and σ_θ (kgm^{-3}) in the northern Gulf of Aqaba on March 6th 1999, R/V Meteor cruise 44/2.

3.4.2 Thermohaline and vertical convection

Several convection events could be detected both during R/V Meteor cruise 44/2 and at the reference station S2 (Figure 3.7, Figure 3.8, and Figure 3.35) in the northernmost part of the Gulf of Aqaba. A well mixed water was recorded down to the maximum depth of the measurements at Station S2 (~400 m) during the spring period February-April. This is an indication of strong convection which is forced by winds, high evaporation, and cooling resulting in a loss of buoyancy at the sea surface during winter and spring seasons. The increase in the density of the surface water causes the surface water to sink and to mix with the underlying water until the density of the deeper layers is greater than the density in the surface mixed layer.

It is known from many studies that vertical convection occurs in convection cells with a characteristic diameter of about 100 m. Due to their small horizontal scale these cells are also denoted as chimneys. In areas of active convection many neighbored convection cells are found. The density of the surface mixed layer is greater within the convection area compared to the surrounding surface water. The resulting baroclinic pressure gradient combined with a depression of the sea surface in the convection area forms after geostrophic adjustment a cyclonic gyre (KILLWORTH 1976; VISBECK et al. 1996; and STRANEO & KAWASE 1999).

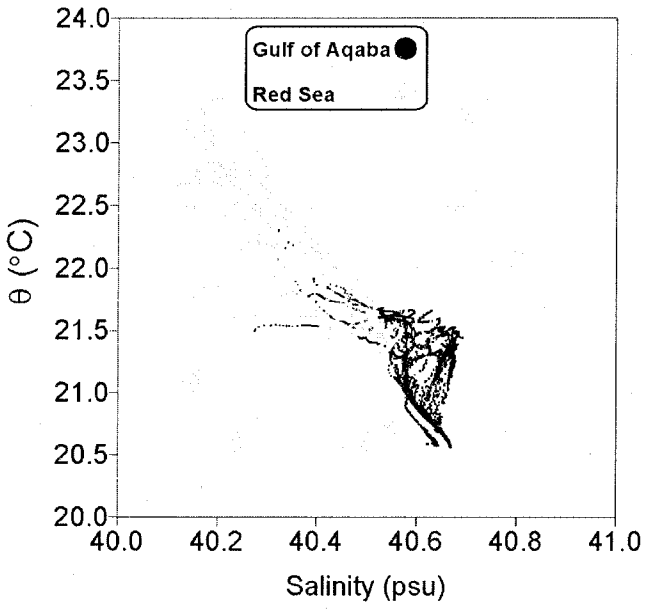

Figure 3.9: θ-S diagram in the Gulf of Aqaba and the northern Red Sea during the R/V Meteor cruise 44/2, during February 21st-March 7th 1999.

An intensive convection event in the northern Gulf of Aqaba was observed on February 26th at position I during R/V Meteor cruise 44/2 (for the location see Figure 2.2). The potential temperature profile shows a mixed surface layer down to 520 m depth, while four days before, on February 22nd, the mixed layer reached 250 m depth only, see Figure 3.10 (a). During these four days, the air temperature did not cool the surface water remarkably and the wind blew quite steady from northern direction. On the other hand, it might be that the constant loss of buoyancy of the surface water due to the winter cooling cause the density of the surface water to pass a critical threshold after which vertical convection occurs. Besides the large deepening by vertical convection, a large variability in the vertical extension of the thermocline was observed on shorter

time scales, probably associated with internal waves. In Figure 3.10 (b), the θ profile taken at the afternoon on March 1st the thermocline descended from 370 m to 470 m during the following night.

The θ-S values at station I between 360 and 390 m at night on March 1st 1999 occurred between 460 and 480 m at afternoon of the same day. Thus, the two profiles at the same station show water of similar characteristic at different depths after about 12 hours, see Figure 3.11.

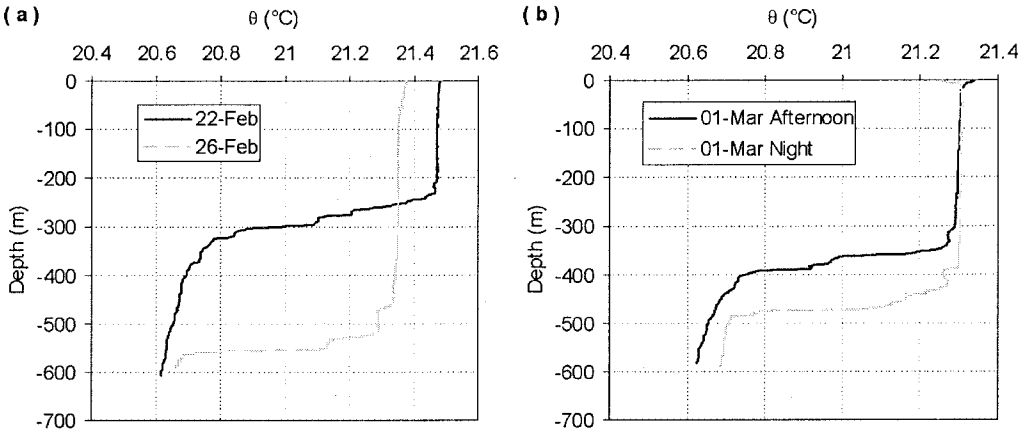

Figure 3.10: θ (°C) profiles measured in the northern Gulf of Aqaba at station I during R/V Meteor cruise 44/2 (a) on February 22nd and 26th, and (b) at afternoon, and night time of March 1st.

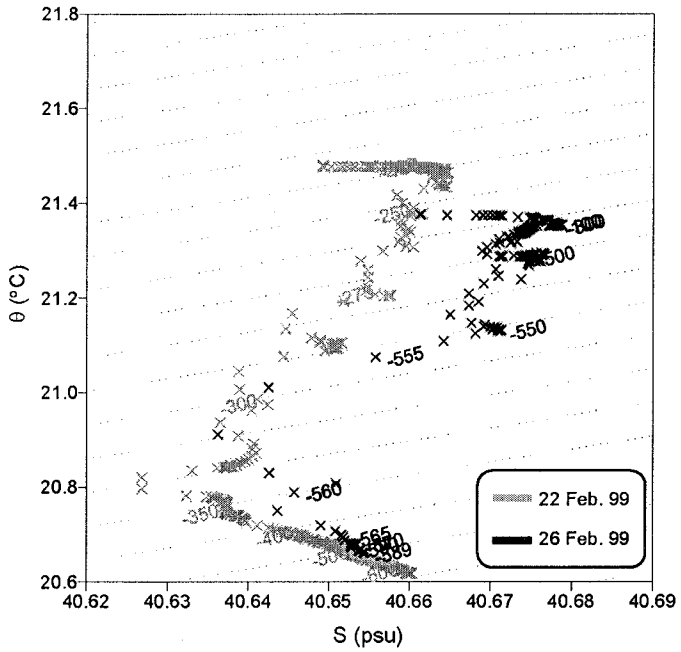

Figure 3.11: θ-S diagram at station I on March 1st 1999 at 04:40 (night) and 16:45 (afternoon), the gray and black numbers refer to the depths at night and afternoon profiles, respectively. R/V Meteor cruise 44/2.

3.4.3 Relative geostrophic velocity (*Vrel*) calculations

An indirect method to estimate the water movement using the T and S data at hydrographic stations is to calculate the geopotential anomaly at each station and to calculate the relative geostrophic velocity (Vrel). These calculations were done for the section in the Gulf of Aqaba along the stations I, II, III, IV, V, and VI on R/V Meteor cruise 44/2 to reveal the currents in the Gulf of Aqaba independent from the relatively strong ageostrophic currents, such as tidal currents. The distribution of the geostrophic velocity component normal to the section referenced to 600 m depth, Vrel, is shown along the section together with the corresponding T and S distribution on different dates February 21st-22nd, 22nd-23rd, 25th-26th, and March 6th-7th 1999, in Figure 3.12, Figure 3.13, Figure 3.14, and Figure 3.15, respectively. A negative sign means Vrel is directed to the east, while a positive signs means Vrel is directed to the west. Both directions are relative to the axis of the gulf, which deviates 18° clockwise form the northern geographical axis.

The stratification is characterized by a depression of the thermocline, obviously forced by vertical convection, at about 300 m depth between station V and II at 22nd February. This depression remains until 23rd February. The northern edge of this depression is moving northward and disappears after 25th February. The resulting pattern of geostrophic currents, shown in Figure 3.12, and Figure 3.13, is an anti-cyclonic one with an eastward current in the northern part of the gulf and westward current in the central part. An eastward geostrophic current occurs also at the Strait of Tiran front in the southern part of the gulf as well. The Vrel distribution ranges between -4.5 to 15.3 cms^{-1} in the water column between 0-600 m.

The eastward current in the northern part disappears after 26th February but the eastward current at the Strait of Tiran front remains, see Figure 3.14, and Figure 3.15. Generally the geostrophic currents vary between -4.6 to 11.9 cms^{-1} at this time.

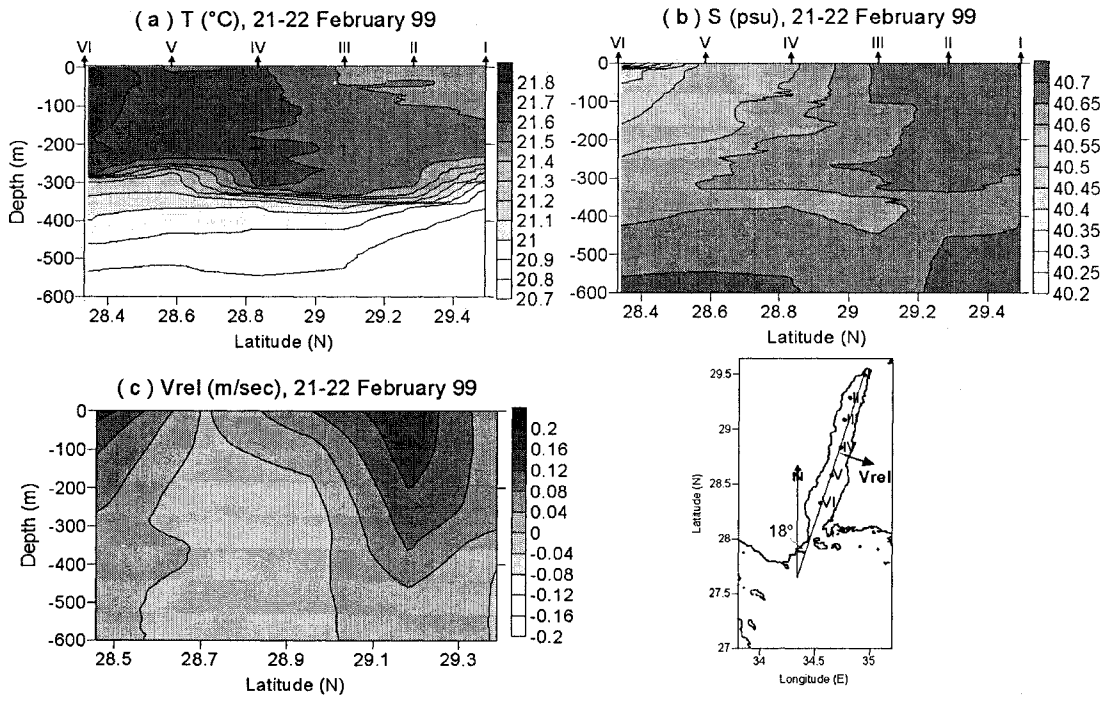

Figure 3.12: Distribution of (a) T (°C), (b) S (psu), and (c) relative geostrophic velocity (Vrel) (ms^{-1}) referenced to 600 m in the Gulf of Aqaba during February 21st-22nd 1999, R/V Meteor cruise 44/2.

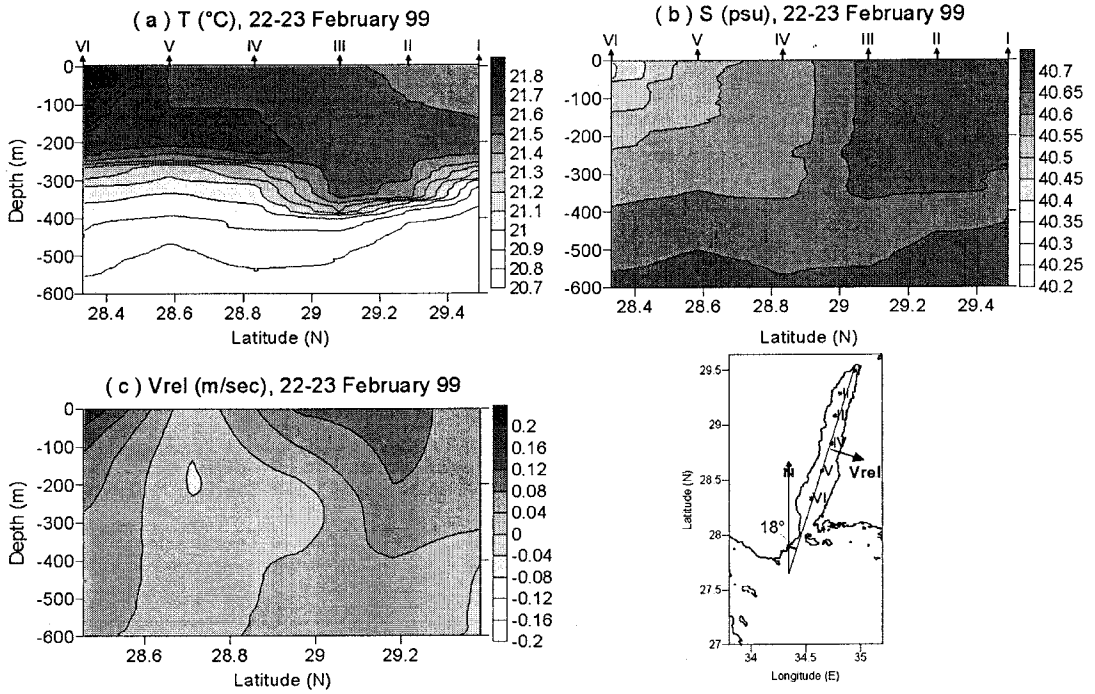

Figure 3.13: Distribution of (a) T (°C), (b) S (psu), and (c) relative geostrophic velocity (Vrel) (ms^{-1}) referenced to 600 m in the Gulf of Aqaba during February 22nd-23rd 1999, R/V Meteor cruise 44/2.

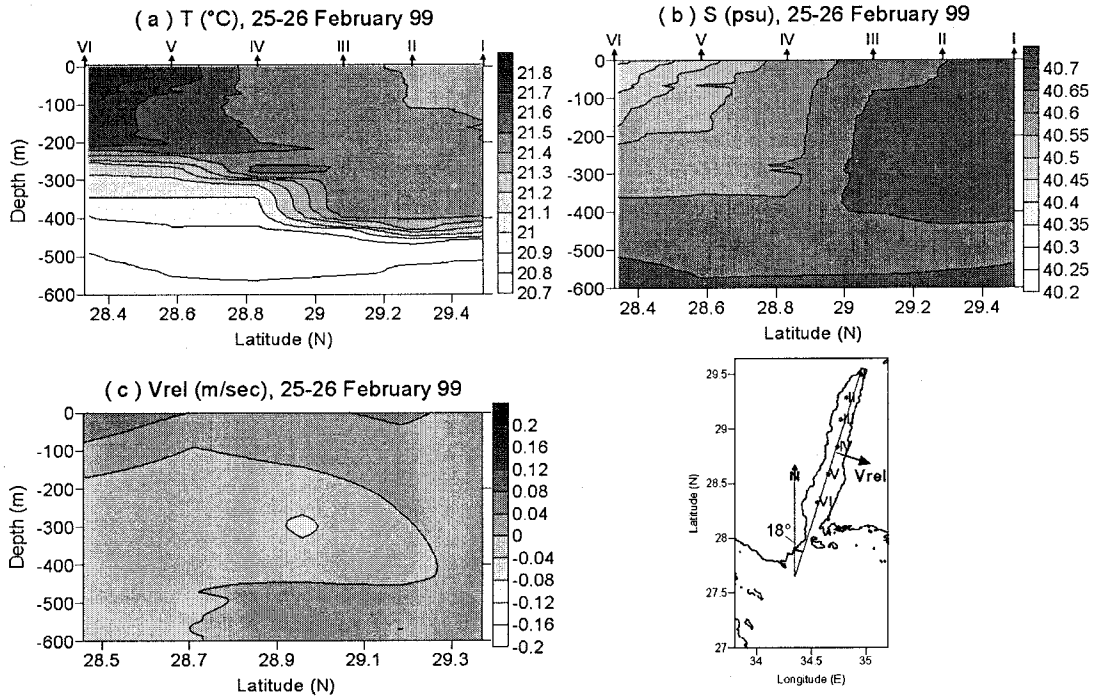

Figure 3.14: Distribution of (a) T (°C), (b) S (psu), and (c) relative geostrophic velocity (Vrel) (ms^{-1}) referenced to 600 m in the Gulf of Aqaba during February 25th-26th 1999, R/V Meteor cruise 44/2.

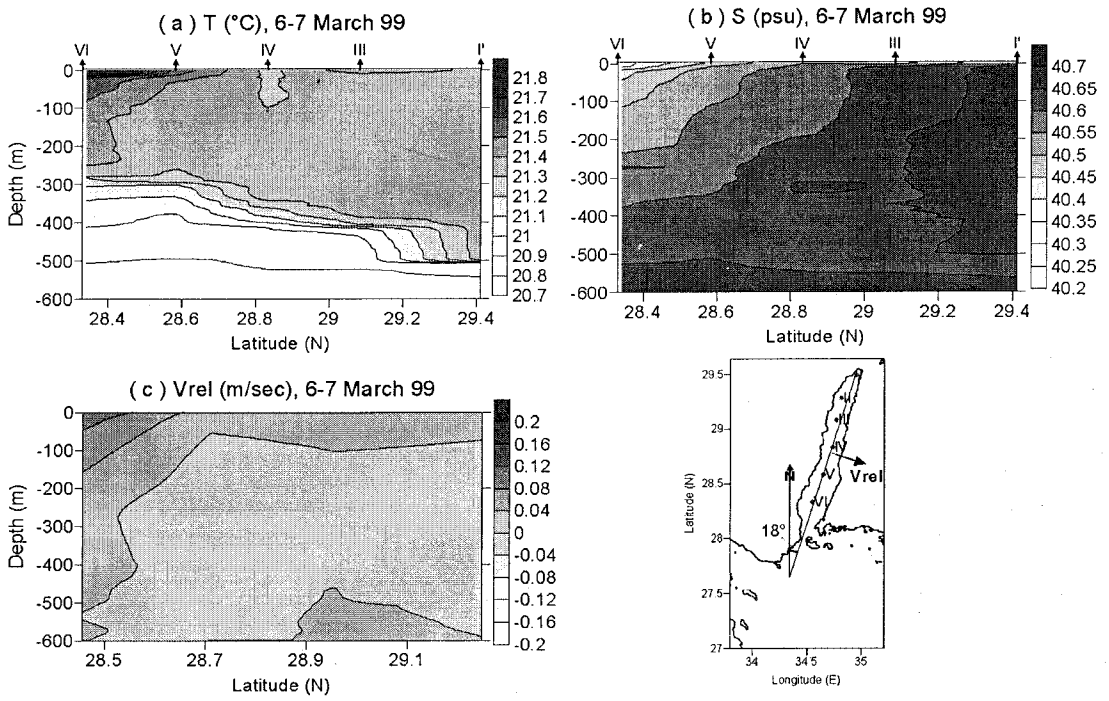

Figure 3.15: Distribution of (a) T (°C), (b) S (psu), and (c) relative geostrophic velocity (Vrel) (ms^{-1}) referenced to 600 m in the Gulf of Aqaba during March 6^{th}-7^{th} 1999, R/V Meteor cruise 44/2.

The minimum and maximum values of geostrophic current, Vrel, in the upper 600 m depth between all stations are summarized in Table 3-4.

Table 3-4: Minimum and maximum values of the relative geostrophic velocity (Vrel) (cms^{-1}) in the upper 600 m depth along the stations from I to VI during R/V Meteor cruise 44/2.

	Relative geostrophic velocity (Vrel) (cms^{-1})												
	21-22 Feb. 1999			22-23 Feb. 1999			25-26 Feb. 1999			6-7 Mar. 1999			
Stn.	Min.	Max.	Std.	Min.	Max.	Std.	Min.	Max.	Std.	Stn.	Min.	Max.	Std.
I-II	-0.3	6.1	2.67	-0.2	6.7	2.89	0.0	3.0	0.86	--	--	--	--
II-III	0.0	15.6	4.90	0.0	10.2	3.41	-1.2	4.6	1.62	I'-III*	-3.4	1.2	1.32
III-IV	-2.4	8.2	2.58	-2.8	8.6	2.86	-4.6	3.5	2.13	III-IV	-1.9	1.2	0.88
IV-V	-3.7	0.0	1.18	-4.4	0.0	1.44	-2.4	3.8	1.19	IV-V	-3.1	2.0	1.16
V-VI	0.0	15.3	4.07	0.0	16.0	4.01	-1.7	8.1	2.59	V-VI	0.0	11.9	2.97

*: The station I' (34.936°E & 29.411°N) is located near the station I.

3.4.4 Direct current measurements

3.4.4.1 Circulation in the northern Red Sea and Strait of Tiran

The currents in the northern Red Sea were scanned with the vessel mounted ADCP of R/V Meteor on the cruise 44/2 for the period from February 21st to March 7th 1999. Figure 3.16 shows the ADCP survey tracks in the northern Red during three time intervals; (a) February 21st-24th 1999, (b) February 25th-28th 1999, and (c) March 3rd-4th 1999.

The horizontal current vectors distribution in the northern Red Sea during the three periods are plotted for different depths in the upper 275 m as shown in Figure 3.17 to Figure 3.19.

These observations covered the area east and southeast of the southern Sinai Peninsula. A well developed cyclonic gyre with a diameter of about 50-60 km and maximum velocity of about 0.4 ms^{-1} was observed in the upper 215 m depth. This gyre, which was quite stable during all three observational periods, may contribute to the preconditioning for the intermediate water formation in the northern Red Sea.

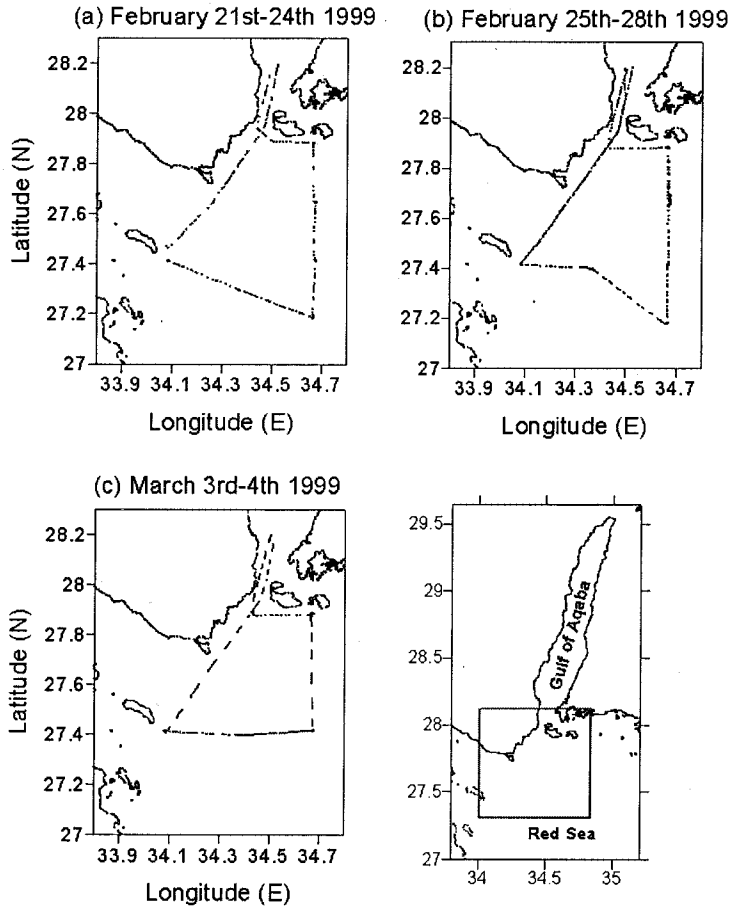

Figure 3.16: ADCP survey tracks in the northern Red Sea during the R/V Meteor cruise 44/2 during (a) February 21st-24th, (b) February 25th-28th, and (c) March 3rd-4th 1999.

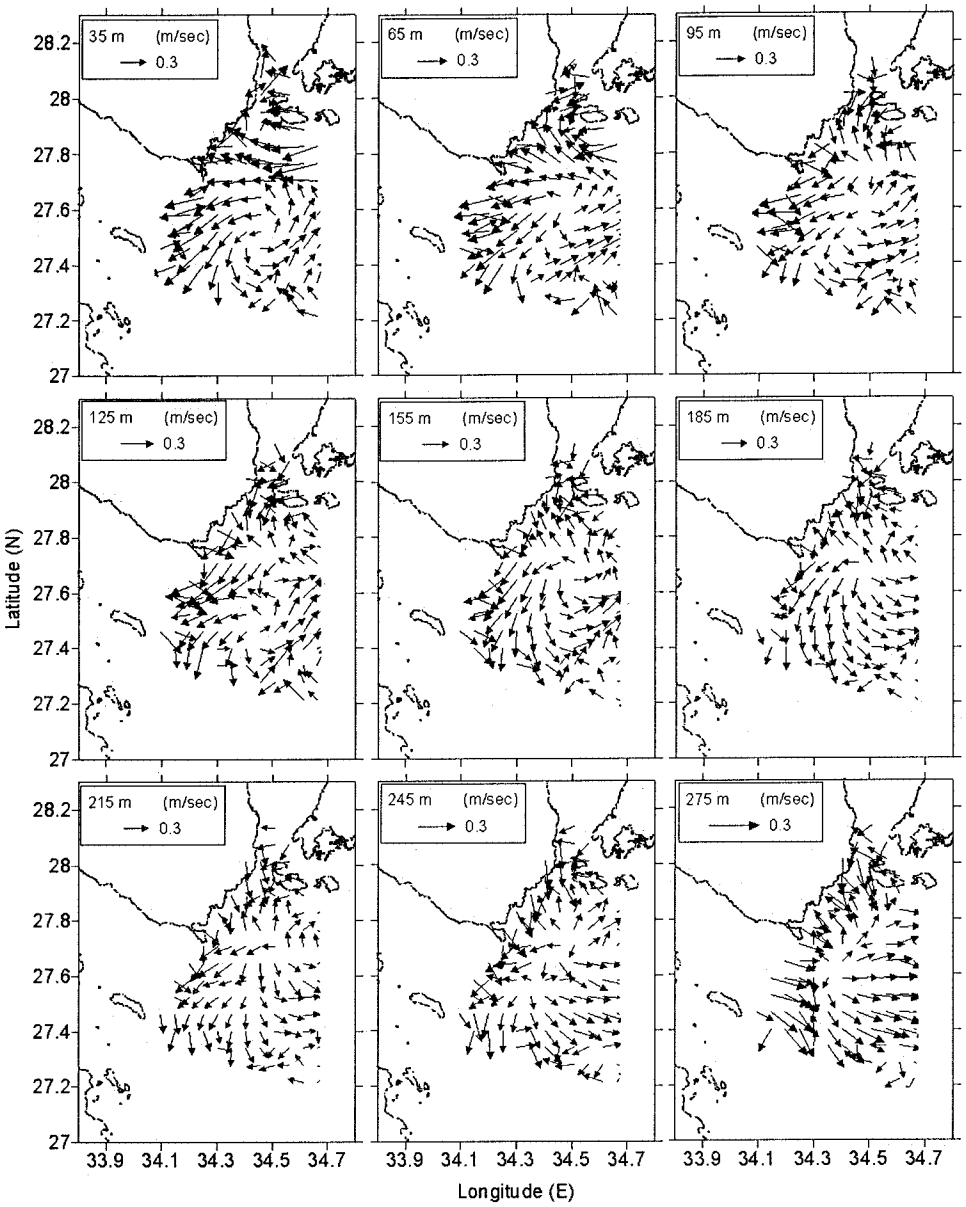

Figure 3.17: Distribution of the horizontal current vectors in the northern Red Sea at different depths in the upper 275 m during February 21st-24th 1999, R/V Meteor cruise 44/2.

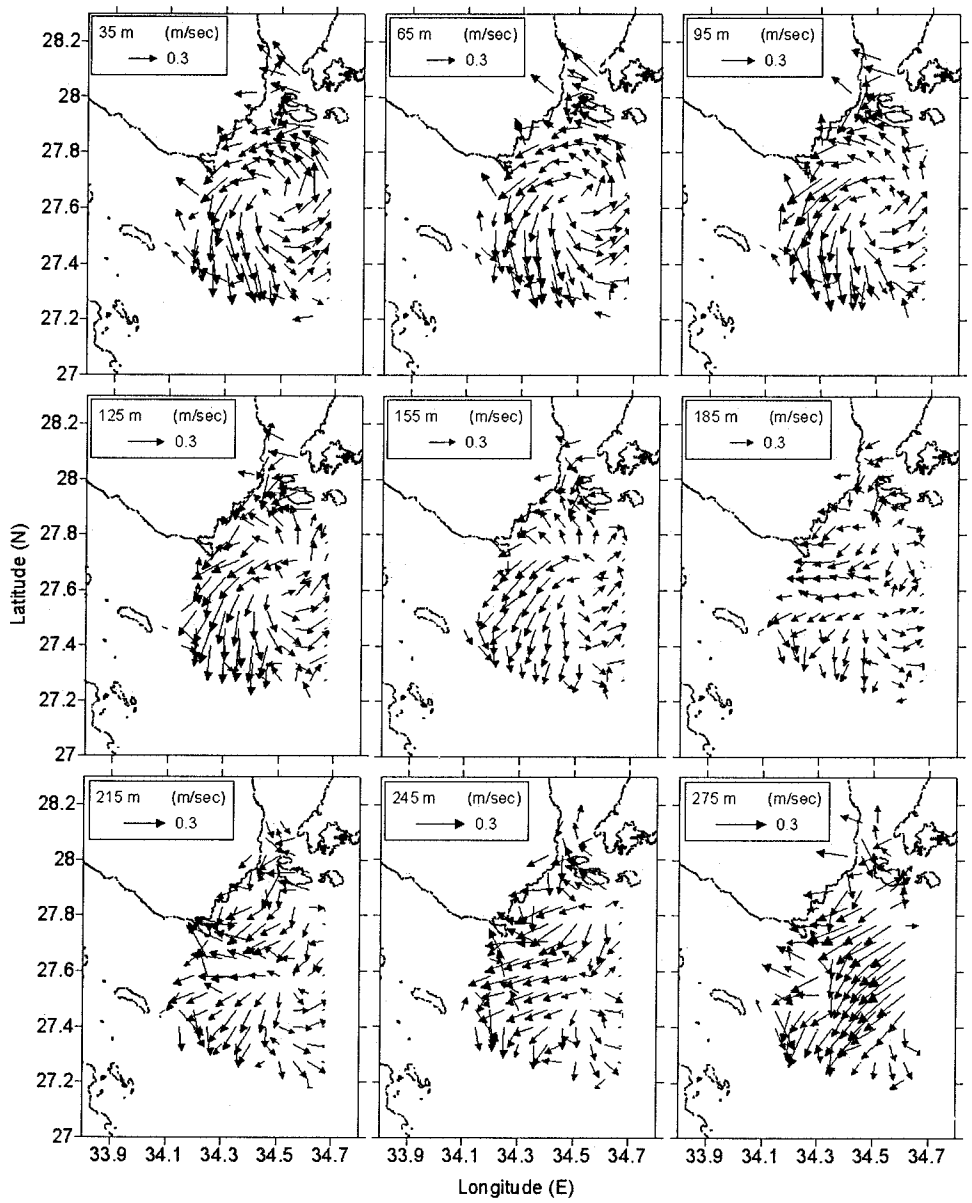

Figure 3.18: Distribution of the horizontal current vectors in the northern Red Sea at different depths in the upper 275 m during February 25th-28th 1999, R/V Meteor cruise 44/2.

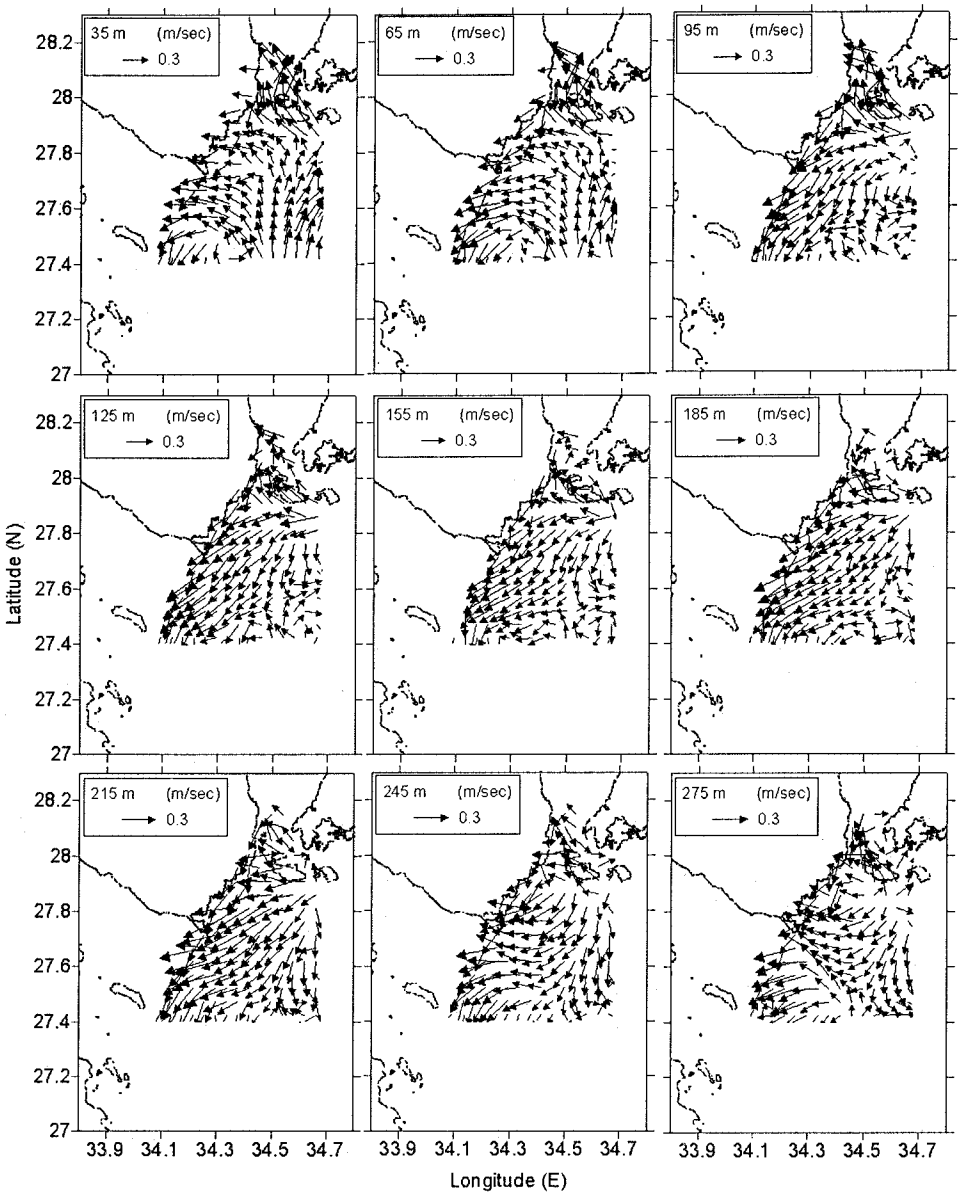

Figure 3.19: Distribution of the horizontal current vectors in the northern Red Sea at different depths in the upper 275 m during March 3rd-4th 1999, R/V Meteor cruise 44/2.

Moreover, the ADCP measurements were used to study the water exchange through the Strait of Tiran as shown in Figure 3.20. A two layer exchange between the northern Red Sea and Gulf of Aqaba was observed. Inflow (NNW) into the Gulf of Aqaba occurred in the 35-70 m of the water column over the sill, and outflow (SSW) into the Red Sea was observed below 70 m depth. The strength of the outflow to the Red Sea was generally linearly increasing with depth and reached up to about 1 ms^{-1} at 200 m depth, see Figure 3.21. The outflowing water of the Gulf of Aqaba is likely to merge with the deeper parts of the cyclonic eddy observed south east of the Sinai Peninsula. The inflow to the Gulf of Aqaba in the upper 70 m depth has maximum velocities of about 0.2 ms^{-1}. These low velocities are not able to compensate the strong outflow in the lower layer; hence, one can expect lateral variation of the interface between in- and outflow across the sill of the strait. Wind forcing may contribute to this effect. This is supported by a time series of the current in the 35-355 water column at station VI, as discussed in the following section.

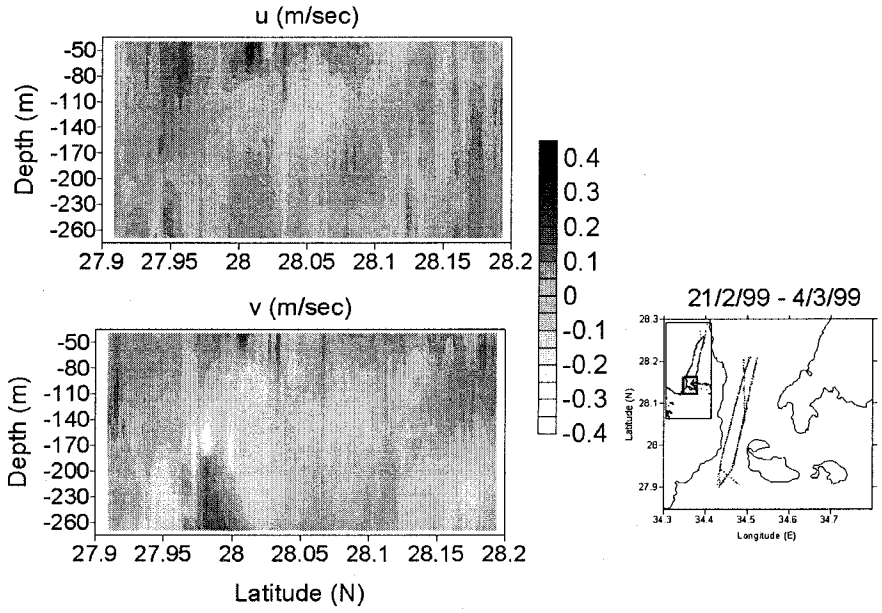

Figure 3.20: Vertical section distribution of the current components (ms^{-1}) through the strait of Tiran during the period of February 21st to March 4th 1999, during R/V Meteor cruise 44/2. The east component of the current is u and the north component is v.

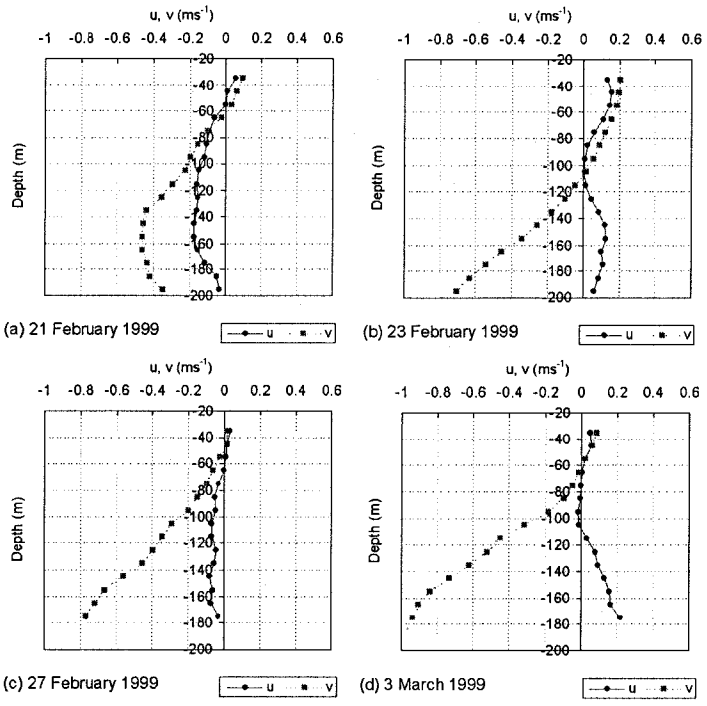

Figure 3.21: The current components (ms^{-1}) profiles at the sill of the Strait of Tiran measured on different dates during R/V Meteor cruise 44/2.

3.4.4.2 Circulation in the Gulf of Aqaba

The circulation in the northern Red Sea and water exchange with the Gulf of Aqaba through the Strait of Tiran studied in the previous section showed a cyclonic gyre in the upper 215 m depth in the northern Red Sea, and a two layer water exchange through the Strait of Tiran. Inflow occurred in the upper 70 m, and outflow below 70 m down to the sill depth at about ~260 m.

Additional information was provided by a time series of the current in the upper 350 m measured near the Strait of Tiran front at the station VI. The observations aims at the time scales of the currents in the southern gulf, and whether it is related to the inflow and outflow between the gulf and northern Red Sea. The current components, vector sticks plots, and the progressive vector diagram at 55, 105, 155, 205, and 255 m depths at the station VI during March 2nd 01:55 to March 3rd 07:53 1999 are shown in Figure 3.22 and Figure 3.23. Two main features can be derived from the figures: (1) The mean current was vertically separated into an easterly flow with a clockwise rotation of about 12.3 hr period in the upper 100 m, and a north westerly current in the 120-280 m of the water column. Profiles of the mean values of the current speed and direction during the period in Figure 3.22 were plotted in Figure 3.24. (2) A baroclinic semidiurnal signal (1.95 cycle/day; 12.3 hr period) of an internal tide wave with amplitude of about 0.2 ms^{-1} was superimposed on the mean value. However, the amplitude of the clockwise tidal rotation decreases with depth and seems not be present in the lower levels (155-255 m, Figure 3.23). In the lower levels only the magnitude of the current vectors vary with the same period, but directions do not change.

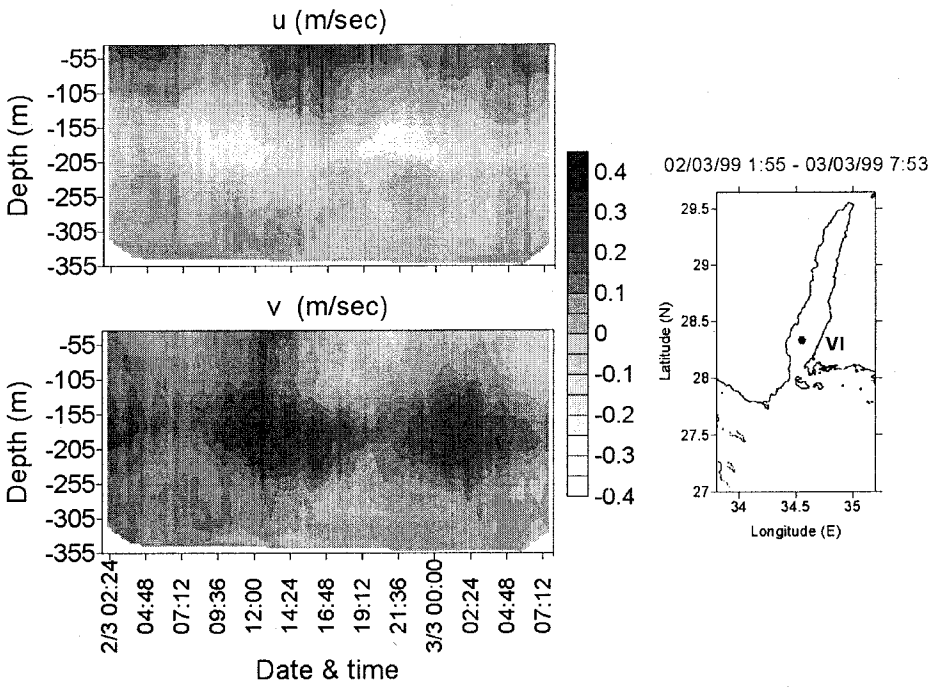

Figure 3.22: Time series records of the current components (ms^{-1}) in the upper 355 m depth at station VI during March 2nd 01:55-March 3rd 07:53 1999. R/V Meteor cruise 44/2.

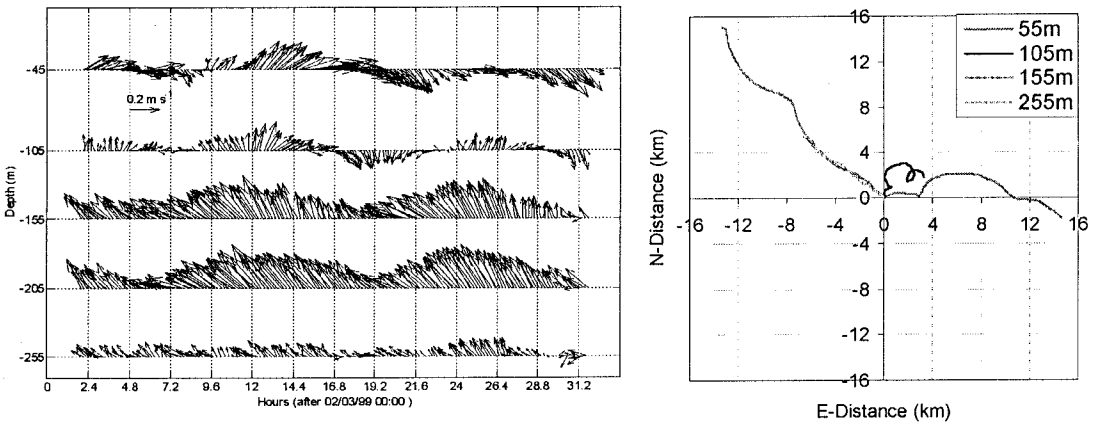

Figure 3.23: Vector sticks distribution (left) and progressive vector diagram (right) at selected depth levels at station VI during March 2nd 01:55-March 3rd 07:53 1999. R/V Meteor cruise 44/2.

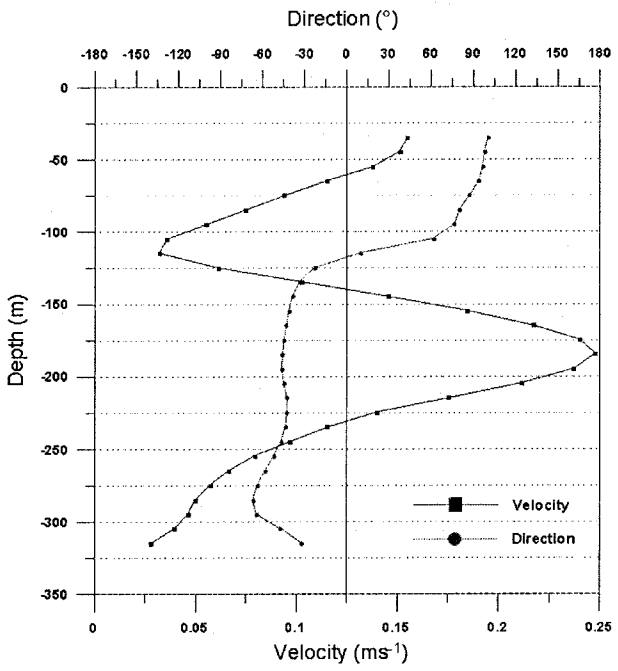

Figure 3.24 Profile of the current speed mean (ms^{-1}) and direction mean (°) at station VI during March 2nd 01:55-March 3rd 07:53 1999. R/V Meteor cruise 44/2.

It is likely that the baroclinic tidal wave is generated by the barotropic tide at the sill of the Strait of Tiran and is propagating north-westward into the Gulf of Aqaba. The range of the traveling internal tide waves is unknown, but at least it does not reach the northern tip of the gulf during February to March as seen in the Figure 3.25.

A further time series of the currents over a period of 21 hours was recorded at the station I in the northern tip of the Gulf of Aqaba on March 2nd 1999, see Figure 3.25. The most significant difference to the time series in the southern gulf is the absence of a significant semidiurnal tidal signal. Instead current fluctuations with a typical time scale of a few hours were found in the northern gulf. The mean current in the 35-335 m of the water column was directed towards NE and

ranged between 0-0.26 ms^{-1} with mean value of 0.06 ms^{-1}. The current direction in the upper 100 m changed from NE to SE (~90° clockwise rotation). The changing direction may be due to the opposite effects of wind forcing, and thermohaline inflow. The NNW wind in the northern gulf induces a SSE surface current in the upper layer, while the thermohaline inflow from the Red Sea creates a NNE current in deeper layers. Thus in summary, the current in the northern Gulf of Aqaba flows to NE and occasionally switches to SE in response to the force exerted by the wind on the upper layers. Diurnal or semidiurnal signals seem not to appear in the current during spring in the northern gulf.

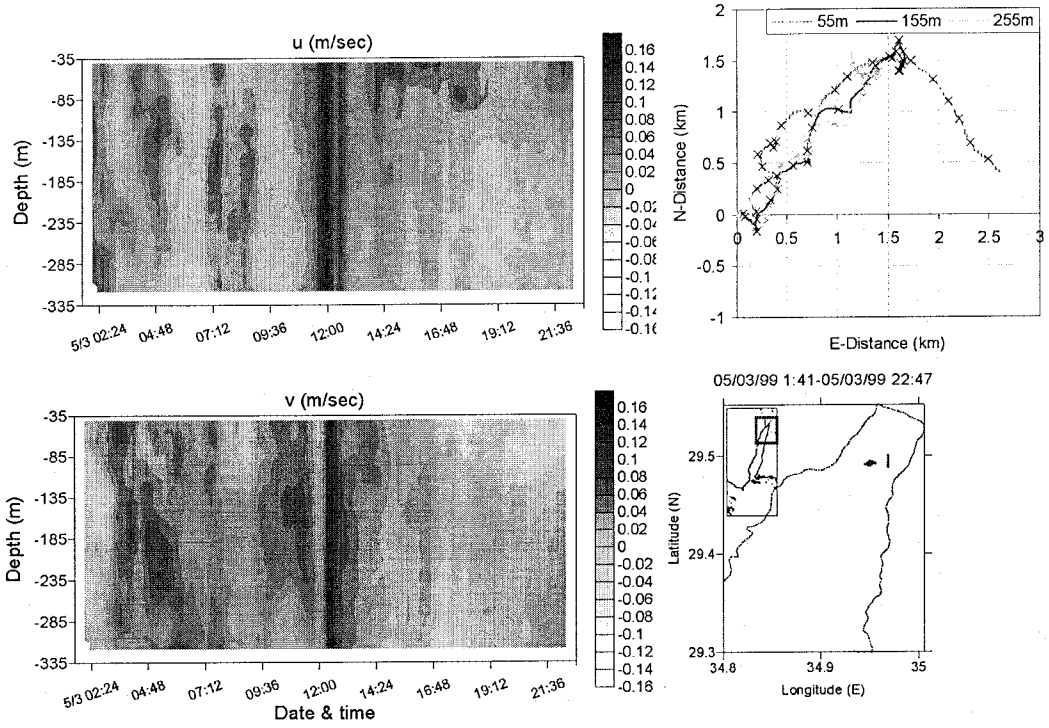

Figure 3.25: Time series records of the current components (ms^{-1}) in the upper 355 m depth (left) and progressive vector diagram (upper right) at 55, 155, and 255 m depths at station I during March 5th 01:44-March 5th 22:47 1999. R/V Meteor cruise 44/2.

Immediately, after the record of the time series at station I, a cross section survey was worked in the northern gulf at the same stations where the CTD casts have been taken. The first survey started at the station "s3", which was worked from March 5th 23:39 to March 6th 03:53 1999 (~4 hours and 30 minutes). A time series of the current profile (ms^{-1}) at s3 was recorded, which is shown in Figure 3.26. The SSE current (ranging between 0.0 to 0.16 ms^{-1}) dominated the upper 200 m. Below the transition layer at 200 m to 335 m depth the NNW current (ranging between 0.0 to 0.10 ms^{-1}) was found. Obviously, the current was rotated 180° clockwise downward in the 35-335 m of the water column. The current pattern remained unchanged during the period of 4.5 hours at station s3. The temporal change on the current seems to have not a strong influence of the spatial distribution between the stations s1, s2, s3, s4, and s5.

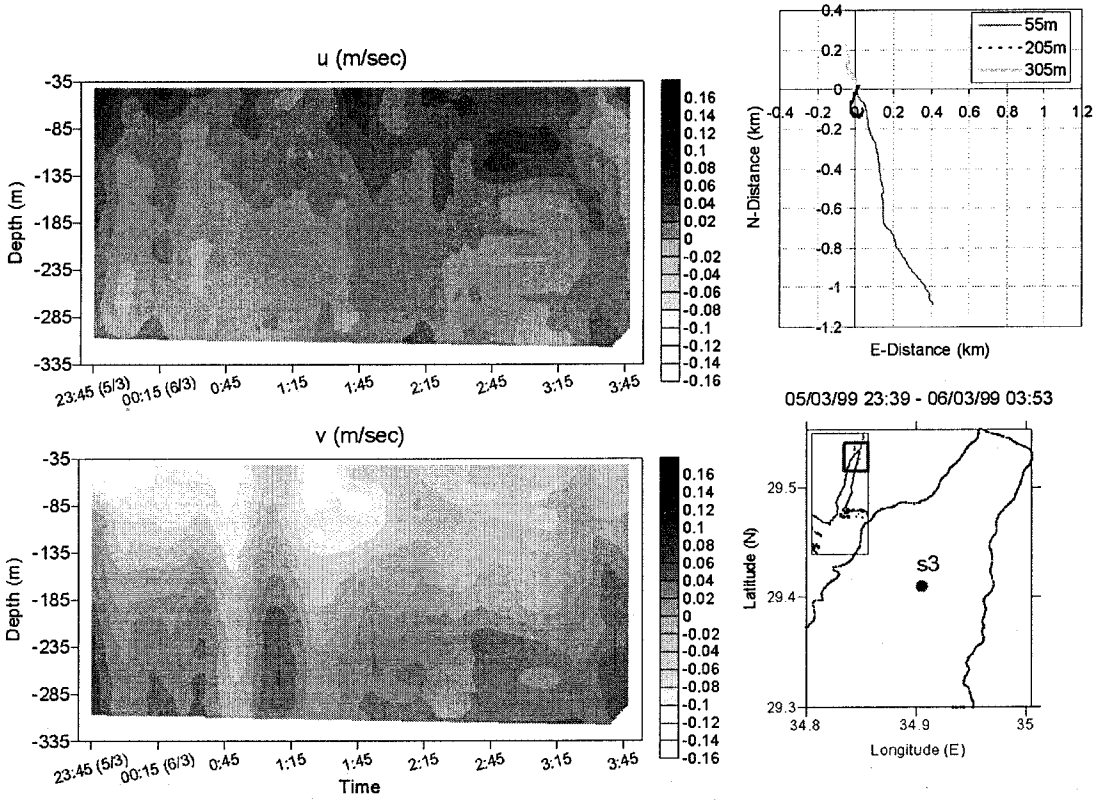

Figure 3.26: Time series records of the current components (ms^{-1}) in the upper 355 m depth (left) and progressive vector diagram (upper right) at 55, 205, and 305 m depths at station s3 during March 5th 23:39-March 6th 03:53 1999. R/V Meteor cruise 44/2.

Figure 3.27 shows a cross section of the current components (ms^{-1}) between the stations s1, s2, s3, s4, and s5 during March 6th 1999 05:05-16:00. Three different features could be seen in the Figure 3.27.

1. A homogeneous NE current pattern over the 35-335 m of the water column at stations s1-s2 (western part).
2. A SE current in the upper 200 m, and a NE current in the 200-335 m of the water column at station s3 (center).
3. A relative strong current reversed at station s4-s5 (eastern part), with a N-NNE current in the upper 200 m, and a S-SSW current below the transition layer at 200 m to 335 m depth.

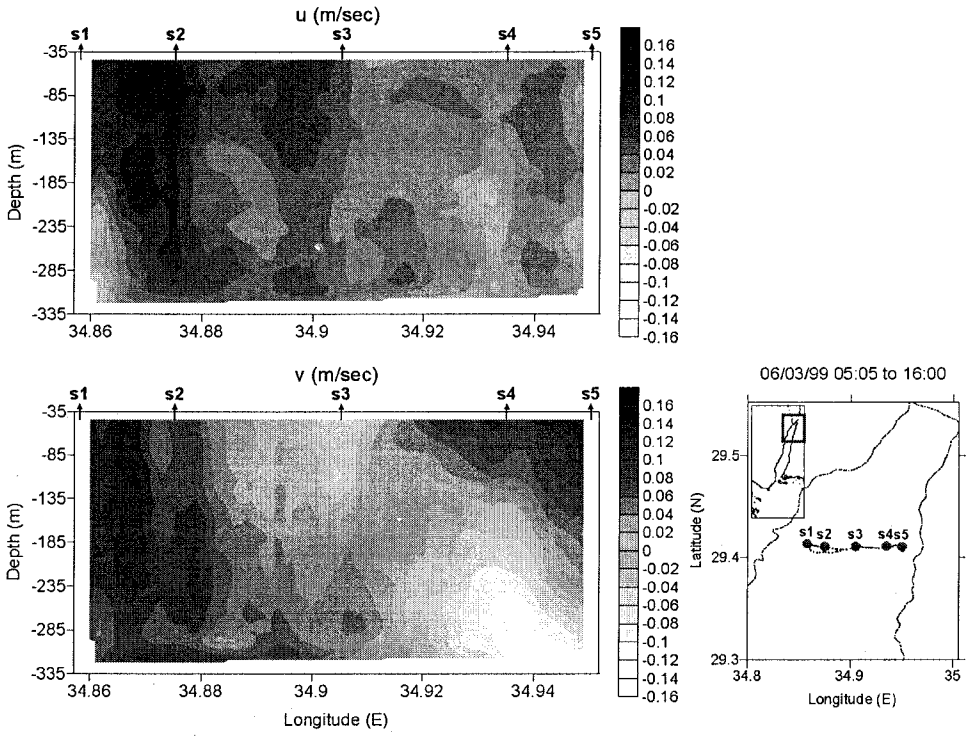

Figure 3.27: Cross section distribution of the current components (ms^{-1}) in the 35-335 m of the water column in the northern Gulf of Aqaba during March 6th1999 05:05-16:00. R/V Meteor cruise 44/2.

In order to visualize the distribution of the horizontal current patterns, the current measurements along the tracks between station I (Figure 3.25 and Figure 3.26) and stations s1, s2, s3, s4, and s5 (Figure 3.27) were interpolated for 40, 100, 150, 200, 250, and 300 m depths. The results are shown in Figure 3.28. The current in the upper 200 m in the western and eastern parts of the northern gulf was directed to the NE, while in the center the current was towards SE. Consequently, an anti-cyclonic circulation is observed between the western and central parts of the section in the upper 150 m. Below 200 m to 300 m depth, the NE current still dominated in the western part, while the transition current from NE to SE can clearly be seen at the eastern part. This agrees with the suggested northward current in upper 300 m, and southward counter current near the bottom, due to the upward and downward shape of the density between 100-300 m and near the bottom, respectively, see section 3.4.1.1. Obviously, the two opposites currents are parts of a larger anti-cyclonic circulation between eastern and western parts. The range and mean of the velocity in the upper 300 m were 0-0.30 and 0.06 ms^{-1}, respectively. The resulting localized eddy has apparently a diameter of about 5 to 8 km.

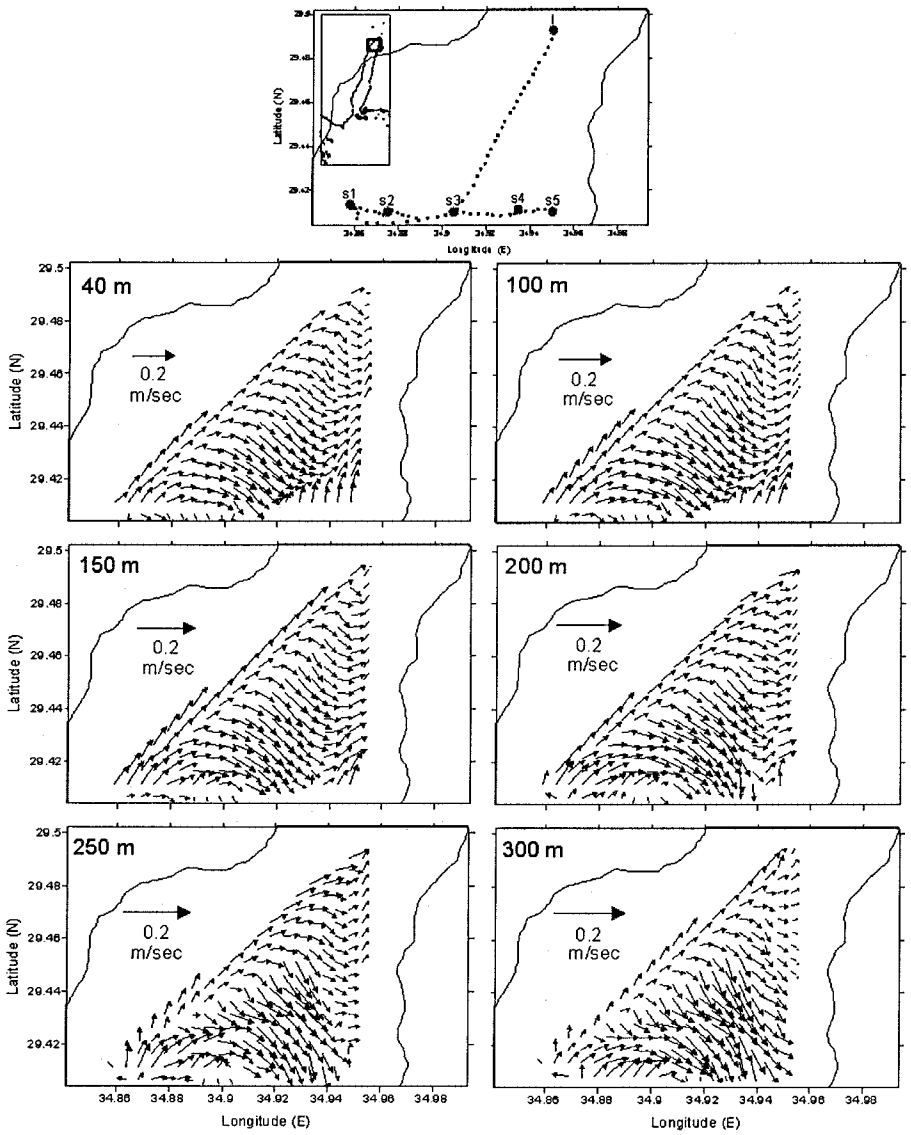

Figure 3.28: Distribution of the horizontal current vectors between the stations I, s1, s2, s3, s4, and s5 at selected depth levels during March 5th 01:40-March 6th 16:00 1999, R/V Meteor cruise 44/2.

In order to study the basin scale current pattern along the gulf axis, four continuous tracks were performed within eight days, on February 26th-27th, February 28th-March 1st, March 1st-2nd, and March 4th-5th 1999. The vertical distribution of the current components (ms^{-1}) are plotted in Figure 3.29 (a), (b), (c), and (d), respectively.

The most significant feature in Figure 3.29 is a wave-like variation of the velocity in the upper 250 m along the gulf with a typical length scale of about 20 km. The distribution of the u component at selected depth levels, shown in Figure 3.30, reveals the baroclinicity of the phenomenon.

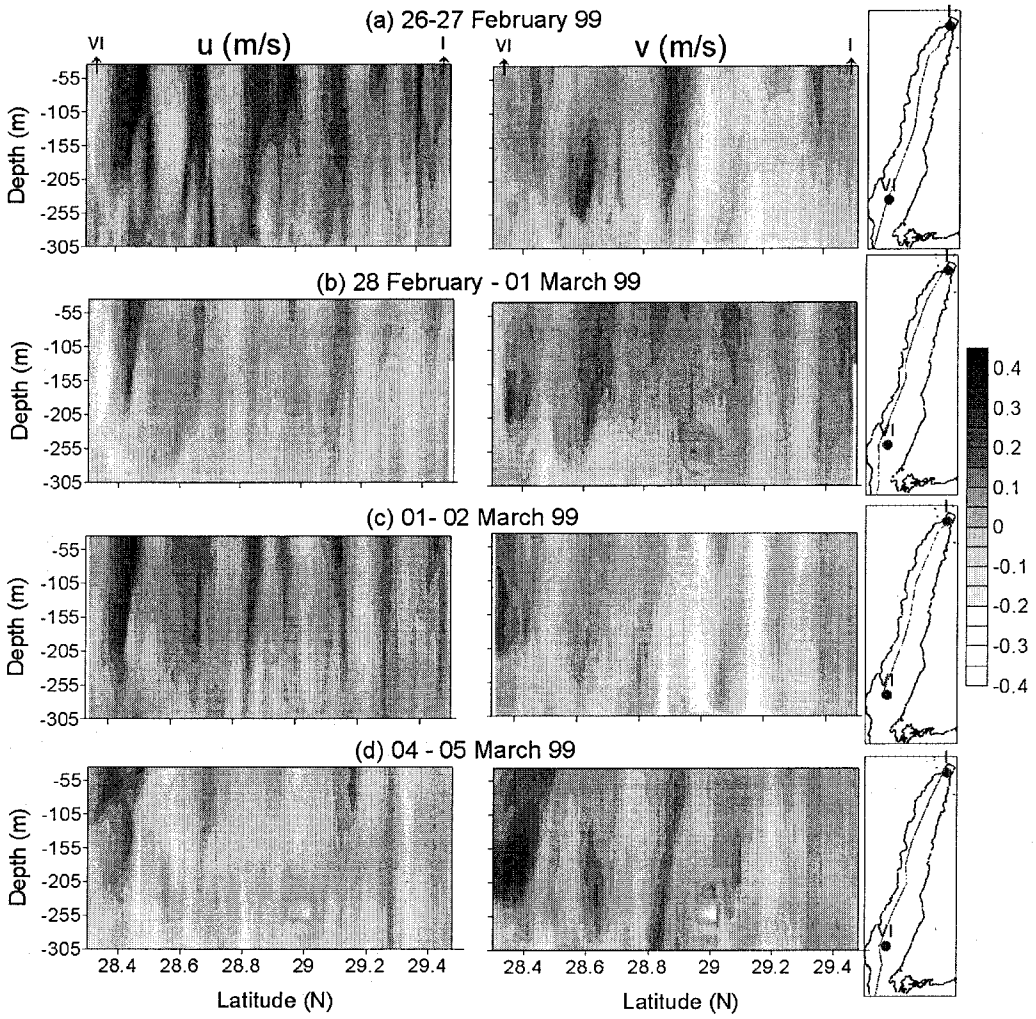

Figure 3.29: Long section of the current components (ms^{-1}) along the axis of the Gulf of Aqaba during the R/V Meteor cruise 44/2.

Moreover, the wave pattern appears to be a typical feature because it could be detected during all the sections within 8 days. Figure 3.31 showing six waves crests of the u component along the gulf axis. The wavelength is ~20 km, which is twice the baroclinic Rossby radius ($R \approx 10$ km).

For some parts of wave pattern, the horizontal current components differ in phase by about 90°, see Figure 3.32. These properties of the current field suggest the existence of wave train, which looks like a chain of cyclonic and anti-cyclonic eddy pairs. The observed current pattern would result if the track of the ship is parallel to the line through the centers of the wave train or eddy centers. The total diameter for each pair equals the wavelength (~20 km $\approx$ 2R). The numerical modeling studies by BERMAN et al. (2000), also suggest that during winter, three eddies in the northern half of the gulf are a typical feature; the northernmost gyre is anti-cyclonic with 18 km diameter, while during spring the northernmost gyre is cyclonic with a 10 km diameter.

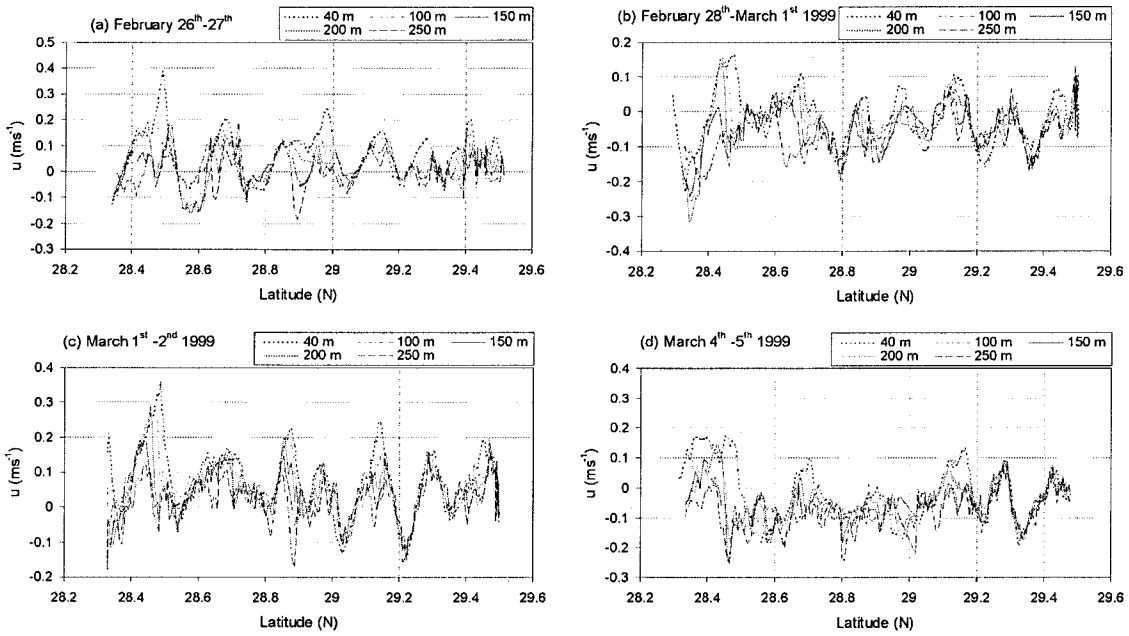

Figure 3.30: Distribution of u (ms^{-1}) component of the current along the axis of the Gulf of Aqaba at selected depth levels during R/V Meteor cruise 44/2.

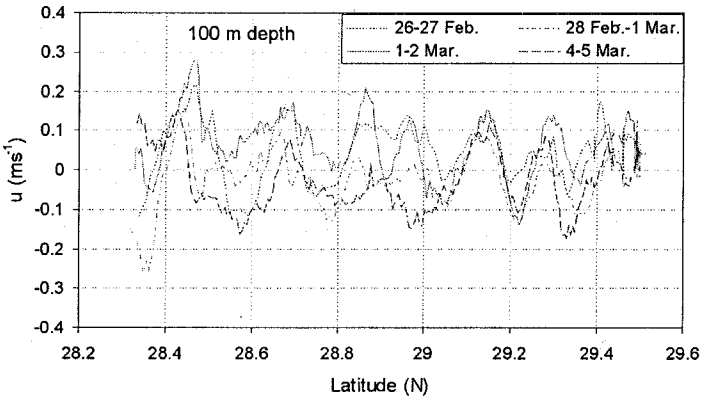

Figure 3.31: Distribution of the u (ms^{-1}) component along the axis of the Gulf of Aqaba at 100 m depth on repeated tracks during R/V Meteor cruise 44/2.

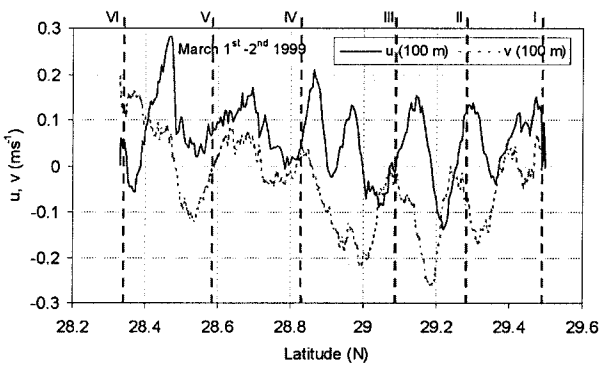

Figure 3.32: Distribution of u and v (ms^{-1}) components of the current along the axis of the Gulf of Aqaba at 100 m depth during March 1st-2nd on the R/V Meteor cruise 44/2.

In order to check whether these eddy patterns are robust features or artificial results generated by poor sampling from a moving ship, we have plotted the current vectors in a time-latitude diagram, Figure 3.33 (a). The stick plots shows that for both slow tracks (the first three tracks were interrupted by CTD stations) and the fast tracks show a similar sequence of changing flow.

A simulation of a purely semidiurnal clockwise rotating current field in the gulf and sampling of these pattern at the same time-latitude points as the observed current vectors is shown in Figure 3.33 (b), where the gray arrows refer to the simulated flow. Although such a simple slab-like tidal motion is an oversimplification we can clearly see that the changes of the currents are not basic tidal motion. This supports the existence of eddy sequences in the Gulf of Aqaba.

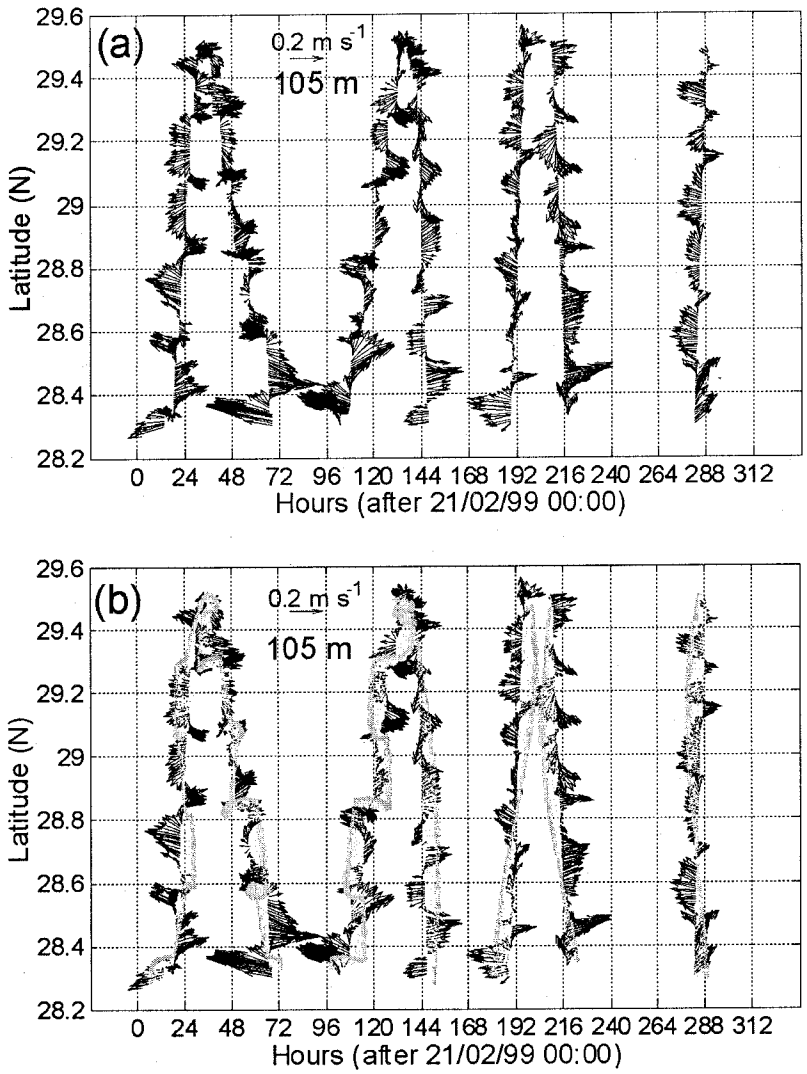

Figure 3.33: Time-latitude distribution of the (a) current vectors Overlaid by (b) a simulation of pure semidiurnal current filed with rotating clockwise (gray arrows) along the axis of the Gulf of Aqaba at 105 m depth on repeated tracks during February 21st-March 6th 1999. R/V Meteor cruise 44/2.

The existence of the energetic variations of the current field with scale of the Rossby radius in the gulf questions the geostrophic current calculations from stations with a distance larger than the baroclinic Rossby radius. The distance between the stations ranged between 25-30 km, therefore, changes in currents between the stations will not be detected by the geostrophic method, while the ADCP measurements make this current variability visible.

The comparison of geostrophic and measured currents clearly reveals the sampling error in the geostrophic current field due to inadequate station distance. Figure 3.34compares the calculated Vrel and the measured u' (ms^{-1}) along the gulf axis during February 21st-22nd 1999. Beside the differences due to the large station distance there is some agreement if u' is averaged along the track.

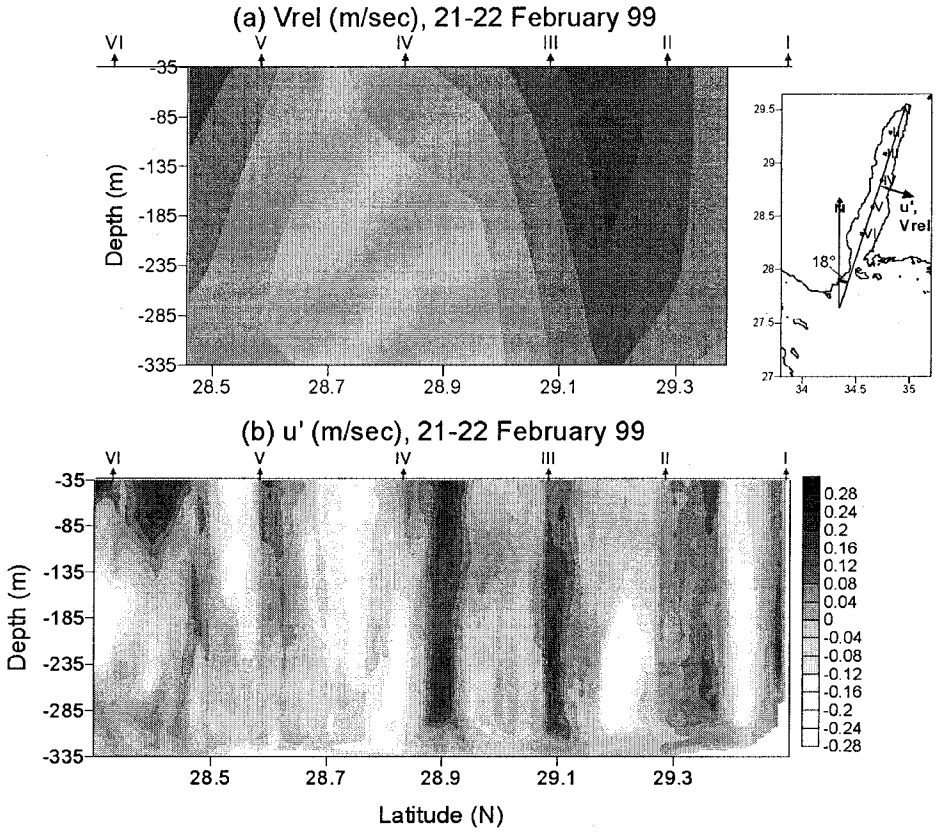

Figure 3.34: Vertical section of the, (a) geostrophic velocity Vrel (ms^{-1}) referenced to 600 m depth calculated from station I-VI, and (b) east current component u' (ms^{-1}) measured simultaneously by the ADCP 150 kHz during the R/V Meteor cruise 44/2.

3.5 Results of the local and seasonal investigation

3.5.1 Water masses and stratifications

3.5.1.1 Seasonal variations of the potential temperature (θ), salinity (S), and density (σ_θ)

In this section we discuss the dynamics of the water mass in parts of the northern gulf. One part of the data base consists of more than four years of biweekly measurements of temperature and salinity in the 0-400 m water column at the reference station S2 (see Figure 2.5) in front of the MSS.

The variations of the temperature profiles recorded form May 1997 to August 2001 are shown in Figure 3.35 (a). The dominating signal is the seasonal variation. The thermal stratification exists during summer (May-December), and is strongest during August where it reached a maximum depth 250 m. The thermocline vanishes during the winter-spring seasons (January-April). The maximum mixing depth reaches as far as 400 m during spring (February-April). The variations of salinity (S) are shown in Figure 3.35 (b). The maximum difference of the salinity was about 0.5 in the upper 400 m during the whole period. This indicates that the changes in S were small, and most of this difference is due to the high evaporation. The phenomenon of higher saline water above lower saline water occurred clearly during the periods of July-November 1997 and July-December 1998, and also appeared, but weakly, during September-November 2000 and July-August 2001. This phenomenon developed in August at 60 m, plunged to 200 m in December. Later it dwindled until it vanishes during spring. The evaporation, which increases the surface salinity, and the low saline water carried by the thermhaline in the intermediate waters from the Red Sea, might be both an explanation for this phenomenon during summer. During April 1999-February 2000, the salinity assumes the lowest values in the upper 400 m during the period of May 1997 to August 2001. In Figure 3.35 (c), it is shown that the behavior of the density σ_θ follows basically the temperature θ with respect to the stratification and mixing time and scale, i.e., salinity plays a minor role.

The maximum range of the temperature θ, salinity and density σ_θ in the 0-250 m of the water column during the strongest stratification periods, which occurred during August months, were between 28.04-20.88 °C, 40.67-40.20, and 26.55-28.63 kgm^{-3}, respectively. During February-March months, where the mixing is dominating, the range mean of the temperature θ, salinity, and density σ_θ in the 0-400 m of the water column were 21.50-21.10 °C, 40.44-40.48, and 28.51-28.63 kgm^{-3}, respectively. Hence the mean annual variation of temperature, salinity, and density in the upper 400 m were about 7.3 °C, 0.5, and 2.3 kgm^{-3}.

The thermal stratification is building from May in the upper 100 m and in ranging between 21.2-22.5 °C, in the same time, the air temperature is ranging maximally between 20-40 °C with mean value of about 29 °C. The minimum air temperature is around the water temperature, while the mean air temperature exceeds the maximum of the water temperature by about 6.5 °C. The increase of air temperature continues gradually until it reaches the maximum in August (ranging between 27-41 °C). Following to that, the stratification develops in both the depth (reaches to 250 m in August) and the value range (21-27 °C in August). The degradation of stratification begins during October in the upper 60 m, while the air temperature drops during night (~18 °C) well below than the water temperature (~25.5 °C). The air temperature decreases progressively, leading to a permanent loss of buoyancy and causes the density of the surface water to pass a critical threshold after which vertical convection occurs, therefore, the continuous deepening of the convection is dominating during winter. Figure 3.36 (a) shows the variation of the stratification

deepness S_h (m) during summers (where the temperature gradient is greater than 0.025 °Cm^{-1}) and the mixed layer deepness M_h (m) during winter-spring seasons (where the temperature gradient is less than 0.005 °Cm^{-1}) together with the low pass filtered air temperature (°C) during the period of May 1997 to August 2001. The variations of S_h and M_h with time are approximated as a polynomial of second order and as a linear one, respectively. The rate dS_h/dt ($mday^{-1}$) represents a linear relationship with respect to the time, and appears fast in early summer (~-3.0 $mday^{-1}$) and then slows down in late summer (~-0.2 $mday^{-1}$) when the stratified layer get thicker, while the rate dM_h/dt is constant. The interannual variations of S_h and M_h are weak, both scale and rate, during the five summer and four winter-spring seasons from 1997 to 2001, see Figure 3.36 (a). The composite variation of S_h for the summers reveals the average deepening of the stratification during summer, which could be given as $S_h(t) = 0.0093t^2 - 2.961t + 21.712$; where t is days number after April 1st, and the unites of coefficients 0.0093, –2.961, and 21.712 are $mday^{-2}$, $mday^{-1}$, and m, respectively, see Figure 3.36 (b). The composite variation of M_h, as seen in Figure 3.36 (c), gives the average deepening of the mixing, which is varying linearly with respect to the time as $M_h(t) = -2.379t - 30.898$, where t is days number after October 1st, and the unites of coefficients –2.379, and –23.898 are $mday^{-1}$, and m, respectively, hence the mean of dM_h/dt equals –2.379 $mday^{-1}$.

The peaks of sea surface temperature, which occurred in August, have different values through the years from 1997 to 2001. The minimum value is 25.48 and the maximum value is 28.04, which were measured in 1997 and 1999, respectively. The differences in the surface temperature advection of heat could be related to interannual variations of the surface heat flow, annual variations of the weather conditions, and to the seasonal differences of the water temperature values, which flow from the Red Sea.

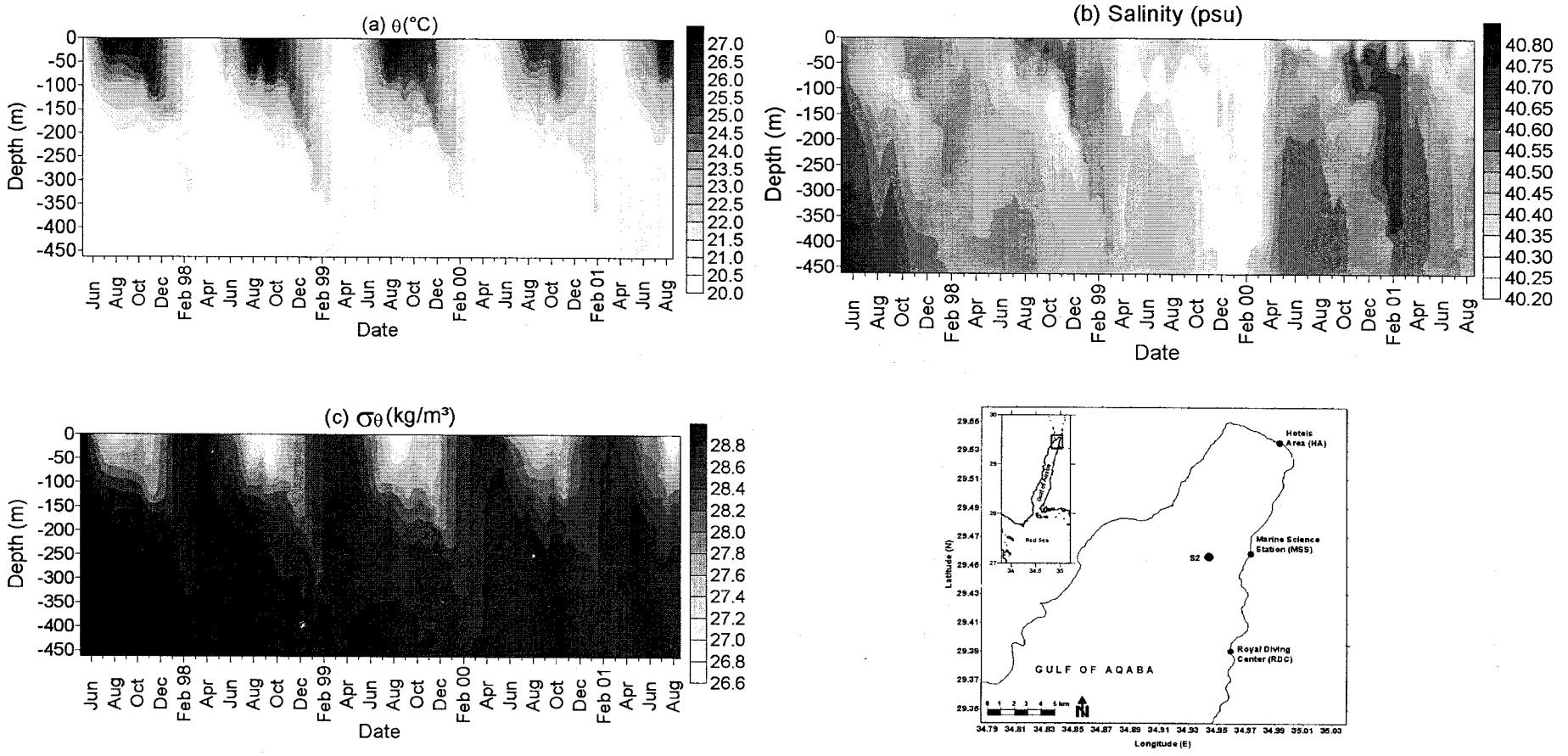

Figure 3.35: Time series measurements of θ (°C), S (psu), andσ_θ (kgm^{-3}) for the 0-400 m water column at the reference station (S2) in front of the MSS during May 1997- August 2001.

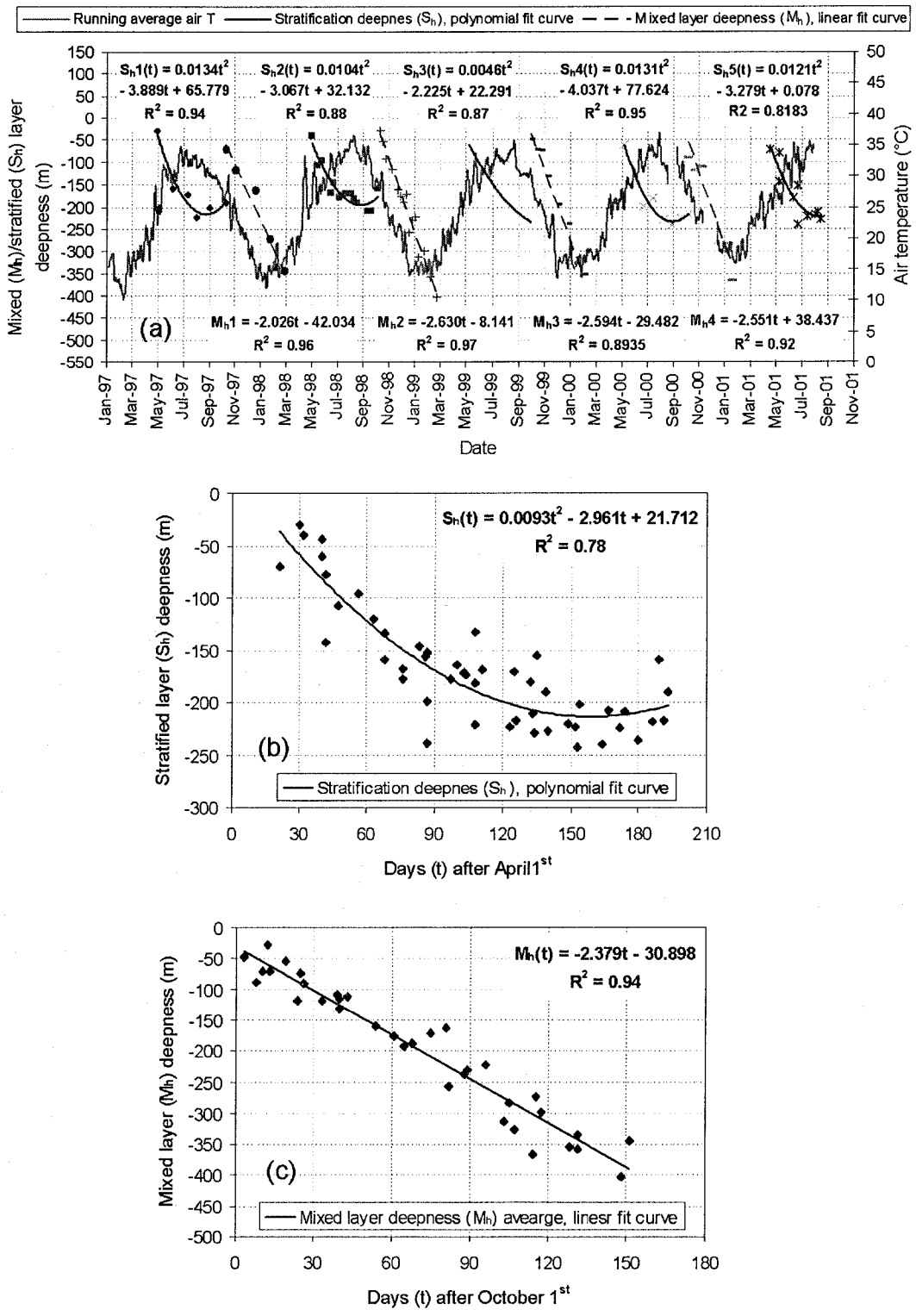

Figure 3.36: (a) The variation of the stratification deepness S_h (m) during summers and the mixed layer deepness M_h (m) during winter-spring seasons together with the low pass filtered air temperature (°C) during May 1997-August 2001. (b) and (c) represent the composite variations of S_h and M_h, respectively.

Figure 3.37 shows the profiles of the mean, minimum, and maximum (a) temperature θ (°C), (b) salinity S (psu), and (c) density σ_θ (kgm^{-3}) values, for the segments 0-20, 20-40,..., 440-460 m of the water column at station S2 in front of the MSS during the period of May 1997 to August 2001. In Figure 3.37 (a), the highest and lowest sea surface θ (°C) were measured during May 1997 till August 2001 were 28.04 °C on August 1999 and 21.13 °C on February 2001, respectively. The sea surface salinity maximum value was 40.67 on August 2001, and the minimum value was 40.20 on March 1998, see Figure 3.37 (b).

In Figure 3.37 (c), the highest and lowest densities σ_θ (kgm^{-3}) near the sea surface were 28.73 kgm^{-3} on February 2001, and 26.54 kgm^{-3} on August 1999, respectively.

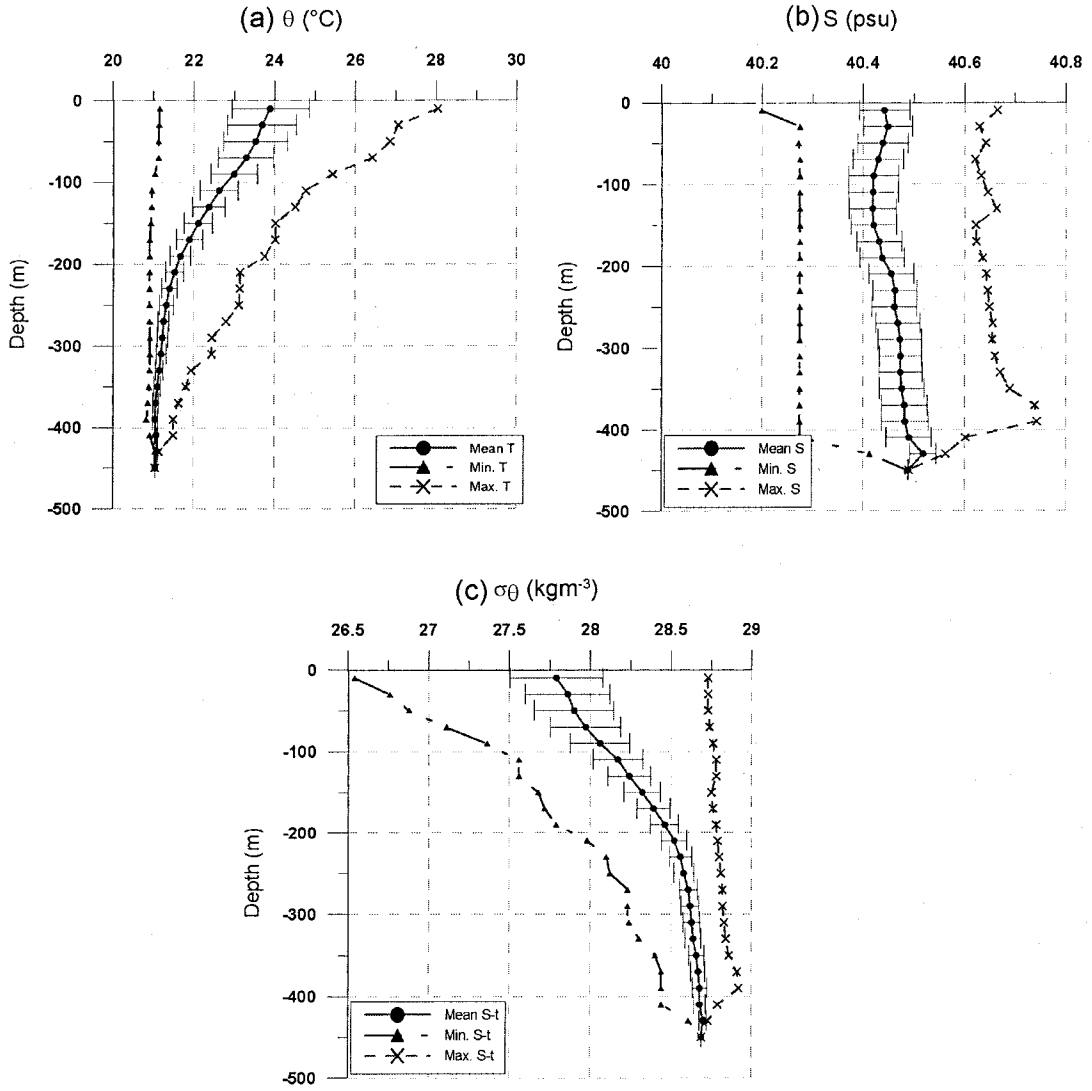

Figure 3.37: Profiles of the mean, minimum, and maximum of the (a) θ (°C) (b) S (psu), andσ_θ (kgm^{-3}) values for the segments 0-20, 20-40,..., 440-460 m at the reference station S2 in front of the MSS during May 1997-August 2001.

3.5.1.2 Water masses properties

Figure 3.38 shows the θ-S diagram for the 0-400 m waters during the period of May 1997 to August 2001 at the reference station S2 in the northern tip of the Gulf of Aqaba. The θ-S diagram shows that the temporal variations of the salinity were confined to a small interval of 40.20-40.75, while the variation of the temperature was large, ranging between 20.84-28.04 °C, as shown in Figure 3.38. Actually, the real effects on the thermodynamics process on the seawater of the Gulf of Aqaba are dominated by θ variations, while S plays a minor role. The upper 200 m and between 200 and 400 m the water had similar characteristics during winter-spring seasons (February-April), i.e., during the convection period in the Gulf of Aqaba, where the 0-400 m water column was well mixed.

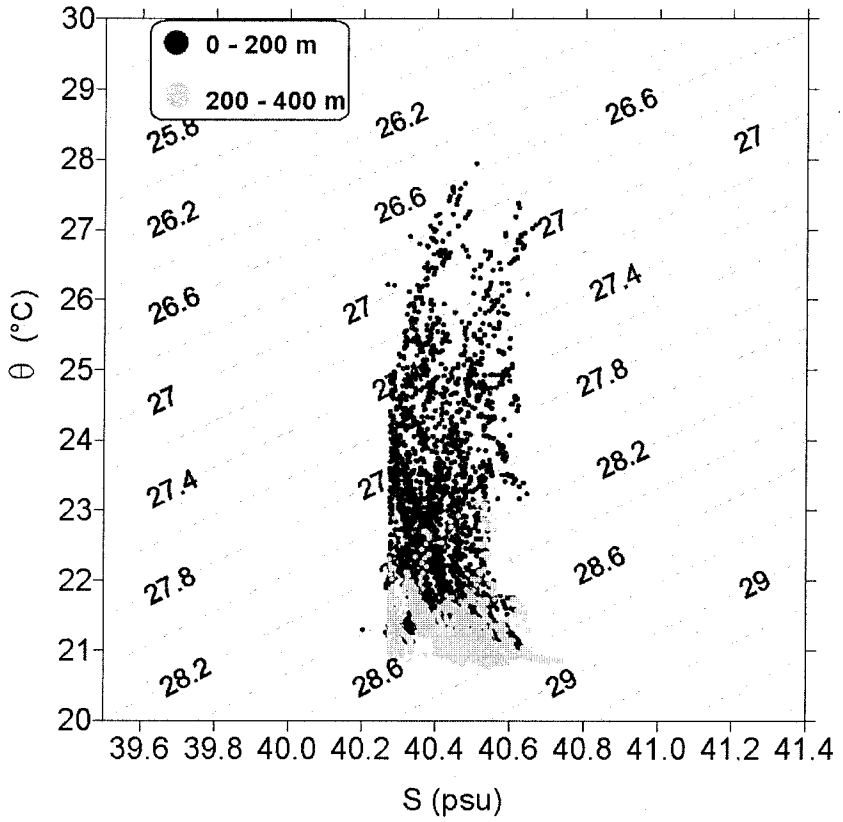

Figure 3.38: θ-S diagram at the reference station S2 for the 0-400 m water column in the northern tip of the Gulf of Aqaba for the period from May 1997 to August 2001.

3.5.1.3 Inter station statistical comparison

In this subsection we compare the findings from the time series at three stations in the northern gulf. The hydrographic conditions at each station exhibited pronounced seasonality, and the annual variations of the hydrographic parameters are much higher than the difference between the stations for the same time and depth. Hence, a straightforward comparison of the statistics of the parameters less useful. Therefore, a technique in which conditions are compared to a reference station was followed. Here, the difference between a specific value and its reference value is calculated and these differences are then used to analysis the variance. The reference was selected as a composite station that includes all the data recorded at the different stations. Two stations are considered significantly different from each other with respect to a certain parameter, if their 95% confidence intervals for the parameters do not intercept, and a station is considered significantly different from the reference composite station, if the difference is significantly different from zero, i.e. if the 95% confidence interval does not include zero.

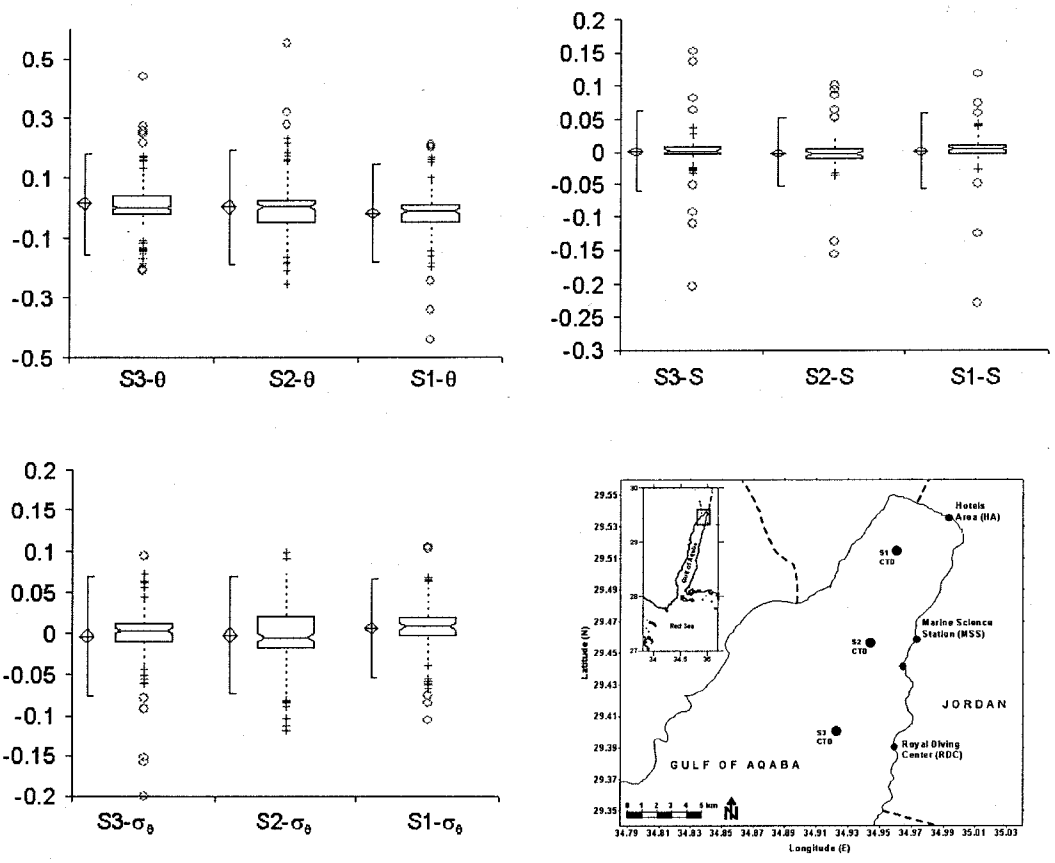

Figure 3.39: Box-Whisker plots of the θ (°C), S (psu), and σ_θ (kgm^{-3}) at three stations S 1, S2, and S3 in the upper 300 m depth during February 2000 -August 2001.

Table 3-5: Statistical comparison analysis between the means of θ (°C), S (psu), and σ_θ (kgm^{-3}) at the stations S1, S2, and S3 in the upper 300 m depth during February 2000 -August 2001.

θ (°C)	**n**	**Mean**	**SD**	**SE**	**95% CI of Mean**
S3	91	0.0143	0.10163	0.01065	-0.0069 to 0.0355
S2	91	0.0035	0.11569	0.01213	-0.0206 to 0.0276
S1	91	-0.0178	0.09771	0.01024	-0.0382 to 0.0025
S (psu)	**n**	**Mean**	**SD**	**SE**	**95% CI of Mean**
S3	91	0.0011	0.03774	0.00396	-0.0067 to 0.0090
S2	91	-0.0017	0.03186	0.00334	-0.0083 to 0.0050
S1	91	0.0005	0.03478	0.00365	-0.0067 to 0.0078
σ_θ (kgm^{-3})	**n**	**Mean**	**SD**	**SE**	**95% CI of Mean**
S3	91	-0.0035	0.04400	0.00461	-0.0126 to 0.0057
S2	91	-0.0024	0.04320	0.00453	-0.0114 to 0.0066
S1	91	0.0058	0.03629	0.00380	-0.0017 to 0.0134

θ (°C)					
Source of variation	SSq	DF	MSq	F	p
Stations (factor)	0.0486	2	0.0243	2.19	0.1136
Within cells (error)	2.9932	270	0.0111		
Total	3.0418	272			
S (psu)					
Source of variation	SSq	DF	MSq	F	p
Stations (factor)	0.0004	2	0.0002	0.17	0.8472
Within cells (error)	0.3284	270	0.0012		
Total	0.3288	272			
σ_θ (kgm^{-3})					
Source of variation	SSq	DF	MSq	F	p
Stations (factor)	0.0047	2	0.0023	1.37	0.2549
Within cells (error)	0.4607	270	0.0017		
Total	0.4654	272			

Here, SD is the standard deviation, SE is the standard error, SSq is the total sum of the square, DF is the degrees of freedom, MSq is the mean of the square, F is the F-ratio or the variance ratio = MSq(stations or factor)/MSq(within cells or error), and p is the probability. For the 95% confidence level to have a significant difference between any two stations, p should be ≤ 0.05.

The above technique was applied for comparison between the means of θ, S, and σ_θ for six profiles in the 300 m water column taken at stations S1, S2, and S3 in the northern tip of the Gulf of Aqaba during the period of February 2000 to August 2001. Figure 3.39 and Table 3-5 show the results of the test. The statistical analysis of θ, S, and σ_θ showed no significant difference between any stations in the upper 300 m depth during that period.

3.5.2 Direct current measurements

3.5.2.1 Time series records near the shore

The time series of current profiles were recorded using Acoustic Doppler Current Profiler (2×Workhorse Sentinel ADCP 300 kHz) at three different positions near the shore. One of the workhorses was deployed in different periods at two positions (w1-a and w1-b; in the canyon and on the shelf areas, respectively), 200 m from the coast (0.02R). The other instrument was deployed at position (w2; on the slope area), 900 m from the coast (0.09R) in front of the MSS, see Figure 2.5. Note that the Rossby radius is R ~10 km.

Thus, we have time series for 12 months at position w1-a and for 3 months at w1-b. The second Workhorse recorded three periods within 5 months. Some gaps in the time series occurred due to battery failures or other technical problems.

In the following, all drawing of time series of the current will be transformed into the cross shore and long shore components relative to the northern Gulf of Aqaba axis. The northern gulf axis deviates 25° to the east of the geographic north.

3.5.2.1.1 Currents in the canyon (w1-a) and shelf (w1-b) areas

Figure 3.40 and Figure 3.41 show the time series records of the cross and long shore current components (cms^{-1}), for the 20-40 m at position w1-a in front of the MSS during March 2000-February 2001. This long term investigation revealed a weak mean current value about 3 cms^{-1}, where the maximum current measured was 17 cms^{-1}. Figure 3.42 shows the dominants current components values (u & v cms^{-1}) at position w1-a, at different depths 20, 28, and 36 m. The percent frequencies of the u and v values from -5 to 5 cms^{-1} at depths 20, 28, and 36 m were ranging between 85-90% and 95%, respectively. Thus, the current at position w1-a in front the MSS was weak and mostly fluctuated between -5 to 5 cms^{-1}.

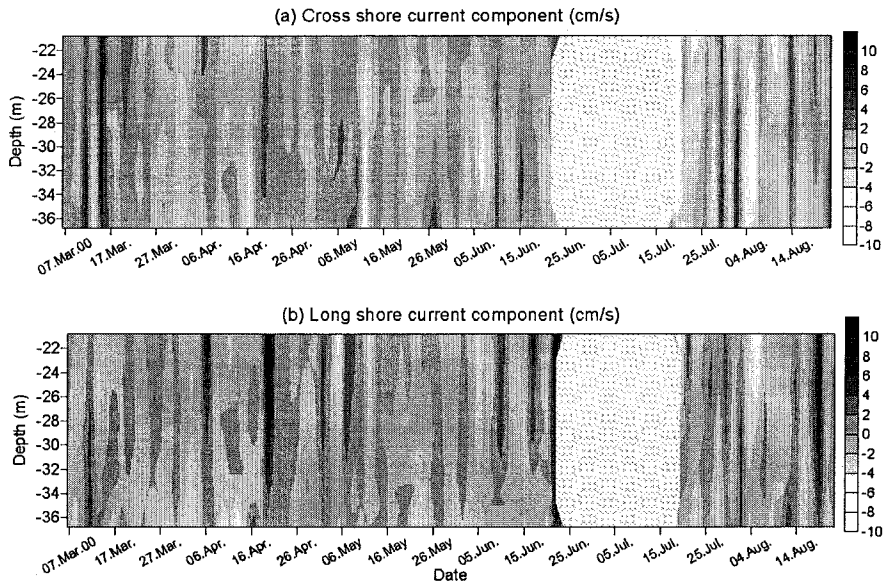

Figure 3.40: Time series records of the (a) cross shore (cms^{-1}) and (b) long shore (cms^{-1}) current components of the 20-40 m water column in front of the MSS at position w1-a during the period of March 6th to August 22nd 2000.

Figure 3.43 shows the progressive vector diagram at depths 20, 28, and 36 m, during the periods of (a) March 6th-June 22nd 2000, (b) July 17th-August 22nd 2000, and (c) October 16th 2000-January 7th 2001. At 20 m depth the current track was to SE in Figure 3.43 (a) and SSW in Figure 3.43 (b). At 28 and 36 m depths, the current flows to NW and SW, respectively, in both intervals in Figure 3.43 (a) and (b). During both periods in (a) and (b) the current was the strongest at 36 m depth. In Figure 3.43 (c), the current tracks changed at the depths 20, 28, and 36 in comparison to the first two periods. The current was towards SE till November 27th 2000 at all the depths, but afterwards the currents at the depths 28 and 36 turned to NW, while at 20 m depth the current did not change until January 7th 2001. In general, the current pattern at position w1-a in front of the MSS is varying between SE and SW with a reversal from SE to NW during the period of March 2000 to February2001.

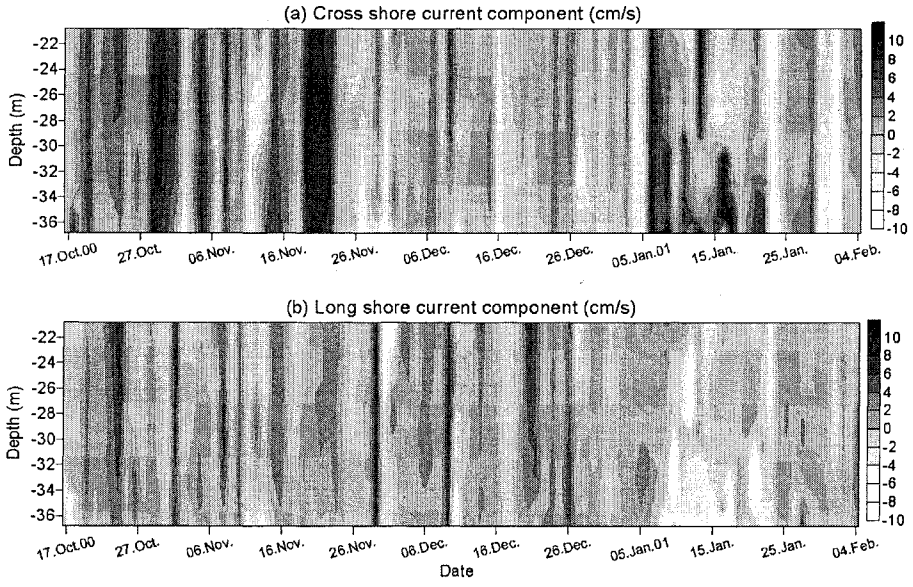

Figure 3.41: Time series records of the (a) cross shore (cms^{-1}) and (b) long shore (cms^{-1}) current components of the 20-40 m water column in front of the MSS at position w1-a during the period of October 16th 2000 to February 4th 2001.

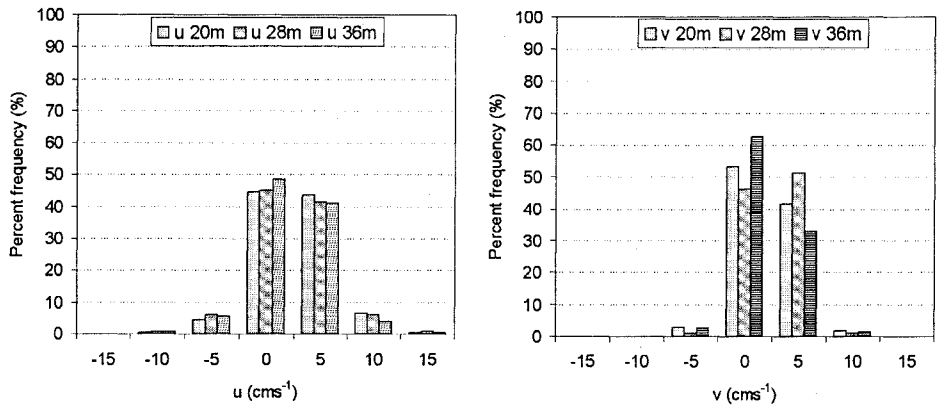

Figure 3.42: Percent frequency distribution of the current components (u & v cms^{-1}), at depths 20, 28, and 36 m, at position w1-a in front of the MSS during March 2000-February 2001.

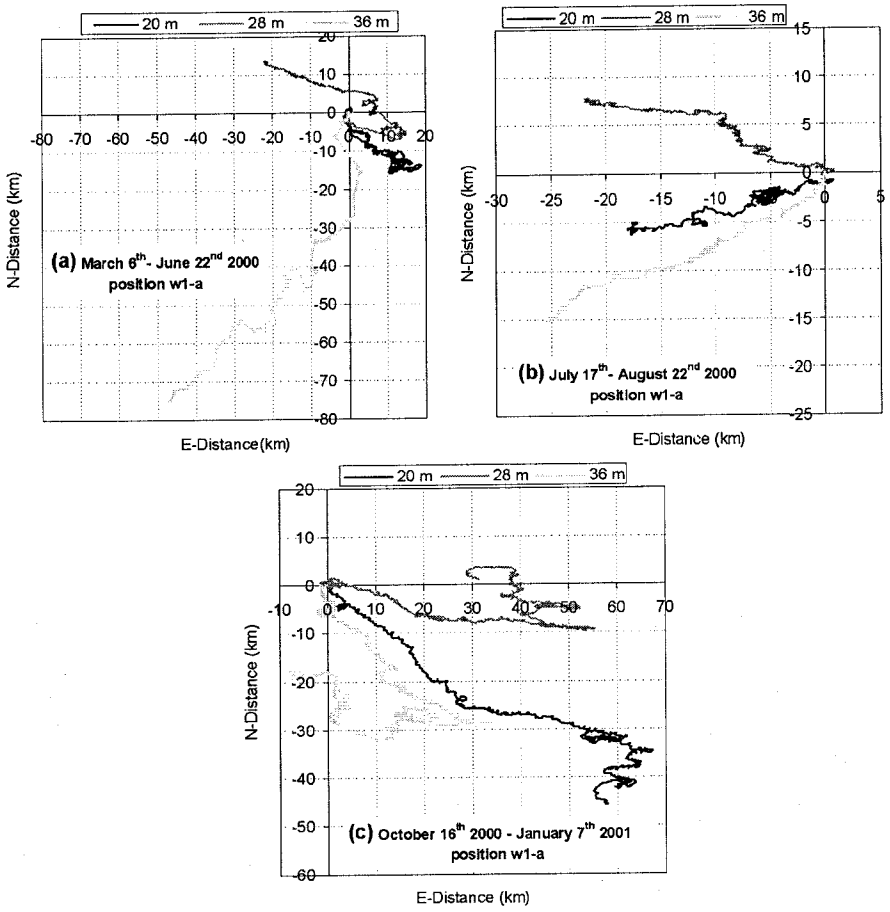

Figure 3.43: Progressive vector diagram at selected depth levels at position w1-a during three time intervals.

Next we look at the seasonality of the coastal current in the canyon area as recorded in front of the MSS from March 2000 to January 2001. To detect differences between the seasons and to looking for any semi-diurnal or diurnal signals of the current, we apply spectral analysis and plot scatter diagrams of the current components, which are shown in Figure 3.44.

The power spectra of the current at position w1-a (in Figure 3.44 (a)) show clearly seasonal differences in the currents. In summer the semi-diurnal signal (T1-sum = 12.19 ± 0.58 hr) and diurnal signal (T2-sum = 24.54 ± 2.36 hr) are obviously present. During winter, the semi-diurnal signal was also clearly detected (T1-win = 12.46 ± 0.61 hr), while the diurnal signal was missing. The tidal signals disappeared during spring. This result agrees with the absence of diurnal or semidiurnal signals in spring 1999 during the Meteor cruise in the northern gulf (Figure 3.25).

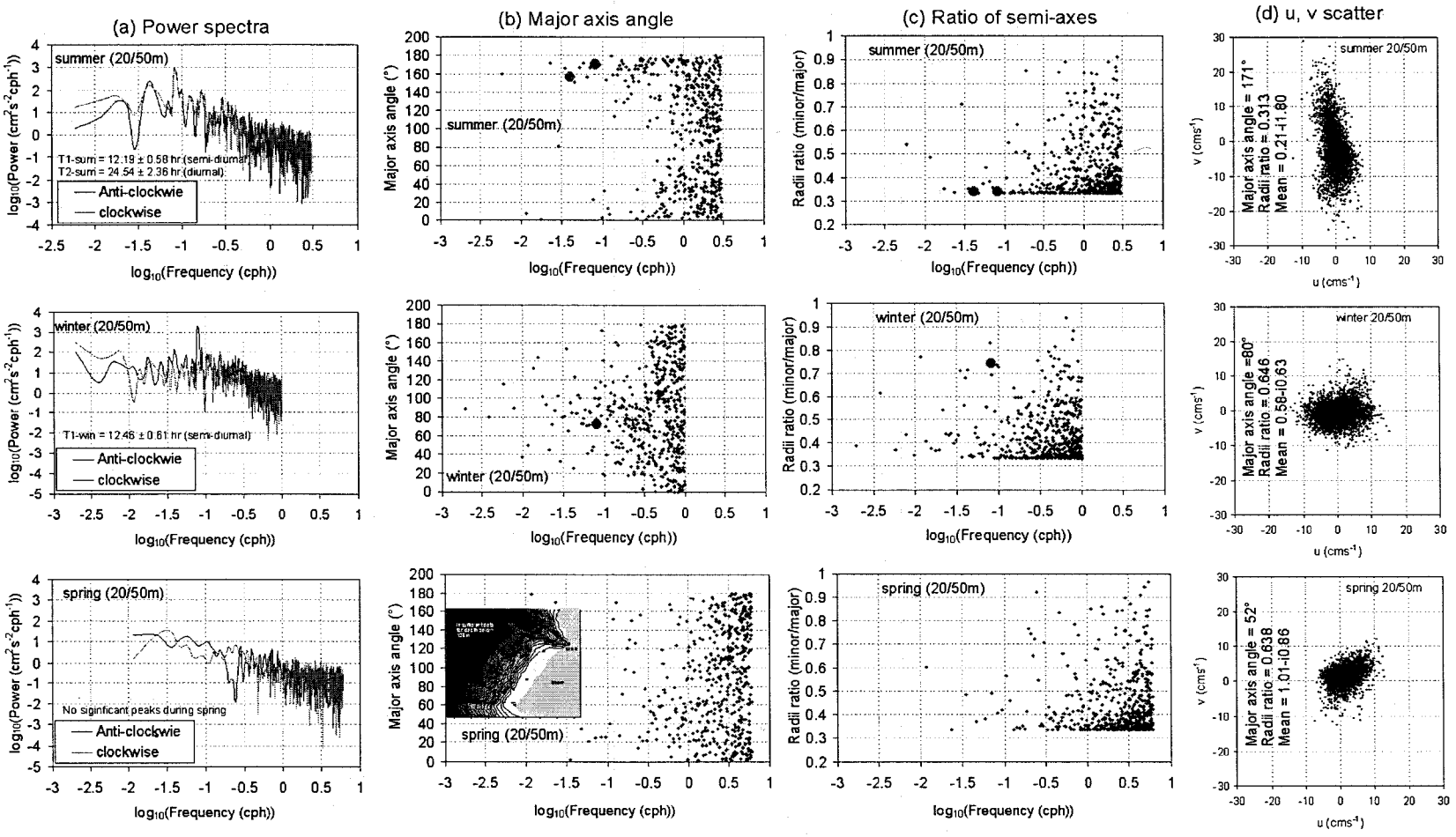

Figure 3.44: Spectrum analysis of the current (a, b, and c), and (d) u v scatter at 20 m at position w1-a in front of the MSS during summer, winter, and spring 2000/2001.

The scatter plots of the currents have an elliptic structure, Figure 3.44 (d). The ratio of the semi-axes (minor/major) of the elliptic shape of the scatter plots of current during summer, winter, and spring were 0.313, 0.646, and 0.638, respectively. During summer the major axis was parallel to the north-south direction, while during winter and spring the scatter plots show an almost circular shape, see Figure 3.44 (d). These agree well with the major axis and radii ratio distribution in Figure 3.44 (b) and (c), which were resulted from the spectrum analysis of the current vector data. In the next section, the same spectrum analysis of the current vector will be applied also to the current in 20 m depth on the slope area (w2).

For the coastal location (w1-b) in the shelf area (see Figure 2.5 and Table 2-4), the time series of the (a) cross shore, (b) long shore, (c) vertical w current components (all in cms^{-1}), and (d) relative backscatter intensity RBI (db) during three different time intervals in summer 2001 are shown in Figure 3.45, Figure 3.46, and Figure 3.47, respectively. It is obvious from the figures (a) and (b), the current in the shelf area was directed to SSE-SSW over the whole water column, 4-32 m. The current decreased with increasing the depth, where the mean value in the upper 11 m was 5.5 cms^{-1}, and near the bottom between 25 to 32 m water column, the current mean was 0.7 cms^{-1}. The mean values of u and v of different depths are listed in Table 3-6.

The progressive vector diagram at three depths ~10, 20, and 32 m is drawn in Figure 3.48, clearly, the current track in the shelf area was towards SSE-SSW during summer 2001 (July-October).

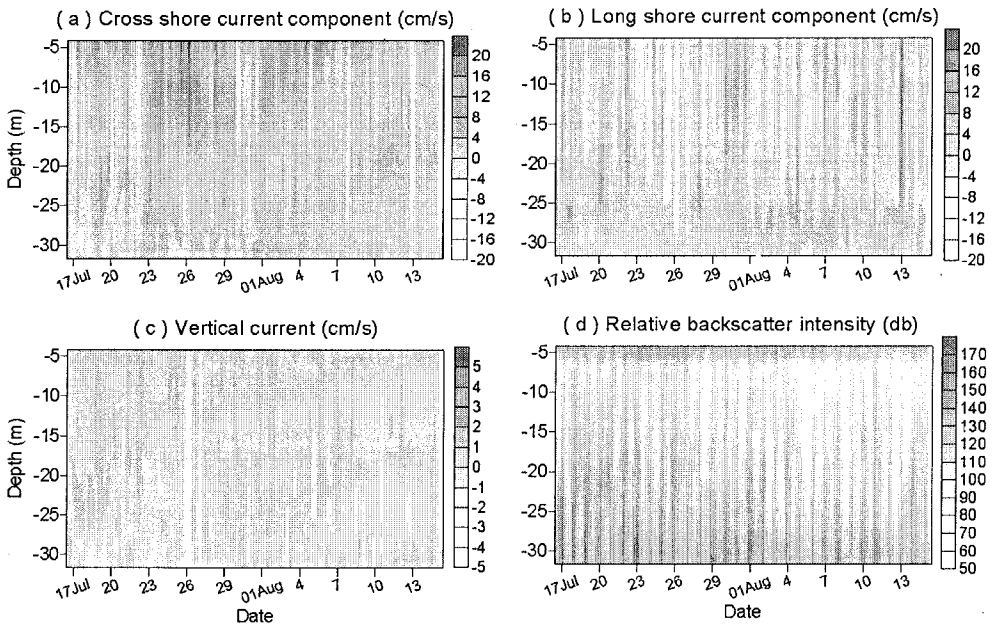

Figure 3.45: Time series records of the (a) cross shore (cms^{-1}), (b) long shore (cms^{-1}) current components, (c) vertical current (cms^{-1}), and (d) relative backscatter intensity (db) of the 4-32 m water column in front of the MSS at position w1-b during the period of July16th to August 15th 2001.

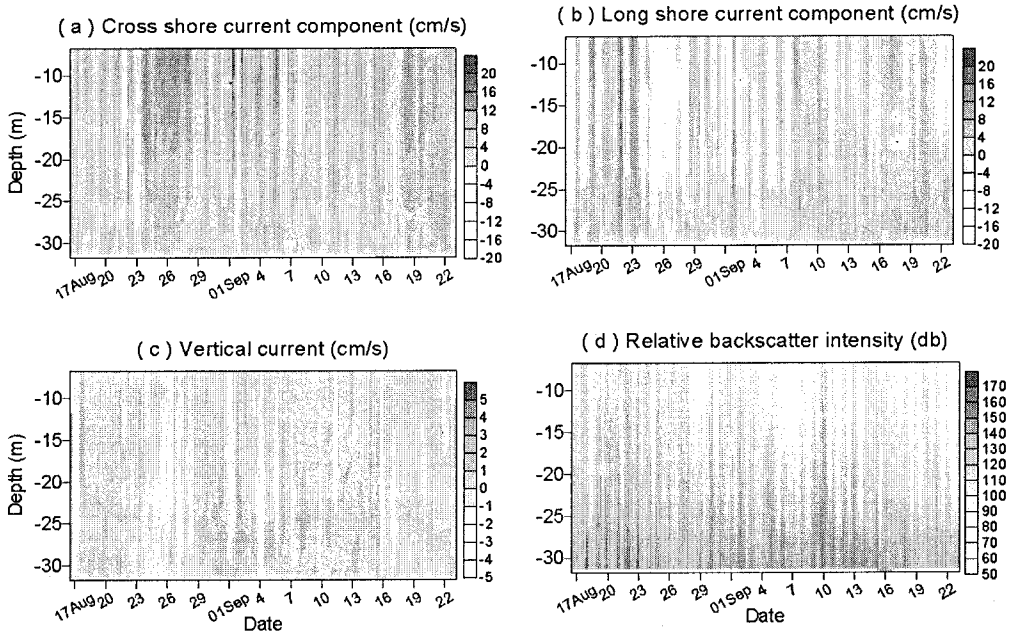

Figure 3.46: Time series records of the (a) cross shore (cms^{-1}), (b) long shore (cms^{-1}) current components, (c) vertical current (cms^{-1}), and (d) relative backscatter intensity (db) of the 4-32 m water column in front of the MSS at position w1-b during the period of August 16th to September 23rd2001.

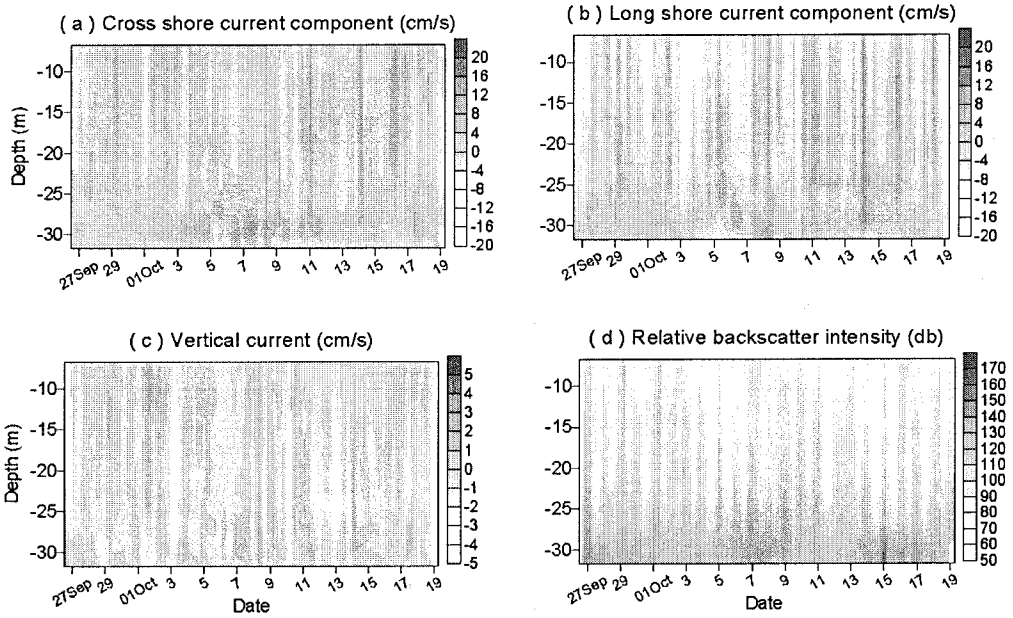

Figure 3.47: Time series records of the (a) cross shore (cms^{-1}), (b) long shore (cms^{-1}) current components, (c) vertical current (cms^{-1}), and (d) relative backscatter intensity (db) of the 4-32 m water column in front of the MSS at position w1-b during the period of September 26th to October16th2001.

Table 3-6: Mean values of the u and v in different depth interval at position w1-b in front of the MSS during three different time intervals in summer 2001.

	Jul. 16th -Aug.15th 01		Aug.16th-Sep. 23rd 01		Sep. 26th-Oct.19th 01	
	Mean (cms^{-1})		Mean (cms^{-1})		Mean (cms^{-1})	
Depth (m)	u	v	u	v	u	v
4-11	2.66	-3.39	3.40	-4.84	-3.21	-5.61
11-19	0.42	-2.21	0.61	-3.41	-3.34	-3.13
18-25	-0.01	-1.36	-0.26	-2.16	-2.74	-1.04
25-32	-0.20	-0.10	-0.33	-0.53	-1.21	-0.52

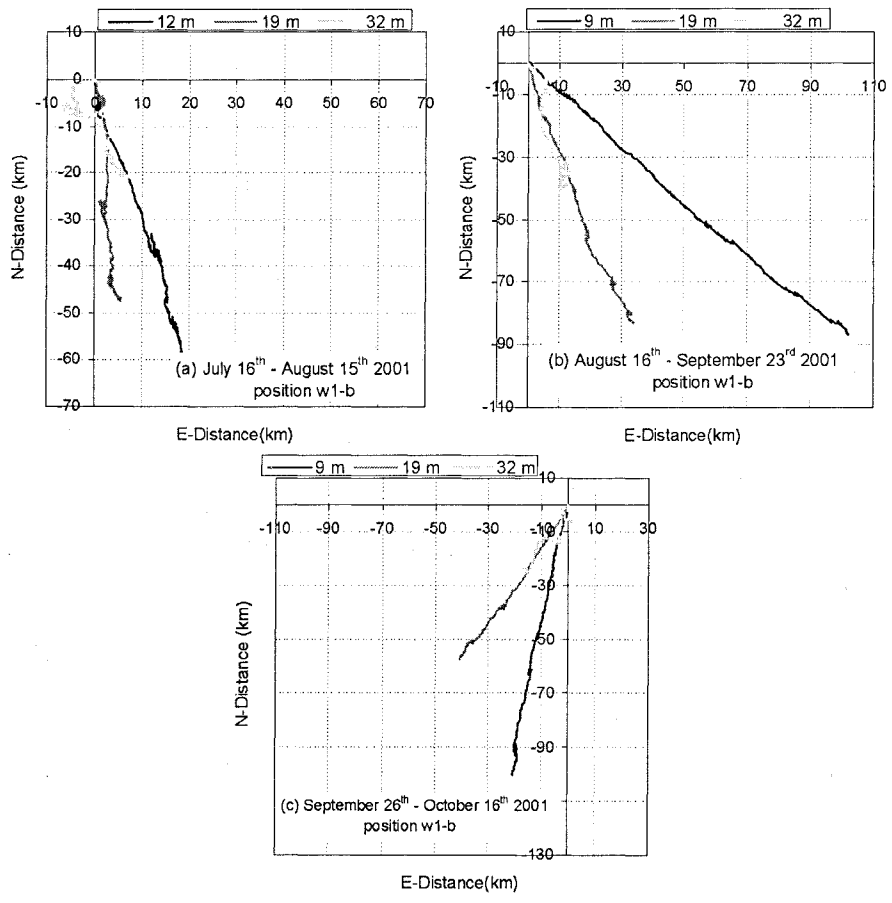

Figure 3.48: Progressive vector diagram at selected depth levels at position w1-b during three time intervals.

The time series of the vertical current (w) and relative backscatter intensity (RBI) in the 4-32 m depth, as shown in Figure 3.45 to Figure 3.47 (c) and (d), reveal four main features: (1) a significant increasing of RBI with depth between 20-32 m, (2) a clear periodic variation in RBI and w, (3) an apparently concurrence between RBI and w especially during scatterers activity, and (4) a prevailing downward motion with relatively high velocities assuming values of a few centimeters per second.

Feature (1) can be well seen in Figure 3.45 to Figure 3.47. In order to study features (2) and (3) in more detail, a spectrum analysis of w and RBI at 20 m depth was performed for the time

between August 16th 2001 and October 16th 2001. The power spectra of both w (cms^{-1}) and RBI (db) are shown in Figure 3.49. Three significant peaks were detected, diurnal (23.36 ± 3.26 h), semidiurnal (11.9 ± 0.83 h) and at a period of 7.91 ± 0.37 h. The periods of all three peaks are close to the periods of the peaks a, b, and d found in the spectrum of the sea level elevation shown in Figure 3.6. This suggests that horizontal motions occurring over an inclined bottom induce vertical motions. However, there might be additionally signals with a diurnal period. Vertical convection forced by buoyancy loss due to the high evaporation and flowing dry air from land might induce downward motion particularly during daytime. Additionally, the vertical migrations of biological scatterers, such as zooplankton, imply a diurnal signal in w, which is independent of the motion generated by physical processes. In Figure 3.50 (a), the time series of w (cms^{-1}) and RBI (db) during 10 days is shown at 20 m depth. The time series of w, u, and v (all in cms^{-1}) over the same period of time at 20 m depth are shown in Figure 3.50 (b).

In principle, the RBI can be considered as a tracer transported by the velocity field, which has an active contribution w_{mig} (vertical velocity of zooplankton's migration) to the vertical component of the velocity. The transport equation of RBI is:

$$\frac{\partial RBI}{\partial t} + (u\frac{\partial}{\partial x} + v\frac{\partial}{\partial y} + w\frac{\partial}{\partial z})RBI = 0 \qquad (3.4)$$

The RBI gradient with respect to x and y is negligible, compared with the vertical component of the gradient. We assume the vertical component of the velocity to be composed of a physical w_p and a biological part w_{mig}

$$w = w_p + w_{mig} \qquad (3.5)$$

Then equation (3.4) becomes:

$$\frac{\partial RBI}{\partial t} + (w_p + w_{mig})\frac{\partial RBI}{\partial z} = 0 \qquad (3.6)$$

From equation (3.6) follows that both physical and biological vertical motions contribute to the temporal variations of RBI. The physical part of w may consist of vertical motions due to vertical convection, due to internal waves, and to vertical motions induced by horizontal motions over an inclined bottom. Vertical motions of internal waves are located in the high frequency part of the internal wave spectrum (GILL 1982). Since the ADCP measurements were performed at a site surrounded by steep bottom topography, horizontal motions may contribute to the observed variability in RBI.

The kinematic boundary condition that no flow is possible through a rigid boundary $A(x, y, z)$ can be expressed by (see e.g. FENNEL & LASS 1989):

$$\frac{dA}{dt} = \vec{u}.\nabla A = -u\frac{\partial H}{\partial x} - v\frac{\partial H}{\partial y} + w_p = 0 \qquad (3.7)$$

Or

$$w_p(x, y, H(x, y)) = u\frac{\partial H}{\partial x} + v\frac{\partial H}{\partial y} \qquad (3.8)$$

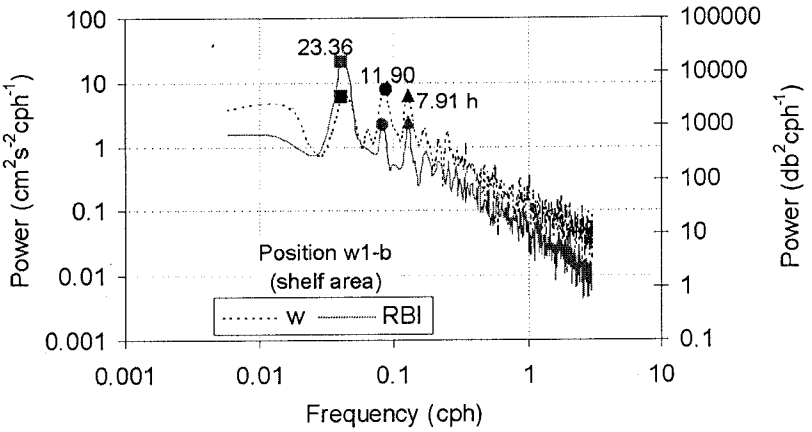

Figure 3.49: Power spectrum of the vertical current w (cms^{-1}) and relative backscatter intensity RBI (db) at position w1-b during August 16th-October 16th 2001.

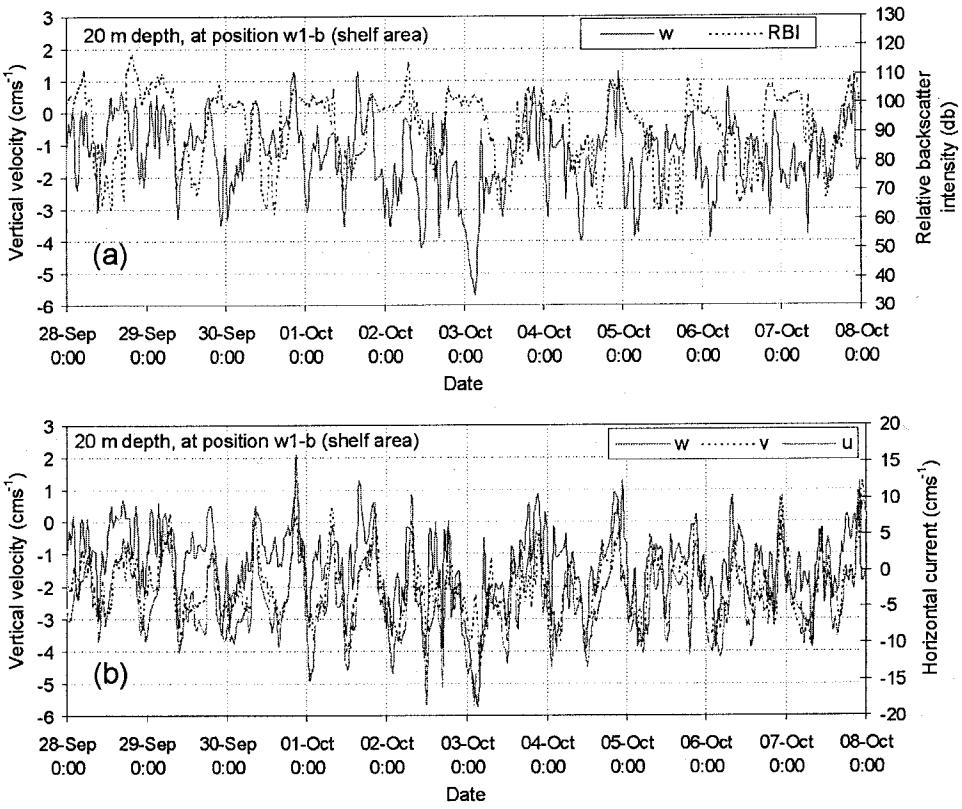

Figure 3.50: Time series of (a) w (cms^{-1}) and RBI (db) during 10 days at 20 m depth, and (b) time series of w, u, and v (all in cms^{-1}) over the same period of time at 20 m, at position w1-b.

Thus horizontal motions of water particles projected on the gradient of the bottom topography induce vertical velocities. Therefore, the semidiurnal and diurnal current signals as well as seiches are likely to contribute to the vertical current signals at the measuring site.

High coherence between the horizontal and vertical current component should exist where the relation (3.8) is valid. However, coherence can be reduced by signals in w, which are not

correlated with u and v. Among these is the white noise of the ADCP current measurement itself and the vertical migration of the scatterers.

The bottom topography in the vicinity of the measuring site is shown in Figure 3.51. The gradient of the topography is directed toward 300° from north. The amount of the bottom gradient was determined by the depth difference along the direction of the gradient between the deepest point $H(x_f, y_f)$=750 m at a distance L=3.5 km from the shore point (x_o, y_o);

$$\frac{H(x_f, y_f) - H(x_o, y_o)}{L} = \frac{750}{3500} = 0.21.$$

The coherence between the horizontal and the vertical current components are shown in Figure 3.52 (a). There is no coherence between u and w except for the diurnal period where the coherence is marginally only. This could be due to the orientation of the tidal motion whose direction of the scatter ellipse is aligned 160 to 170° north. Hence, the east component of the tidal motion has a minor contribution compared to the north component. However, the convection forcing the water to move down slope could cause the marginal coherence at the diurnal period. Significant coherence between the v and w components of current is found at the semidiurnal period and marginally coherence at the 7.48 h period. This pattern of coherence can be explained by the strong signal in v and the low uncorrelated motion of w at both the semidiurnal and the seiches period whereas the uncorrelated signals may be strong at the diurnal period.

The transfer function and the phase between the north and the vertical current components are shown in Figure 3.52 (b). The phase is not significantly different from zero for periods larger than the seiches period. The transfer function varies between 0.1 and 0.15 in the relevant range of periods. From equation (3.8) we obtain the coherent transfer between the north and the vertical current component due to the bottom boundary condition as:

$$\left|\frac{w}{v}\right| = |\nabla H \cos\alpha| = 0.21\,|\cos(120°)| = 0.105 \qquad (3.9)$$

This agrees quite well with the observed value of the transfer function, indicating that the rough estimation of ∇H represents the real bottom gradient at position w1-b.

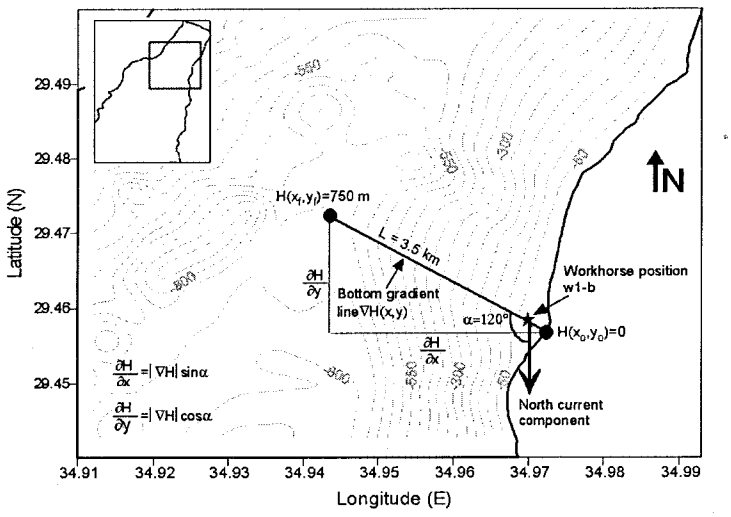

Figure 3.51: The bottom topography in the vicinity of the measuring site (w1-b).

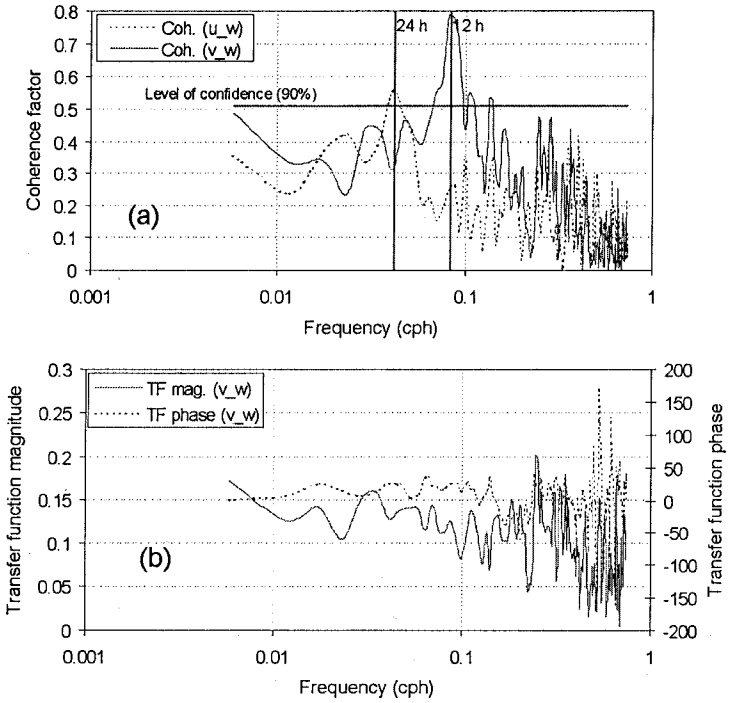

Figure 3.52: Cross correlation test of w with u and v (all in cms^{-1}), occasioning (a) the coherence factor distribution versus the frequency between u and w, and between v and w, and (b) the transfer function and phase distribution versus the frequency between v and w, at position w1-b during August 16th-October 16th 2001.

The coherence between the vertical component of the current and the RBI is shown in Figure 3.53. There is a marginal coherence of about 0.5 between both parameters at the diurnal and the semidiurnal periods. This means that the signal to noise ratio is of O(1) with a slightly stronger signal at the diurnal period. This implies that either the vertical motion at the diurnal period due to the migration of zooplankton or due to convection or both together are of the same order as the vertical motion induced by the horizontal motion over the inclined bottom.

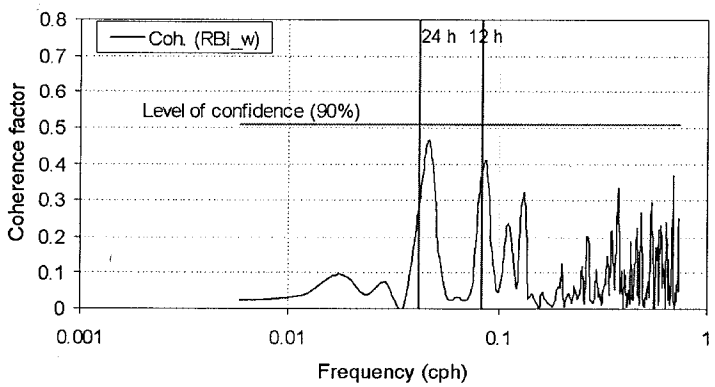

Figure 3.53: Coherence factor distribution versus the frequency between RBI (db) and w (cms^{-1}), at position w1-b during August 16th-October 16th 2001.

In order to study the stability of the distribution of RBI and w, which were represented mainly by a diurnal signal, the mean variation of RBI (db) and w (cms^{-1}) for 24 hours was calculated over 94 days during the measurements period at position w1-b (Figure 3.54) to estimate the distinguished variation from that of noise, particularly, the feature of the prevailing downward motion with relatively high velocities. Statistically, the maximum variation range of RBI and w during 24 hours exceed by about 4.3 and 2.9 times, respectively, that of $2\sigma_N/(N)^{-1/2}$, where σ_N is the standard deviation and N is the sampling number. The statistical term $2\sigma_N/(N)^{-1/2}$ represents the maximum error band where the variations through it are not significant. This implies that the periodic variation of RBI is not influenced significantly by noise, while w variation was relatively perceivable, see Figure 3.54. It can be seen from Figure 3.54 that the vertical current at position w1-b remained downward all time, which may related to the convection resulting from the high evaporation affined with dry air flowing from land to the coastal surface waters, particularly during daytime. Therefore, a permanent convection is likely to occur during summer in coastal waters, which are characterizing of (1) relatively high inclined bottom (2) high evaporation and (3) blowing of dry air. Moreover, the decreasing magnitude of the vertical current |w| from 1.0 cms^{-1} at midday to about 0.3 cms^{-1} on nighttime was clear (Figure 3.54), which could attributed to the upward migration of zooplanktons. Thus, the migrating zooplanktons affect the measured vertical speed; they reduce the signals when they move upward and may enhance the signal during their downward motion. This indicates the importance of migration leverage on w measurements. After the scatterers became passive, |w| started to increase, which obviously indicates the dominance of the convection on w. In general these results support the suggested of the influence of the convection and the migration of zooplankton on the vertical motion measurements.

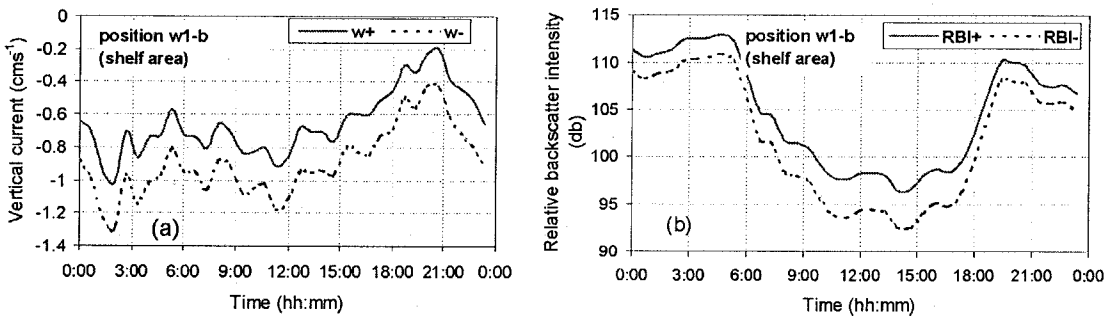

Figure 3.54: Distribution of the maximum and minimum deviation about the daily average of (a) w (cms^{-1}) and (b) RBI (db) at 20 m depth at position w1-b. The ± sign means: mean value ± $\sigma_N/(N)^{-1/2}$, where N is the sampling number (94 days) andσ_N is the standard deviation.

3.5.2.1.2 Currents on the slope area (w2)

Time series of the horizontal and vertical w current components, all in cms^{-1}, and the relative backscatter intensity RBI (db) are shown for the 20-80 m water column in Figure 3.55, Figure 3.56, and Figure 3.57, for the periods March 6th-April 12th 2000 (spring), April 17th-May 16th (early summer) 2000, and May 17th -July 9th 2000 (summer), respectively. Figure 3.58 shows the mean value of the u and v profiles for the 20-80 m water column from March 6th to July 9th 2000. In Figure 3.59 the progressive vector diagram during spring, and summer periods at depths 20, 40, 60, and 80 m are plotted.

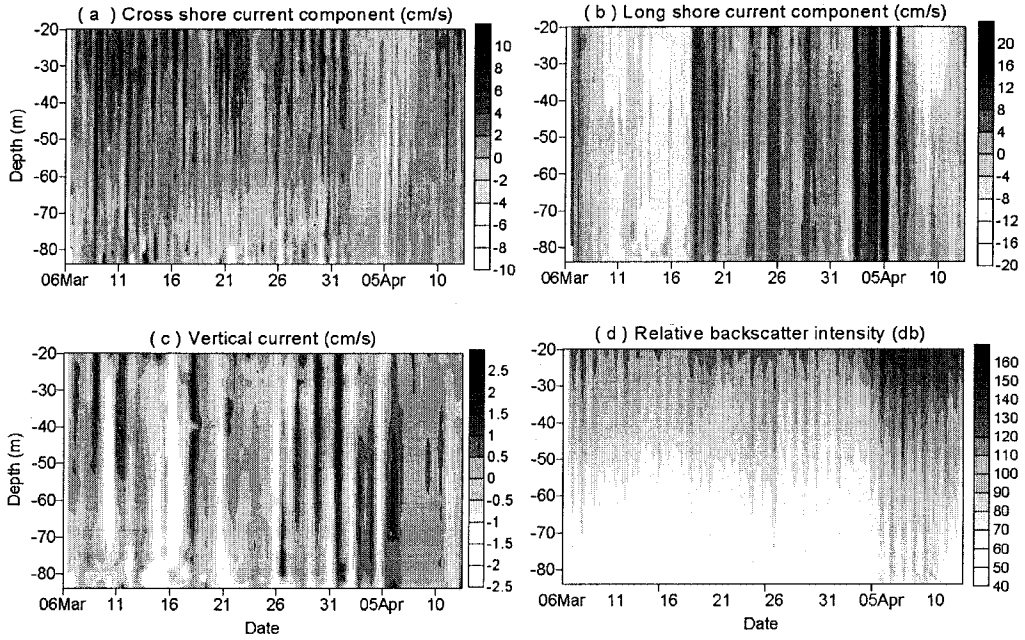

Figure 3.55: Time series records of the (a) cross shore (cms^{-1}), (b) long shore (cms^{-1}) current components, (c) vertical current (cms^{-1}), and (d) relative backscatter intensity (db) of the 20-80 m water column in front of the MSS at position w2 during the period of March 6th to April 12th 2000.

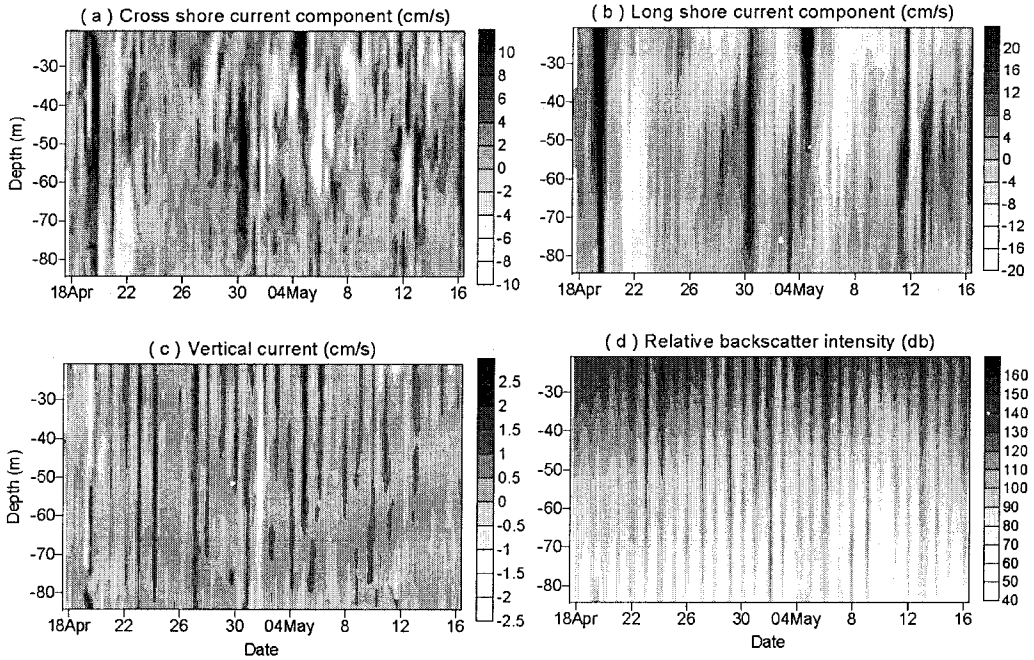

Figure 3.56: Time series records of the (a) cross shore (cms^{-1}), (b) long shore (cms^{-1}) current components, (c) vertical current (cms^{-1}), and (d) relative backscatter intensity (db) of the 20-80 m water column in front of the MSS at position w2 during the period of April 17th to May 16th 2000.

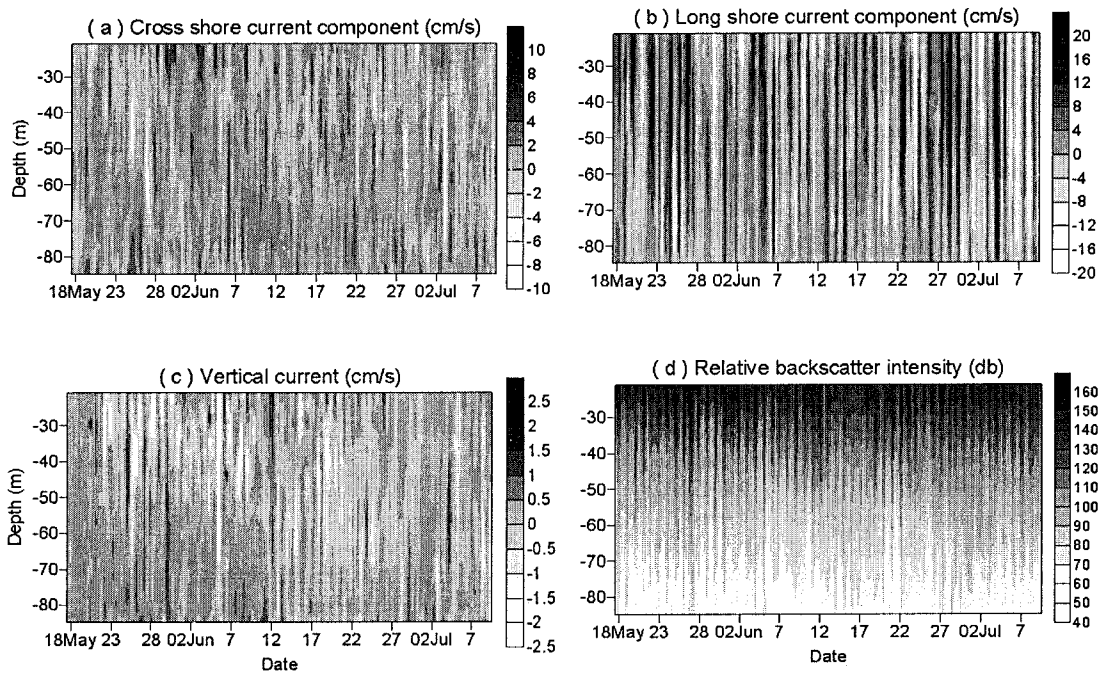

Figure 3.57: Time series records of the (a) cross shore (cms^{-1}), (b) long shore (cms^{-1}) current components, (c) vertical current (cms^{-1}), and (d) relative backscatter intensity (db) of the 20-80 m water column in front of the MSS at position w2 during the period of May 17th to July 9th 2000.

The currents are mainly parallel to the axis of the gulf, i.e. the east current component was weak compared to the north component. In general, the current track during spring-summer seasons was fluctuating from NNE to SSW direction, mostly with a regular frequency. The transition period of the direction was nearly 3.5 days. The factors, which controlled the reversed of the currents at position w2, were the reversed winds and thermohaline forces. The coherence between the filtered north component of the wind (Vy) and the current (v) at 20 m depth appeared well compatibility with respect to the time in spring-summer seasons, but with a delay of v relative to Vy, see Figure 3.60. While the wind was directing to the south with $|Vy|>4$ ms^{-1}, v was following in the same direction, but when Vy became calmer or switched to north direction, v began to has the opposite direction to the north.

The current pattern during summer had a clearer trend in comparison to the spring. The current pattern during summer could be separated into three main layers, one from 20-60 m water column with northward current, second, a transition layer around 60 m depth, and third, from 60-80 m with southward current, see Figure 3.58 and Figure 3.59. The speed range in the 20-80 m at position w2 was between 0 to 45 cms^{-1}, with a mean value of 6.4 cms^{-1}, and a standard deviation of 4.7 cms^{-1}.

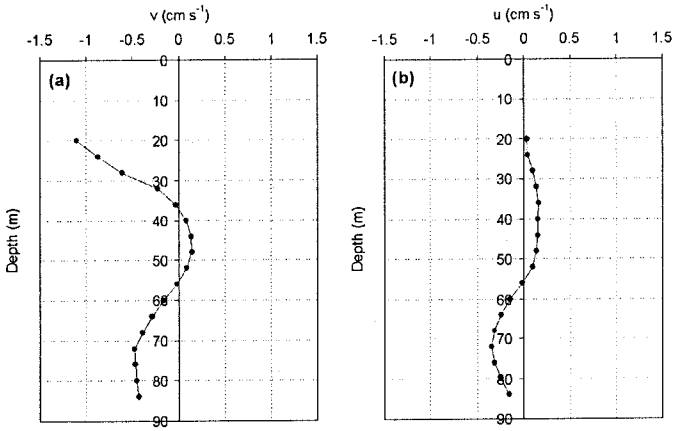

Figure 3.58: Mean profiles of the (a) north (v cms^{-1}) and (b) east (u cms^{-1}) current components for the 20-80 m water column at position w2 in front of the MSS during the period of March 6th to July 9th 2000.

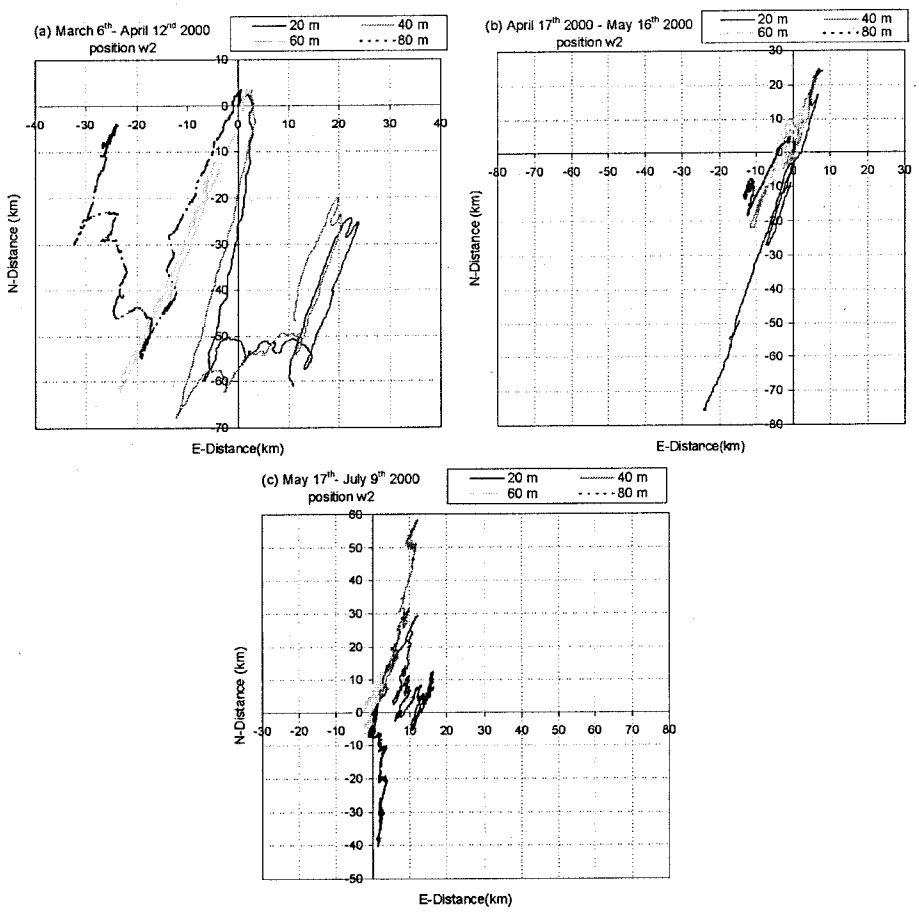

Figure 3.59: Progressive vector diagram at selected depth levels at position w2 during three time intervals.

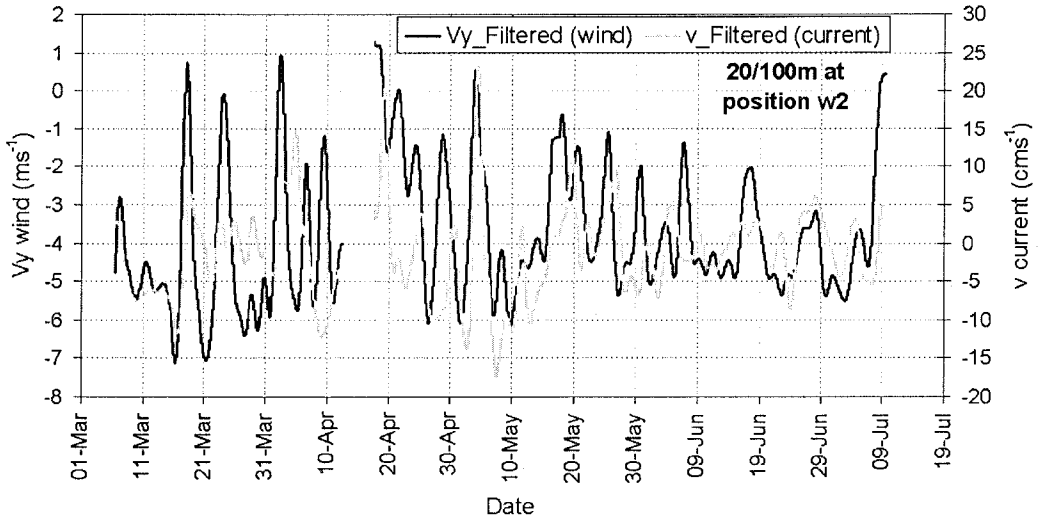

Figure 3.60: Time series variation of the north components of the wind and the current at 20 m depth at position w2 during March 6th-July 9th 2000.

The power spectra and the scatter plots of the currents at position w2 were estimated for summer and spring seasons, as seen in Figure 3.61. This analysis shows no significant signal for a semi-diurnal or diurnal current pattern during spring, while a clear semi-diurnal signal occurred during summer (T1-sum = 12.19 ± 0.58 hr), see Figure 3.61 (a). This agrees completely with the results of the spectral analysis at position (w1-a) during spring 2000 (Figure 3.44), and is in accordance with the absence of diurnal or semidiurnal signals during spring 1999 in the northern gulf during R/V Meteor 44/2 (Figure 3.25). The ratio of the semi-axes (minor/major) of the elliptic scatter plot of the current components during summer and spring were 0.217 and 0.264, respectively. The major axis deviated about 20° clockwise of the north-south axis during summer and spring, see Figure 3.61 (d). These findings agree well with the results from the spectrum analysis of the current data, shown in Figure 3.61 (b) and (c).

The time series of w and RBI in slope area (w2) in Figure 3.55 to Figure 3.57 during spring-summer 2000 have similarities with those during summer 2001 in shelf area (w1-b) as shown in Figure 3.45 to Figure 3.47. The major difference of RBI distributions between both positions is that at position w2 RBI decreases with depth below 20 m, while at position w1-b it increases with depth between 20-32 m. This is due to larger bottom depth of about 100 m at compared with the bottom depth of 37 m at position w1-b. The spring bloom could be seen in Figure 3.55, when the RBI increased significantly after April 5th.

Figure 3.62 shows the spectral analysis of w (cms^{-1}) and RBI (db) at position w2 during the spring-summer season. The analysis reveals three peaks of w and RBI; 23.36 ± 2.15 hr (diurnal), 11.90 ± 0.55 hr (semidiurnal), and 5.95 ± 0.09 hr (half of semidiurnal). These signals are approximately the same signals as those found at position w1-b (see Figure 3.49), but the spectral level of the signals 11.90 and 5.95 hr is about one order of magnitude smaller compared with those at position w1-b. Figure 3.63 shows (a) RBI (db) and w (cms^{-1}) distribution, and (b) u, v, and w (all in cms^{-1}) distribution during 10 days at 20 m depth.

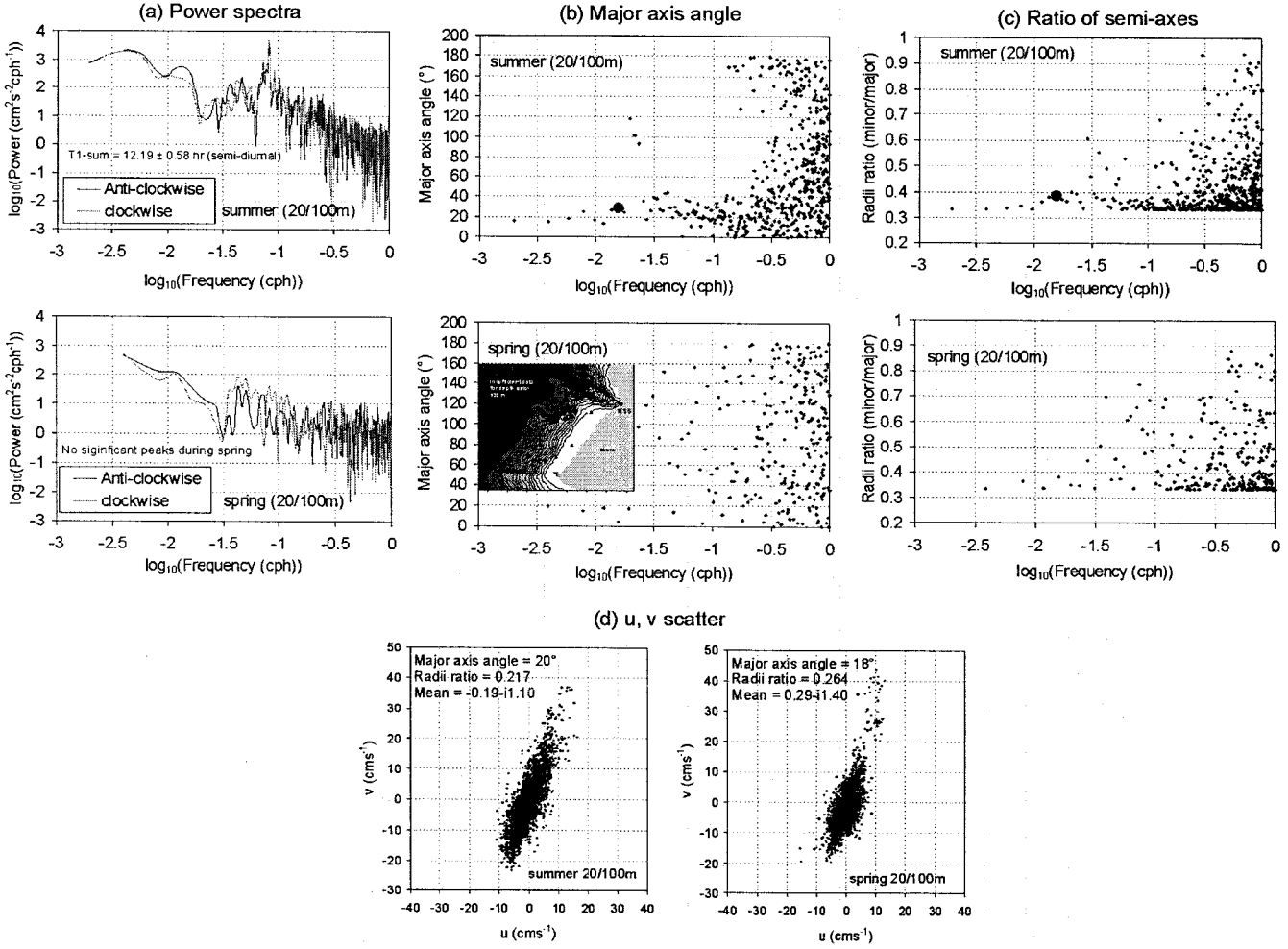

Figure 3.61: Spectrum analysis of the current (a, b, and c), and (d) u v scatter at 20 m depth at position w2 in front of the MSS during summer, and spring 2000/2001.

The spectrum analysis (Figure 3.61) of u and v showed only a semidiurnal signal at position w2. Moreover, the u and v scatter plot depicted an elliptic shape with the major axis perpendicular to the bottom gradient, i.e. horizontal motions will not induce vertical motions at this site. Figure 3.64 shows the cross correlation test between RBI (db) and w, u and w, and between w and v, (u, v, and w are in cms^{-1}). No coherence is found between the horizontal and the vertical component of the current. This means that the signal, indicated by the peaks in Figure 3.63, of the measured vertical current is lower than the noise. The coherence between the vertical component and the RBI is marginal at the diurnal period. This implies that the vertical migration of zooplankton occurs at a velocity of the order of the instrumental noise of the instrument.

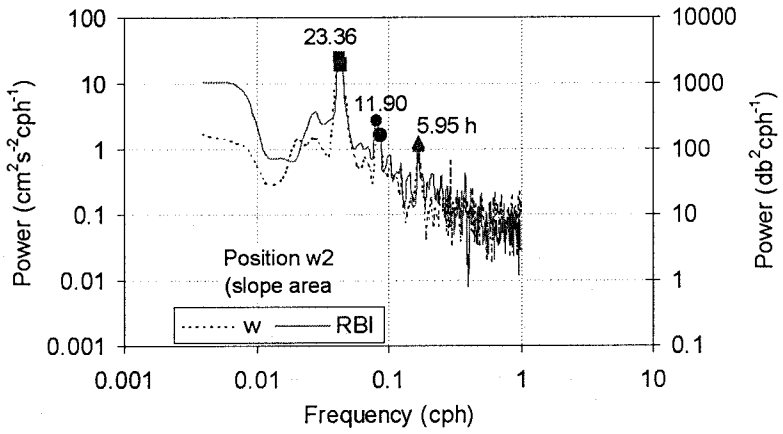

Figure 3.62: Power spectrum of the vertical current w (cms^{-1}) and relative backscatter intensity RBI (db) at position w2 during spring-summer 2000.

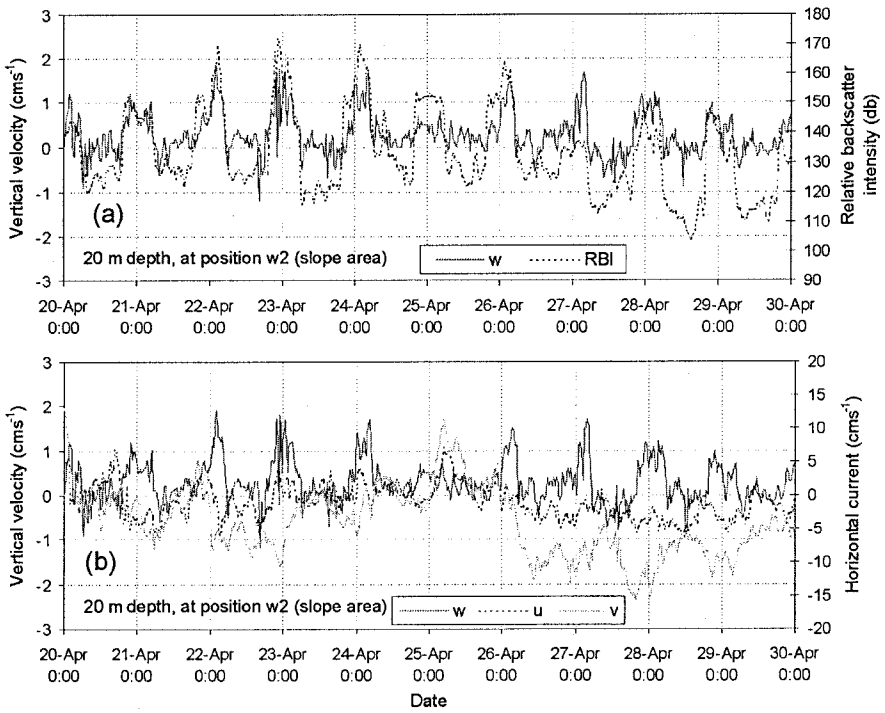

Figure 3.63: Ttime series of (a) w (cms^{-1}) and RBI (db) during 10 days at 20 m depth, and (b) time series of w, u, and v (all in cms^{-1}) over the same period of time at 20 m, at position w2.

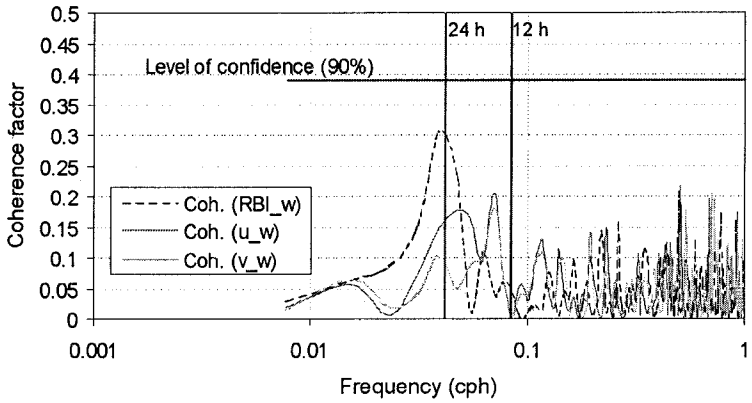

Figure 3.64 Coherence factor distribution versus the frequency between RBI (db) and w, u and w, and between v and w (u, v, and w all in cms^{-1}) at position w2 during spring-summer 2001.

To detect the interfered signal to noise ratio on w and RBI, the daily average of the variations of RBI (db) and w (cms^{-1}) over 80 days, shown in Figure 3.65. It follows that the influence of noise is weak on RBI and relatively stronger on w. The measurement errors represent 41% and 22% of the maximum variation range of w and RBI, respectively. Therefore, it is not likely to find an obvious coherence between w and RBI in case of the high ratio (3:2) between the vertical speed and instrumental noise. Moreover, vertical current was not distinguishable whether it was upward or downward.

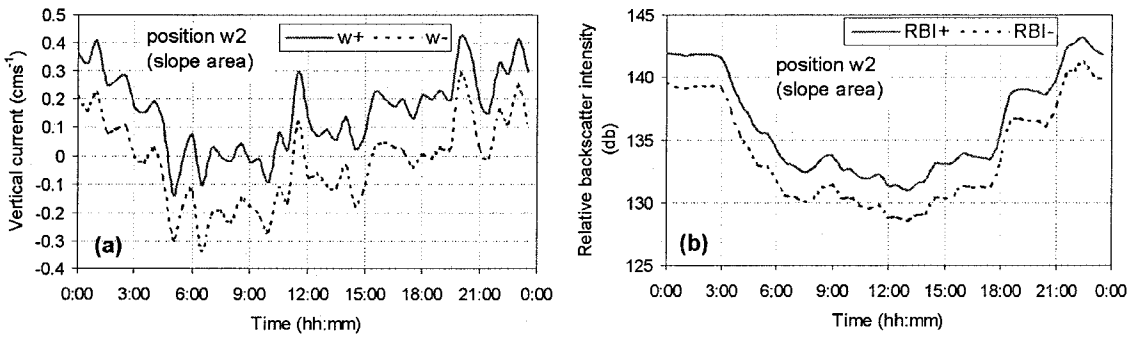

Figure 3.65 Distribution of the maximum and minimum deviation about the daily average of (a) w (cms^{-1}) and (b) RBI (db) at 20 m depth at position w1-b. The ± sign means: mean value ± $\sigma_N /(N)^{-1/2}$, where N is the sampling number (80 days) and σ_N is the standard deviation.

3.5.2.2 Circulation in the northern tip of the Gulf of Aqaba

3.5.2.2.1 Current patterns

In this investigation, many tracks have been worked to measure the current patterns in the northern tip of the Gulf of Aqaba. These are the first direct current measurements in the deeper waters of this area. Several tracks have been made along the gulf axis in the Jordanian sector of the Gulf of Aqaba using ADCP 150 kHz during January-August 2001.

All tracks scanned by the ADCP, which will be discussed in this and the next section, were performed in the Bottom Track Mode with average time interval of 50 seconds for each ensemble, 40 pings per ensemble, and 6 m depth cell size (see Table 2-3), where the average boat speed was about 1.5 ms^{-1}.

Figure 3.66 to Figure 3.73 show the distribution of the (a) cross shore u' (cms^{-1}) and (b) long shore v' (cms^{-1}) current components in the Jordanian waters along the gulf axis on different dates during January-August 2001. Figure 3.66 shows that the general current was towards NNW-NNE. In the southern part of the track, the current was stronger in the upper 150 m than below, in the 150-240 m water column, while the direction did not change and was mainly to the north. The u' and v' mean values were -1.4 cms^{-1} and 9.9 cms^{-1}, respectively. The current pattern differed during March 15th 2001 and August 1st 2001, Figure 3.67 and Figure 3.71, show two opposite currents in the southern Jordanian waters. In the upper 140 m, the current was towards SSE-SSW, while in the 140-240 m water column directed to NNE-NNW. In the northernmost part of the track a NE-NW current occurred in the whole water column.

On May 1st, June 14th, and July 11th 2001, the currents distribution along the track represented a two layers system, with inflow in the upper 120 m northernmost part of the gulf (NNW), and outflow below 120 to 240 m, see Figure 3.68, Figure 3.69, and Figure 3.70. The mean values of u' and v' in these two layers measured on the May 1st, June 14th, and July 11th 2001 are summarized in Table 3-7.

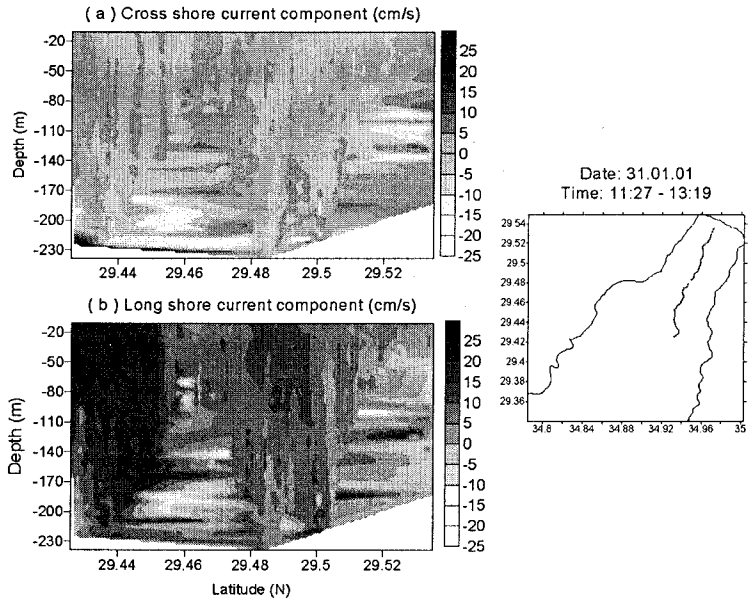

Figure 3.66: Vertical distribution of the (a) cross shore (cms^{-1}) and (b) long shore (cms^{-1}) current components along the axis of the Gulf of Aqaba, on January 31st 2001 from 11:27 to 13:19.

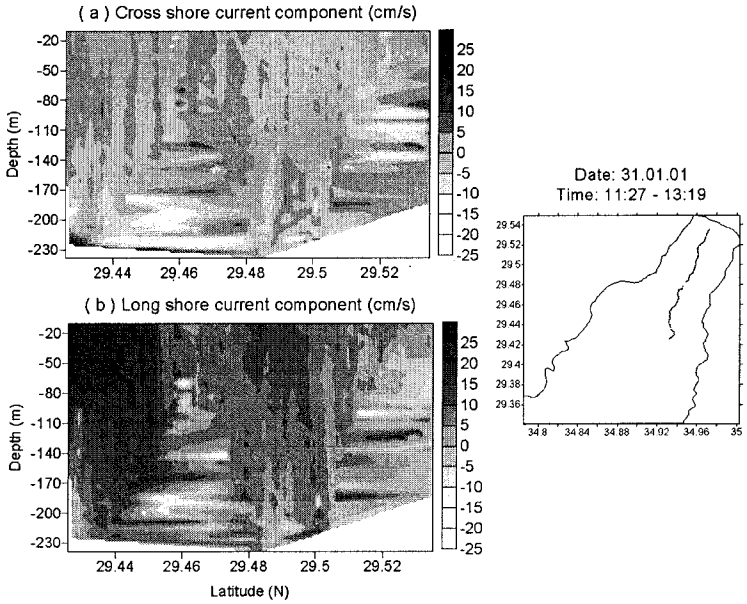

Figure 3.67: Vertical distribution of the (a) cross shore (cms^{-1}) and (b) long shore (cms^{-1}) current components along the axis of the Gulf of Aqaba, on March 15th 2001 from 11:35 to 13:11.

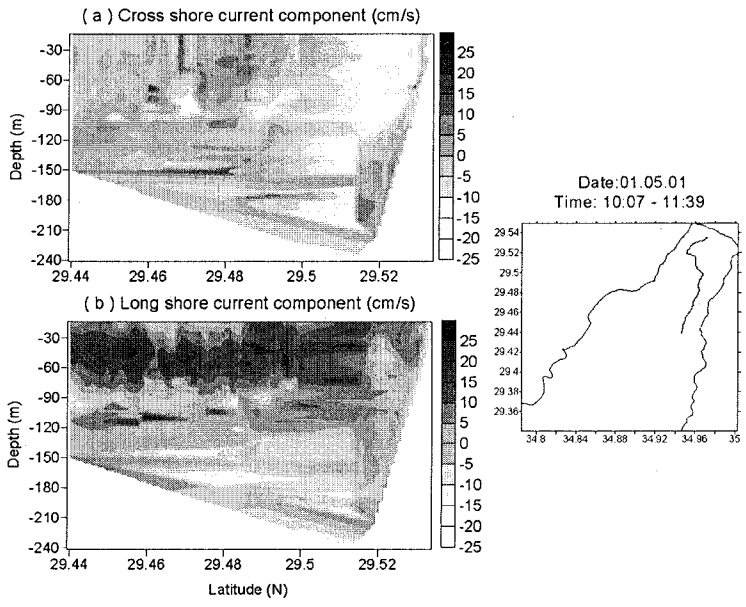

Figure 3.68: Vertical distribution of the (a) cross shore (cms^{-1}) and (b) long shore (cms^{-1}) current components along the axis of the Gulf of Aqaba, on May 1st 2001 from 10:07 to 11:39.

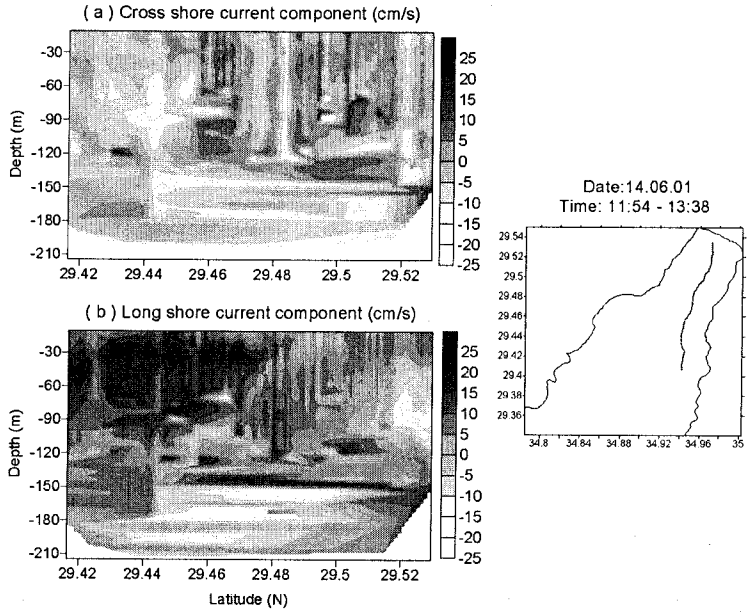

Figure 3.69: Vertical distribution of the (a) cross shore (cms^{-1}) and (b) long shore (cms^{-1}) current components along the axis of the Gulf of Aqaba, on June 14th 2001 from 11:54 to 13:38.

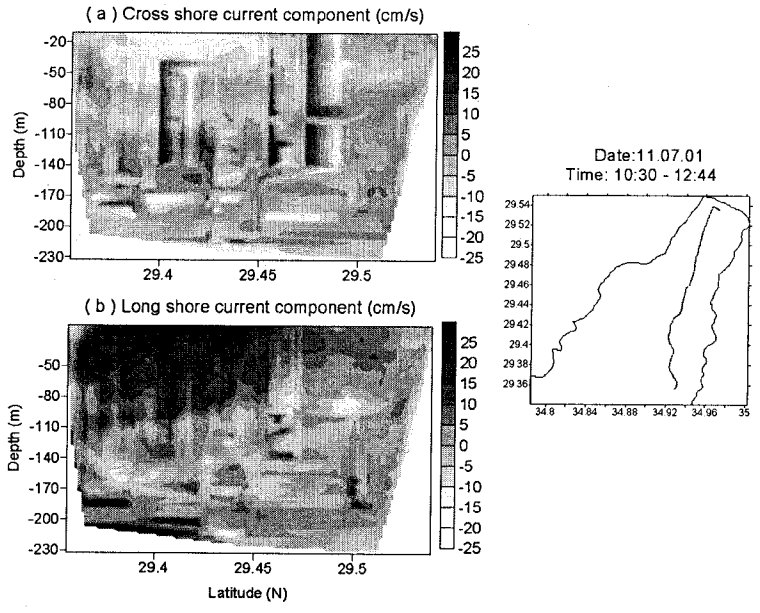

Figure 3.70: Vertical distribution of the (a) cross shore (cms^{-1}) and (b) long shore (cms^{-1}) current components along the axis of the Gulf of Aqaba, on July 11th 2001 from 10:30 to 12:44.

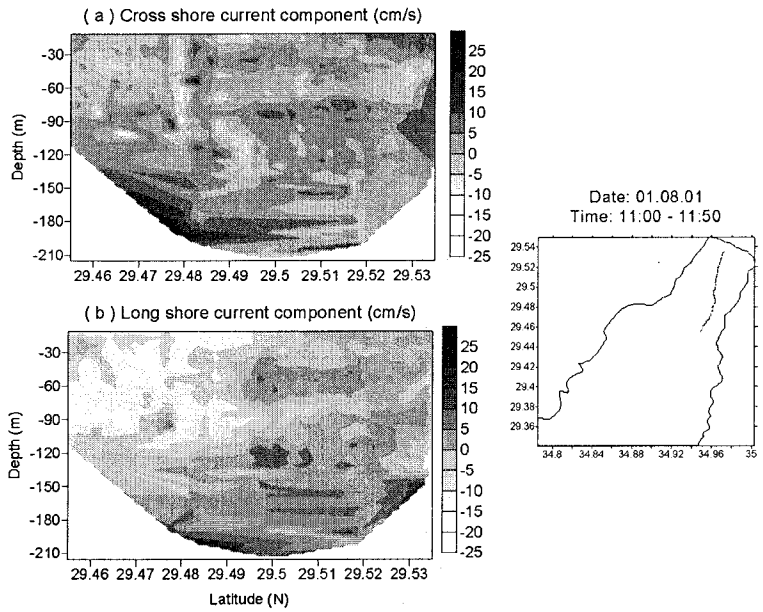

Figure 3.71: Vertical distribution of the (a) cross shore (cms^{-1}) and (b) long shore (cms^{-1}) current components along the axis of the Gulf of Aqaba, on August 1st 2001 from 11:00 to 11:50.

Table 3-7: Mean values of u' and v' (cms^{-1}) in the 0-120 m and 120-240 m of the water column on different dates along the gulf axis.

	May 1st 2001		June 14th 2001		July 11th 2001	
(cms^{-1})	0-120 m	120-240 m	0-120 m	120-240 m	0-120 m	120-240 m
u' mean	-5.6	-3.3	-1.5	-6.0	-3.4	0.1
v' mean	8.0	0.5	6.1	2.5	9.1	0

In Figure 3.72, and Figure 3.73 the current in the 0-240 m water column had similar current structures at different dates (August 5th and 19th 2001). In the upper 50 m, the current direction was SSE, and in the 50-240 m water column the current was fluctuating from SSE to SW. The mean values of u' and v' in the upper 50 m and between 50-240 m water column measured on the August 5th and 19th 2001 are summarized in Table 3-8.

Table 3-8: Mean values of u' and v' (cms^{-1}) in the 0-50 m and 50-240 m of the water column on different dates along the gulf axis.

	August 5th 2001		August 19th 2001	
(cms^{-1})	0-50 m	50-240 m	0-50 m	50-240 m
u' mean	3.0	2.0	0.9	-0.1
v' mean	-10.6	-4.1	-7.6	-0.6

The findings of this study on the currents in the deeper waters near the Jordanian coast of the Gulf of Aqaba from January 2001 to August 2001 can be summarized as:

- The main current is parallel to the axis of the Gulf of Aqaba (northward and/or southward). It was controlled by winds, which drive a SSE current in the upper part of the water column.
- A thermohaline inflow to the north in the upper 120 m depth is prevailing, while below 120 m a general outflow to the south is found.
- The current in the southern part of the Jordanian waters is stronger than in the northern part, i.e. there is an established longshore gradient of the current.
- The current patterns in the northern tip of the Gulf of Aqaba show a substantial temporal variability.

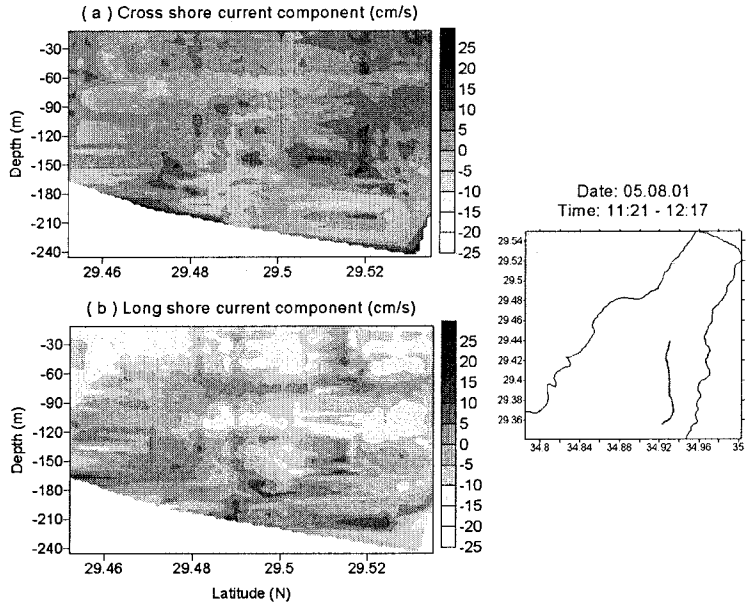

Figure 3.72: Vertical distribution of the (a) cross shore (cms^{-1}) and (b) long shore (cms^{-1}) current components along the axis of the Gulf of Aqaba, on August 5th 2001 from 11:21 to 12:17.

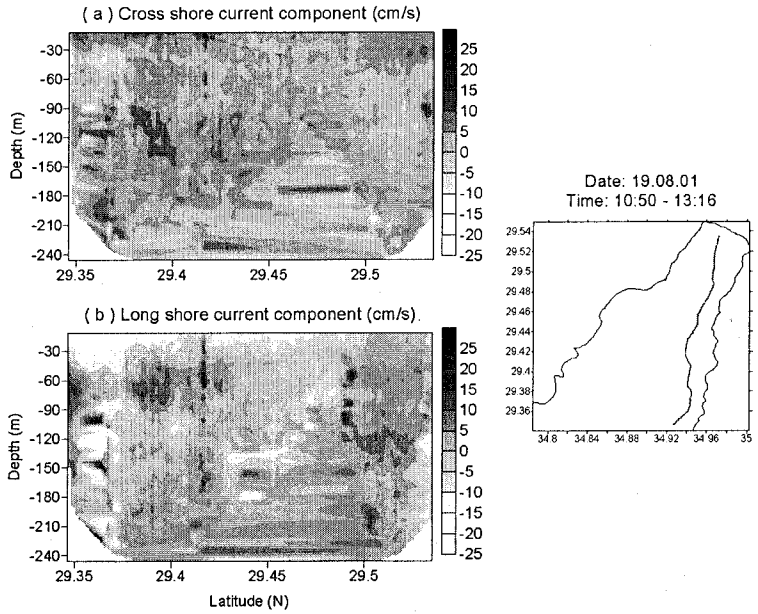

Figure 3.73: Vertical distribution of the (a) cross shore (cms^{-1}) and (b) long shore (cms^{-1}) current components along the axis of the Gulf of Aqaba, on August 19th 2001 from 10:50 to 13:16.

3.5.2.2.2 Eddy currents

The current patterns in the northern tip of the Gulf of Aqaba are changing as mentioned in the previous section. In order to obtain a more detailed view and understanding of the different type of patterns we performed several zigzag surveys in the northernmost tip of the Gulf of Aqaba between Aqaba and Eilat during summer 2001 (July-September), see Figure 3.74.

In order to understand how the flow patterns are generated we have to take local and far field aspects into account. The local aspects are mainly the topographical feature (bottom shape), while the local winds are probably of minor importance for such a small region. The far field aspect is that the flow is mainly driven by the currents in the gulf.

Owing to the summer conditions, the diurnal and semidiurnal currents are a further driving force.

Several aspects should be considered: (a) the NNW wind is dominating over the northern tip of the gulf (refer to Figure 3.2), (b) the inflow (to the north) current in the upper 120 m depth was observed (refer to Figure 3.66, Figure 3.68, Figure 3.69, and Figure 3.70), (c) the high bottom slope in this region, which reaches depths of about 700 m, (d) the phase of the tidal signals, and (e) the narrow width (5-8 km), and the semi-enclosed basin.

The results of surveys are shown in Figure 3.75-Figure 3.79, where snapshots of the horizontal currents are drawn. Each surveys lasted about 2 to 2.5 hours. The main external forces, the wind driven SSE surface current and the deeper thermohaline inflow.

These different currents are interacting with the bottom topography and can create eddies and waves. In Figure 3.75, current convergences near the eastern shore and current divergences in far waters from the coast were found upper 90 m, while seems the northern current was dominating

in deeper waters. Figure 3.76 shows an indication of small anti-cyclonic eddy in the upper 60 m, while current convergences were dominating at 90 and 125 m depths. In Figure 3.77, a SSE current obeyed with current convergence found at 10 m, while a NNE current found at 30 and convoyed with divergence at 60 m.

Figure 3.78 shows different type of patterns, SE current dominated in the upper 40 m, which could be interpreted to the wind force, N flow with anti-cyclonic eddy were found at 60 m depth, a small cyclonic eddy was observed at 90 m depth, S flow with current convergence were found at 125 m depth, and a small anti-cyclonic eddy with divergence were observed at 170 m depth.

In Figure 3.79, the thermohaline inflow seems was dominating in the upper 125 m, where the NNE current was observed complied with current convergence near the northern shore.

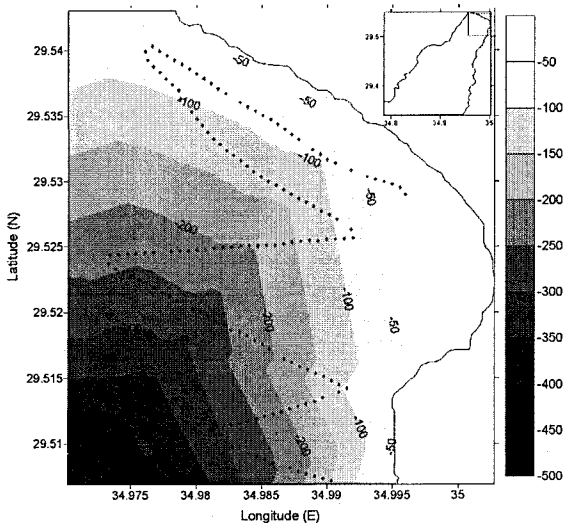

Figure 3.74: ADCP survey track in the northernmost of the Gulf of Aqaba during summer 2001.

It can be assumed that the different patterns are developing in response to variations of tidal and other diurnal and semidiurnal currents in combination with the topographical features, which play an import role in shaping the flow patterns.

Figure 3.80 shows the simultaneous measurements of current (cms^{-1}) at 11 and 23 m depths at position w1-b (refer to section 3.5.2.1.1), and the sea level variation (m) during the surveys times that were performed in the northern tip of the gulf during July-September 2001.

During the survey time on July 17th, the tide was rising, which yields a tidal current onward the northern coast, while the current measured at the same time was stably southward, see Figure 3.80 (a). Consequently, it was likely to observe a divergence of the current in the upper layers, which could be used to explain the findings seen in Figure 3.75. The second case, on July 31st, the tidal current remained northward, but the current changed from southward to northward (Figure 3.80 (b)), therefore, the two parallel currents had the ability to reverse smoothly by hitting the northern coast and contributed to create an eddy in the upper 30 m, moreover, a part of the current downwells after hitting the coast and reverses in deeper waters, where it meets the northern current to create a convergence, as shown in Figure 3.76. The southward current and tidal current, which was induced due to the sea level falling, were observed during the survey time on August 7th and 20th, see Figure 3.80 (c) and (d). The two parallel currents induce a southward current in the upper layers, where a northward current found in deeper waters to compensate the upper outflow. This

feature could be used to explain the findings seen in Figure 3.77 and Figure 3.78. The last survey was on September 5th, where the current was northward and sea level was falling (Figure 3.80 (e)), which yields a tidal current outward the northern coast. Following to that, the northward current dominates and complies with a convergence of the current near the northern coast in the upper layers, see Figure 3.79.

In summary, the variation of the phase of the tidal signals, and the diurnal and semidiurnal currents play a major role to create the different current patterns, which were mapped in the northern tip of the Gulf of Aqaba.

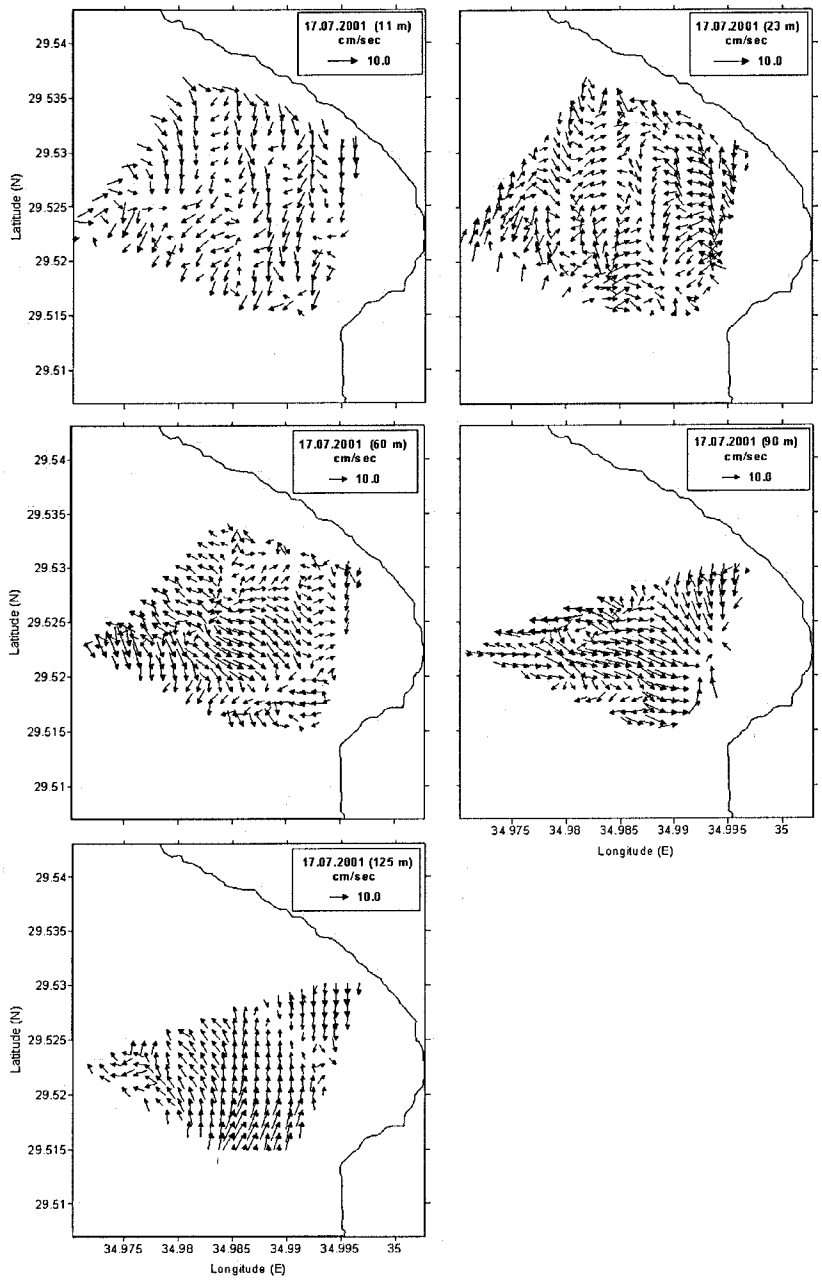

Figure 3.75: Horizontal current vector distribution in the northernmost of the Gulf of Aqaba at selected depth levels between 10-125 m water column on July 17th 2001.

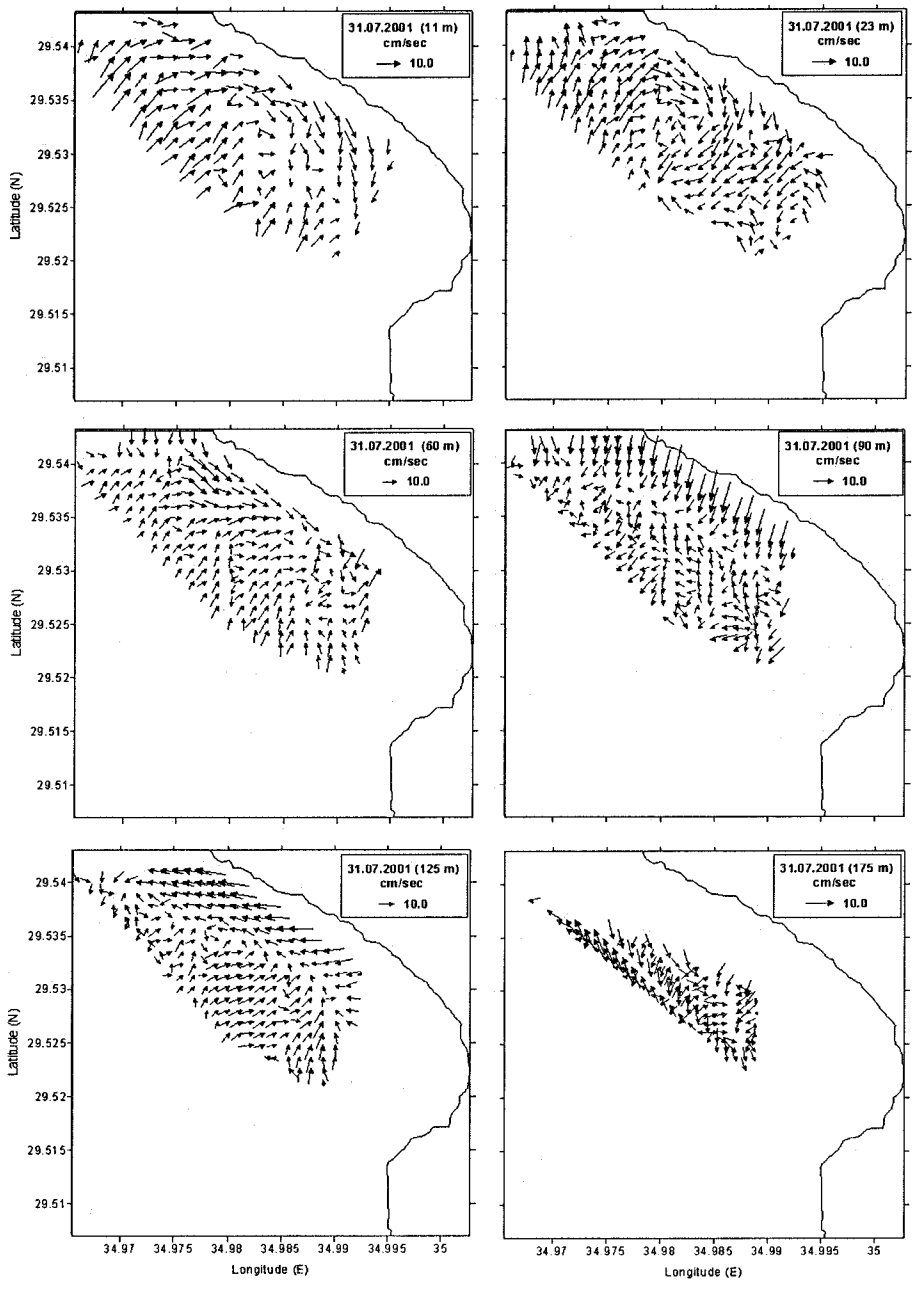

Figure 3.76: Horizontal current vector distribution in the northernmost of the Gulf of Aqaba at selected depth levels between 10-170 m water column on July 31st 2001.

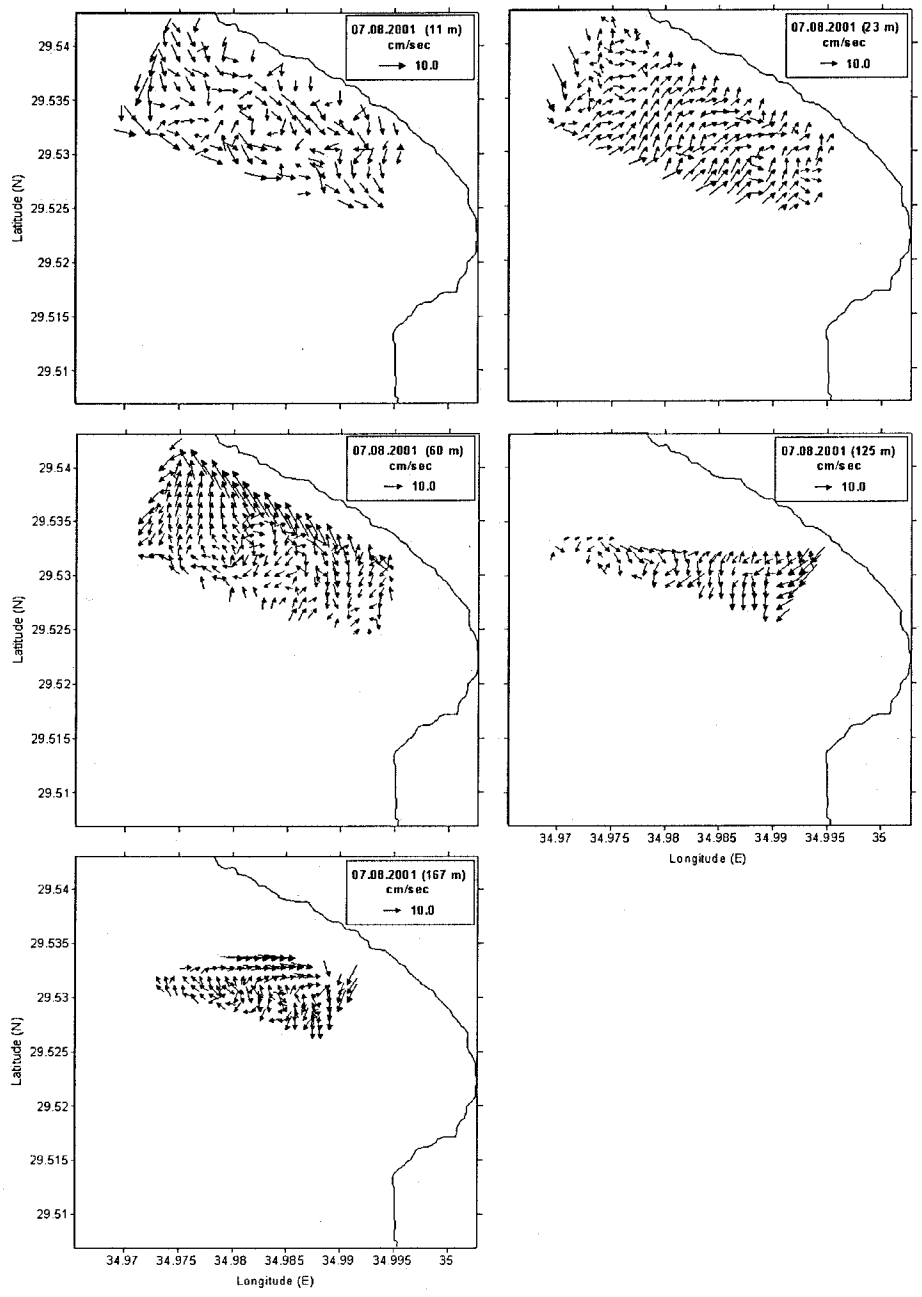

Figure 3.77: Horizontal current vector distribution in the northernmost of the Gulf of Aqaba at selected depth levels between 10-170 m water column on August 7th 2001.

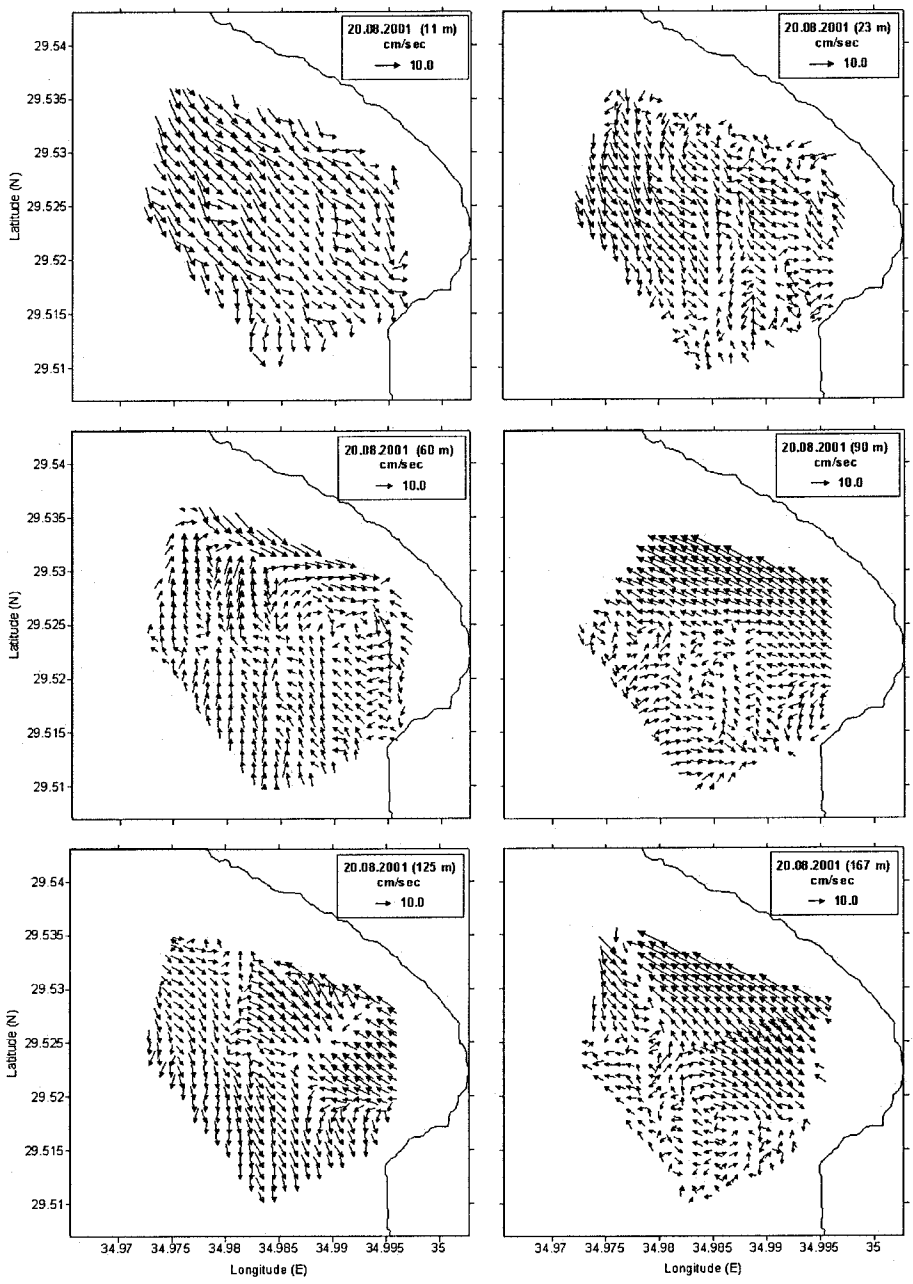

Figure 3.78: Horizontal current vector distribution in the northernmost of the Gulf of Aqaba at selected depth levels between 10-125 m water column on August 20th 2001.

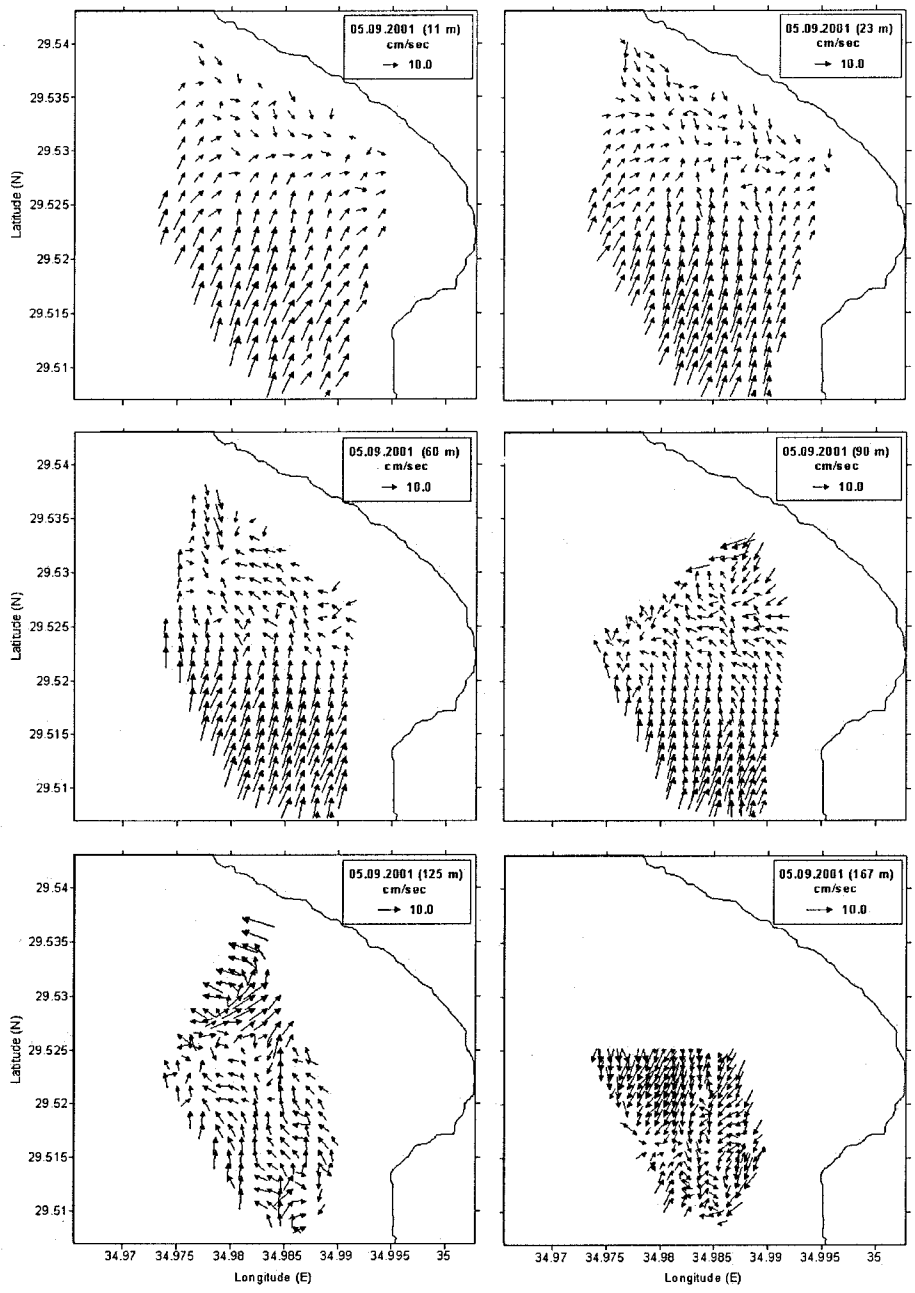

Figure 3.79: Horizontal current vector distribution in the northernmost of the Gulf of Aqaba at selected depth levels between 10-125 m water column on September 5th 2001.

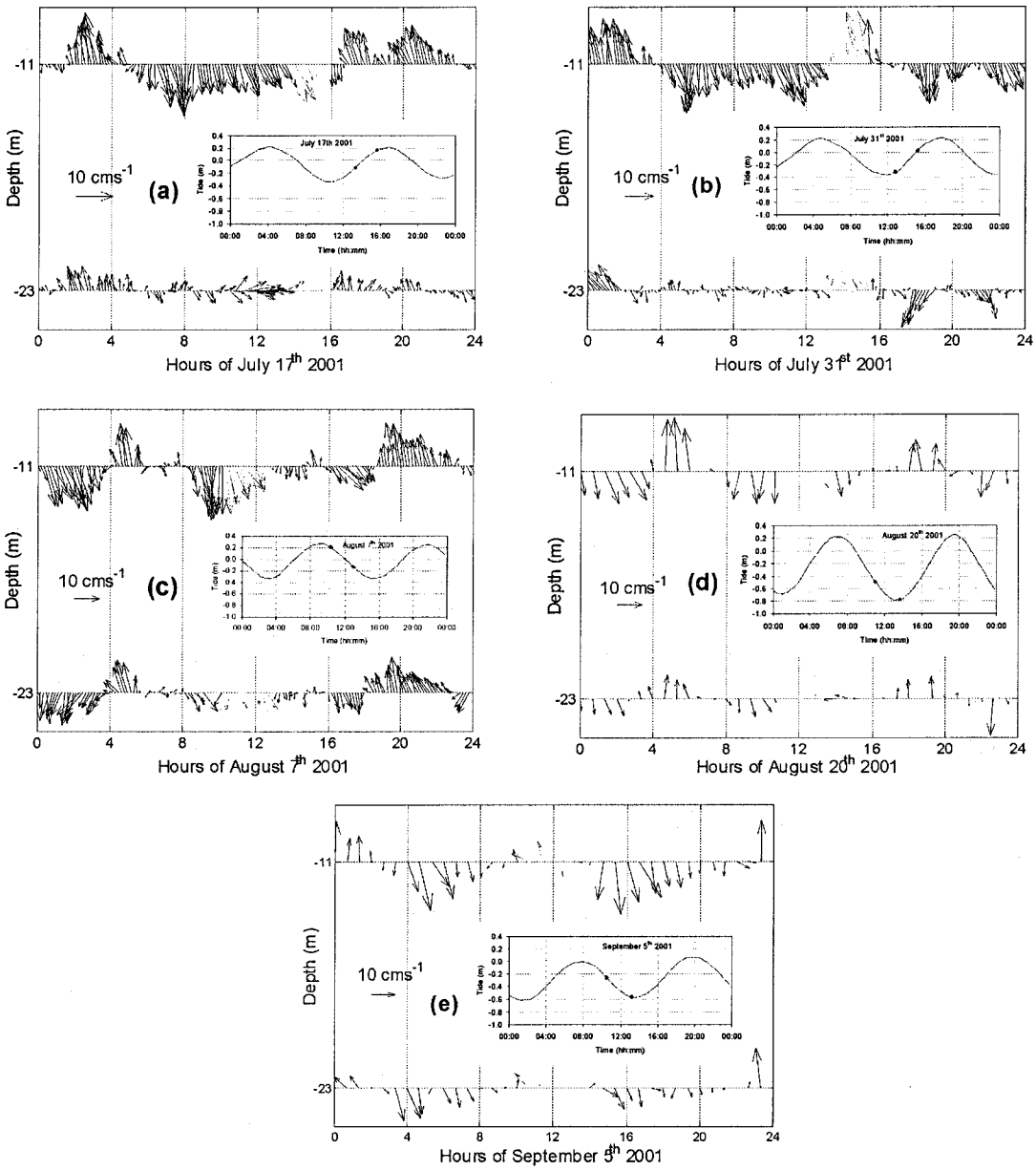

Figure 3.80: Distribution of current vectors (cms^{-1}) at position w1-b, and sea level variation (m) Simultaneous with the surveys times in Figure 3.75 to Figure 3.79 referred by the gray arrows and black dots.

4 Conclusions and recommendations

The present work consists of three main subjects: First, the wind and sea level variation in the northern Gulf of Aqaba. Second, the large scale investigation during spring 1999 on R/V Meteor cruise 44/2 in northern Red Sea and the Gulf of Aqaba. Third, the seasonal study in the northern tip of the Gulf of Aqaba.

❖ Wind and sea level variations

- The calm NNE-NNW winds are prevailing over the northern Gulf of Aqaba during the year. Where the speeds below 6 ms^{-1} represent about 70% of the wind speed, and the frequency of the wind direction from NNE to NNW is about 92%. The southern winds blow for several hours but are switching again to northern winds. The wind during summer nights is calmer than during the day, resulting in the diurnal peak (24.04 ± 0.85 hr). The winds are strongest during the summer season and relatively calm conditions prevail during the rest of the year.
- The seal level anomalies depict a yearly cycle at the northern tip of the Gulf of Aqaba with a minimum in the summer, -0.16 m was measured in August. The maximum of the sea level anomaly occurred in the winter-spring seasons. The maximum of 0.19 m was recorded in March. The yearly cycle of the anomalies follows the corresponding sea level variations of the northern Red Sea.
- Four distinguished peaks were detected from the spectrum analysis of the sea level in the northern Gulf of Aqaba. Semidiurnal (12.39 ± 0.22 hr) and diurnal (23.72 ± 0.82 hr) barotropic tides. The other signals periods 1.05 and 8.03 hr are related to the seiches that are generated in the Gulf of Aqaba and the Red Sea, respectively. The fundamental periods, 1.13 hr in Gulf of Aqaba and 8.38 hr in the Red Sea, agree well with the observed seiches periods.

❖ Large scale investigation in the northern Red Sea and the Gulf of Aqaba during spring 1999 on RV Meteor cruise 44/2

- The deep-water in the Red Sea has the same characteristics as the surface water in the upper 450 m in the Gulf of Aqaba. This indicates that the upper and intermediate water layers of the Gulf of Aqaba contribute to the deep-water formation of the northern Red Sea due to the strong cooling and evaporation in the Gulf of Aqaba during February and March. The deep- water in the gulf (>450 m) seems to be rather passive and plays no specific role in the water mass formation of the northern Red Sea.
- Intensive vertical convection and large variability in the vertical excursion of the thermocline are likely to occur in the northern Gulf of Aqaba within few days or may be few hours.
- A well developed cyclonic gyre with a diameter of about 50-60 km and maximum velocity of about 0.4 ms^{-1} was observed in the upper 215 m waters in the northern Red Sea.

The gyre may contribute to the preconditioning for the intermediate water formation in the northern Red Sea.

- The water exchange between the northern Red Sea and Gulf of Aqaba through the Strait of Tiran is organized in two layers. Inflow (NNW) into the Gulf of Aqaba occurred in the upper 70 m over the sill while and outflow (SSW) into the Red Sea was below 70 m. The strength of the outflow to the Red Sea generally increases linearly with depth and reached up to about 1 m/s at 200 m depth.
- The transition of stratification from the northern Red Sea (21.5-23.5 °C, and 40.0-40.3) to the Strait of Tiran front (21.6-22.0 °C, and 40.3-40.5) was observed in the upper 200 m, while the well mixed conditions was dominating in the upper 300 m in the northern Gulf of Aqaba (21.4-21.6 °C, and 40.6-40.7).
- Three main features can be summarized from current measurements near the Strait of Tiran front (station VI). First, an easterly flow with a clockwise rotation of about 12.3 hr period in the upper 100 m, and a north westerly current in the 120-280 m of the water column. Second, the amplitude of the clockwise tidal rotation decreases with depth and seems not be present in the lower levels (155-255 m), where only the magnitude of the current vectors vary with the same period, but directions do not change. Third, a baroclinic semidiurnal signal (12.3 hr period) of an internal tide wave with amplitude of about 0.2 ms^{-1} was superimposed on the mean value.
- A sequence of flow changes was the robust feature along the axis of the Gulf of Aqaba. These changes do not match the basic tidal motion, and represent in some parts a phase difference in the horizontal current components of about 90°. These finding reveals a chain of cyclonic and anti-cyclonic eddy pairs are the dominant signal along the gulf axis. The total diameter for each pair is twice the baroclinic Rossby radius ($R \approx 10$ km).
- A single anti-cyclonic eddy was observed in the upper 300 m in the northern tip of the Gulf of Aqaba. The diameter of the eddy ranged between 5-8 km.

❖ Seasonal variations in the northern tip of the Gulf of Aqaba

- The temperature variations in the northern tip of the Gulf of Aqaba appear to be seasonal signals. The thermal stratification exists during summer (May-December), and is strongest during August where it reached a maximum depth 250 m. The stratification vanishes during the winter-spring seasons (January-April). The maximum mixing depth reaches as far as 400 m during spring (February-April). The maximum range of the temperature θ, salinity and density σ_θ in the 0-250 m of the water column during the strongest stratification periods, which occurred during August months, were between 28.04-20.88 °C, 40.67-40.20, and 26.55-28.63 kgm^{-3}, respectively. During February-March months, where the mixing is dominating, the range mean of the temperature θ, salinity, and density σ_θ in the 0-400 m of the water column were 21.50-21.10 °C, 40.44-40.48, and 28.51-28.63 kgm^{-3}, respectively.
- The composite variations of the stratification deepness S_h (m) during summers (where the temperature gradient is greater than 0.025 $°Cm^{-1}$) and the mixed layer deepness M_h (m) during winter-spring seasons (where the temperature gradient is less than 0.005 $°Cm^{-1}$) during the period of May 1997 to August 2001 are approximated as polynomials. The stratification deepness rate dS_h/dt ($mday^{-1}$) represents a linear relationship with respect to

the time, and appears fast in early summer (~-3.0 $mday^{-1}$) and then slows down in late summer (~-0.2 $mday^{-1}$) when the stratified layer get thicker, while the mixed layer deepness rate dM_h/dt ($mday^{-1}$) is constant equals –2.379 $mday^{-1}$

- The phenomenon of higher saline water above lower saline water occurred clearly during summer season in the northern tip of the Gulf of Aqaba. This phenomenon develops in August at about 60 m. It reaches a depth of 200 m in December and then it dwindles until it vanishes during spring. The evaporation and the low saline water carried by the thermhaline in the intermediate waters from the Red Sea are assumed to the reason for this phenomenon during summer.

- The interannual variation of the salinity during the four years ranged between 40.20-40.75 in the upper 400 m, while the variation of the temperature was large, ranging between 20.84-28.04 °C. Obviously, the thermodynamics processes in the seawater of the Gulf of Aqaba are dominated by the temperature variations, while the salinity plays a minor role.

- No significant difference of the annual variations of the potential temperature, salinity, and potential density could be detected between the stations in the northern tip of the Gulf of Aqaba in the upper 300 m depth.

- The followings seasonal differences in the current were observed near shore waters at positions w1-a (canyon area), w1-b (shelf area), and w2 (slope area) in front of the Marine Science Station (MSS).

  (a) Summer. The semidiurnal signal (12.19 ± 0.58 hr) was obvious at all positions, while and diurnal signal (24.54 ± 2.36 hr) was appeared at w1-a and w1-b, and disappeared at w2. The current flows at w1-a and w1-b towards SSE-SSW. At w2, the current was fluctuating from NNE to SSW, mostly with regular frequency.

  (b) Winter. Only the semidiurnal signal (12.46 ± 0.61 hr) was detected at w1-a, where the current was varying between SE and SW with a reversal from SE to NW. Unfortunately, data from positions w1-b and w2 were not available.

  (c) Spring. No tidal signals appeared at w1-a and w2 (data from position w1-b was not available), which agrees with the absence of diurnal or semidiurnal signals in spring 1999 during the Meteor cruise in the northern gulf. The currents at w1-a were the same during winter, while at w2, the current was fluctuating from NNE to SSW with regular frequency, as detected during summer.

- The spectrum analyses and cross correlation tests of the horizontal and vertical current components and relative backscatter intensity at position w2 and w1-b during spring-summer 2000 and summer 2001, respectively, reveal that the vertical motion at the diurnal period are either due to the migration of zooplankton or due to the convection. Both are of the same order as the vertical motion induced by the horizontal motion over the inclined bottom. On the other hand, the semidiurnal and seiches periods were detected in the vertical current due to the strong signal in the north current component and the low uncorrelated motion of the vertical current at both the semidiurnal and the seiches period. Moreover, the vertical migration of zooplanktons may occur at a velocity of the order of the instrumental noise of the instrument, which indicates that the signal of the measured vertical current might be lower than the noise.

- A permanent convection, particularly during daytime, is likely to occur in a shallow coastal waters during summer, which are characterizing of (1) relatively high inclined

bottom (2) high evaporation and (3) blowing of dry air. Such as the observed dominance of the downward vertical current at position w1-b during summer 2001.

- The factors, which controlled the reversal of the currents at w2, were the reversed winds and thermohaline forces. The coherence between the filtered north component of the wind and the current at 20 m depth appeared to be well compatibility with respect to the time in spring-summer seasons, but with a delay of north current relative to north wind components. The transition period of the direction was nearly 3.5 days.
- In the deeper parts of the Jordanian waters, the currents are mainly parallel to the gulf axis and controlled by winds, which drive a SSE current in the upper part of the water column, by the deeper thermohaline inflow (to NNE), and by the outflow to the south below 120 m depth.
- The current patterns in the northern tip of the Gulf of Aqaba show a substantial temporal variability. These variations are related to: (1) the variation of the phase of the tidal signals, (2) the diurnal and semidiurnal currents, and (3) the topographical feature.

The work is based on field work that had to struggle with many obstacles due to the complicated political situation in this area and the restrictive application of the Sea Law by the administration of some countries. Nevertheless, it is important to carry on and to work with the material that could be provided. We could commence to develop a first understanding of the different classes of processes working and interacting at basin scale and in narrow local areas. Of course, more investigations are required to generalize and prove the mechanism of the circulation in whole gulf in different seasons. The individual studies and investigations by the riparian countries in parts of the gulf are not yet sufficient to obtain a clear picture, but a first step is done.

This was a first exploration, now some ideas are suggested and developed, but these ideas raise new questions, which are helpful for new, more focused work.

My recommendations and wishes are that a comprehensive research program in the Gulf of Aqaba should be organized with participation of the surrounding countries and supported by international cooperation to better understand this fascinating system. This seems to be the only way for a sustainable use and protection of our small but unique GULF OF AQABA.

References

ALLAN, T. D. 1966: A bathymetric chart of the Red Sea. International Hydrographic Review, 43, 35-38.

ANATI, D. A. 1974: Water transport in the Gulf of Aqaba. Puls Cent. Nata. Exploit. Oceans, CNEXO, Act. Colloq., 2:165-173.

ASSAF, G., and J. KESSLER. 1976: Climate and energy exchange in the Gulf of Aqaba. Mon. Weath. Rev., 104:381-385.

BADRAN, M. 1996: Nutrient chemistry and UV absorption characteristics of waters of the Gulf of Aqaba, Red Sea. Ph.D. thesis, University of Wales, Bangon, U.K.

BEN-AVRAHAM, Z., G. ALMAROG, and Z. GARFUNKEL. 1979 a: Sediments and structure of the Gulf of Eilat (Aqaba)-northern Red Sea. Sedim. Geol., 23:239-267.

BEN-AVRAHAM, Z., R. HANEL, and H. VILLINGER. 1978: Heat flow through the Dead Sea rift. Mar. Geol., 28:253-269.

BEN-AVRAHAM, Z., Z. GARFUNKEL, G. ALMAROG, and K. HALL. 1979 b: Continental breakup by a leaky transform: the Gulf of Eilat (Aqaba). Science, 206:239-267.

BERMAN, T., N. PALDOR, and S. BRENNER. 2000: Simulation of wind-driven circulation in the Gulf of Elat (Aqaba). Journal of Marine System 26 (2000) 349-365.

BOGDANOVA, A. K. 1974: Indirect estimation of the seasonal variation of the water exchange through Bab El Mandeb. Center National Pour L'exploitation des Ocean (CNEXO), no. 2, p. 253-265. 1974.

BRENNER, S., Z. ROZENTRAUB, J. BISHOP, and M. KROM. 1990: The mixed layer/thermocline cycle of a persistent warm eddy in the eastern Mediterranean. Dynamics Atmospheres Oceans.

CEMBER, R. P. 1988: On the sources, formation, and circulation of Red Sea deep water. J. Geophys. Res. C. Oceans, 93 (C7). 8175-8191.

CLIFFORD, M., C. HORTON, J. SCHMITZ, and L. H. KANTHA. 1997: An oceanographic nowcast/forecast system for the Red Sea, J. Geophys. Res. C. Oceans,102 (C11), 25, 101-25, 122.

DAVID, S., and S. WALTER. 1996: Global Bathymetric Prediction for Ocean Modeling and Marine Geophysics. http://topex.ucsd.edu/marine_topo/text/topo.html#net.

DEACON, G. E. R. 1952: The "Maniline" Expedition to the Gulf of Aqaba. II. Preliminary hydrological report. Bull. Br. Mus. nat. Hist., Zool., 1:159-162.

DEFANT, A. 1961: Physical oceanography Vol. II. Pergamon press, Oxford-London-New York-Paris. 1961.

ENCYCLOPEDIA BRITANNICA 2001: © 1999-2001 Britannica.com Inc.

ESHEL, G., M. CANE, and M. BLUMENTHAL. 1994: Modes of subsurface, intermediate, and deep water renewal in the Red Sea. Journal of physical oceanography, v. 99, No. C8, pp. 15,941-15,952, August 1994.

ESHEL, G., N. NAIK. 1996: Climatological coastal jet, intermediate water formation, and general circulation of the Red Sea. Journal of physical oceanography, v. 27, pp. 1233-1257, July 1997.

FENNEL, W., and H. U. LASS. 1989: Analytical theory of forced oceanic waves. Akademie-Verlag, Berlin 1989, 312 pp.

GENIN, A., and N. PALDOR. 1998: Changes in the circulation and current spectrum near the tip of the narrow, seasonally mixed Gulf of Elat (Aqaba). Isr. J. Earth Sci.; 47:87-92.

GILL, A. E. 1982: Atmosphere-Ocean Dynamics. Academic Press, New York.

GREGORY, J. 1929: The rift valley and geology of east Africa. Seelly, Service and co., London. In: G. M. Friedman (ed.), 1968.

HALL, J., and Z. BEN-AVRAHAM. 1978: New bathymetric map of the Gulf of Eilat (Aqaba). Tenth Int. Conf. Sedimentol., Jerusalem, 1:285 (Abst.).

HALL, J. K. 1975: Bathymetric chart of the Straits of Tiran. Israel J. Earth-Sci., 24:69-72.

HULINGS, N. C. 1979: Currents in the Jordan Gulf of Aqaba. Dirasat, 6:21-31.

HULINGS, N. 1989: A review of Marine Science Research in the Gulf of Aqaba, Marine Science Station.

JOHNS, E., D. BROWING. 1971: Cold water layer in the southern Red Sea, Limnol, Oceanogr. 16, 3, 503-509.

JOHNS, E., J. GORMAN, and D. BROWING. 1974: Circulation between the Red Sea and the Gulf of Aden in late summer. Center National Pour L'exploitation des Ocean (CNEXO), no. 2, p. 203-227. 1974.

KILLWORTH, P. D. 1976: The mixing and spreading phases of MEDOC.I. Progress in Oceanography [Prog. Oceanogr.], vol. 7, no. 2, pp. 59-90, 1976.

KLINKER, J., Z. REISS, C. KROPACH, I. LEVANON, H. HARPAZ, E. HALICZ, and G. ASSAF. 1976: Observation on the circulation pattern in the Gulf of Aqaba, Red Sea. Israel. J. Earth Sci. 25:85-103.

LEVANON-SPANIER, I., E. PADAN, and Z. REISS. 1979: Primary production in a desert-enclosed sea-the Gulf of Eilat (Aqaba). Red Sea. Deep-Sea Res., 26:673-685.

MAILLARD, C. 1974: Formation d'eau Profonde en Mer rouge, in La Formation des Eaux Océaniques Profondes, pp. 115-125. CNRS, Paris, 1974.

MAILLARD, C., and G. SOLIMAN. 1986: Hydrography of the Red Sea and exchange with Indian Ocean in summer. Oceanologica Acta, v. 9, no. 3, 1986.

MANASREH, R. S. 1998: Circulation of the Jordanian waters of the Gulf of Aqaba, Red Sea. Master thesis, Yarmouk Uni. Irbid.

MANINS, P. C. 1973: A filling box model of the deep circulation of the Red Sea, Mem. Soc. R. Sci. Lieges, tome VI, 153-166, 1973.

MORCOS, S. A. 1970: Physical and chemical oceanography of the Red Sea. Oceanogr. mar. Biol. a. rev., 8:73-202.

MURRAY, S. P., and W. JOHNS. 1997: Direct observations of seasonal exchange through the Bab el Mandeb Strait, Geophys. Res. Let., 24, 2557-2560.

MURRAY, S. P., A. HECHT, and A. BABCOCK. 1984: On the mean flow in the Tiran Strait in winter. J. Mar. Res., 42:265-287.

MURRAY, S. P., and A. L. BABCOCK. 1982: Characteristics of tidal Reynolds stresses and low frequency turbulence in the Tiran Strait. EOS, vol. 64, no. 45, November 8, 1983.

NEUMANN, C., and D. MC GILL. 1961: Circulation of the Red Sea in early summer, Deep-sea Res., 8, 223-235.

NEUMANN, G., and W. PIERSON. 1966: Principles of physical oceanography.

PALDOR, N., and D. A. ANATI. 1979: Seasonal variation of temperature and salinity in the Gulf of Aqaba. Deep-Sea Res., 26:661-672.

PATZERT, W. C. 1972a: Volume and heat transports between the Red Sea and the Gulf of Aden, and notes on the Red Sea heat budget. Center National Pour L'exploitation des Ocean (CNEXO), no. 2, p. 191-201. 1974.

PATZERT, W. C. 1972b: Seasonal reversal in the Red Sea circulation . Center National Pour L'exploitation des Ocean (CNEXO), no. 2, p. 55-89. 1974.

PATZERT, W. C. 1974a: Wind-induced reversal in Red Sea circulation. Deep-sea Res., v. 21, pp. 109-121. 1974.

PLAEHN, O., B. BASCHEK, T. BADEWIEN, M. WALTER, and M. RHEIN. 2001: The important of the Gulf of Aqaba for the formation of bottom water in the Red Sea. In press.

POND, S., and G. L. PICKARD 1983: Introductory dynamical oceanography. 2nd edition. Pergamon International library of science, technology, engineering, and social studies.

POR, F. D., and R. LERNER-SEGGEV. 1966: Preliminary data about the benthic fauna of the Gulf of Eilat (Aqaba), Red Sea. Israel J. Zool., 15:38:50.

QUADFASEL, D., and H. BAUDNER. 1993: Gyre-scale circulation cells in the Red Sea, Oceanol. Acta, 16, 221-229.

ROBINSON, M. K. 1973: Monthly mean surface and subsurface temperature and depth of the top of the thermocline, Red Sea, Fleet numerical Weather Central, Monterey, Tech. note 73-4, 117 p.

SIEDLER, G., 1969: General circulation of water masses in the Red Sea, in: Hot bines and recent heavy metal deposits in the Red Sea, edited by E. T. Degens and D. A. Ross, Springer, New York, 131-137.

STRANEO, F., and M. KAWASE. 1999: Comparisons of Localized Convection due to Localized Forcing and to Preconditioning. Journal of Physical Oceanography: Vol. 29, No. 1, pp. 55-68, Jan 1999.

SVERDRUP, H. U., M. W. JOHNSON, and R. H. FLEMING, 1961: The oceans their physics, chemistry, and general biology.

TOMCZAK, M., and J. S. GODFREY, 2001: Regional oceanography: An introduction. Pdf version 1.0, 2001. http://www.cmima.csic.es/mirror/mattom/regoc/pdfversion.html.

THOMPSON, E. F. 1939b: Chemical and physical investigation. The exchange of water between the Red Sea and the Gulf of Aden over the "sill." John Murray Exped. 1933-34, Sci. Repots., v. 2, p. 105-119, 1939.

VISBECK, M., J. MARSHALL, and H. JONES. 1996: Dynamics of Isolated Convective Regions in the Ocean. Journal of Physical Oceanography: Vol. 26, No. 9, pp. 1721–1734, September 1996.

WERNER, F., and K. LANGE. 1975: A bathymetric survey of the sill area between the Red Sea and the Gulf of Aden, Geol. Jahrb., D 13, 125-130.

WESSEL, P., and W. SMITH. 1996: GSHHS - A Global Self-consistent, Hierarchical, High-resolution Shoreline Database, http://www.soest.hawaii.edu/wessel/gshhs/gshhs.html.

WOLF-VECHT, A., N. PALDOR, S. BRENNER. 1992: Hydrographic indications of advection/convection effects in the Gulf of Eilat (Aqaba). Deep-Sea Res., v. 39, no. 7/8, pp. 1393-1401. 1992.

WÜST, G. 1934: Salzgehalt und Wasserbewegung im Suezkanal. Naturwissenschaften, 22 Jahrg. Heft 36, p. 447-50, 1934.

WYRTKI, K. 1974: On the deep circulation of the Red Sea, in La Formation des Eaux Oceanigues Prefondes, pp. 91-106. CNRS, Paris, 1974.

Meereswissenschaftliche Berichte

MARINE SCIENCE REPORTS

---

1 (1990) Postel, Lutz:
Die Reaktion des Mesozooplanktons, speziell der Biomasse, auf küstennahen Auftrieb vor Westafrika (The mesozooplankton response to coastal upwelling off West Africa with particular regard to biomass)

2 (1990) Nehring, Dietwart:
Die hydrographisch-chemischen Bedingungen in der westlichen und zentralen Ostsee von 1979 bis 1988 - ein Vergleich (Hydrographic and chemical conditions in the western and central Baltic Sea from 1979 to 1988 - a comparison)
Nehring, Dietwart; Matthäus, Wolfgang:
Aktuelle Trends hydrographischer und chemischer Parameter in der Ostsee, 1958 - 1989 (Topical trends of hydrographic and chemical parameters in the Baltic Sea, 1958 - 1989)

3 (1990) Zahn, Wolfgang:
Zur numerischen Vorticityanalyse mesoskaler Strom- und Massen felder im Ozean (On numerical vorticity analysis of mesoscale current and mass fields in the ocean)

4 (1992) Lemke, Wolfram; Lange, Dieter; Endler, Rudolf (Eds.):
Proceedings of the Second Marine Geological Conference - The Baltic, held in Rostock from October 21 to October 26, 1991

5 (1993) Endler, Rudolf; Lackschewitz, Klas (Eds.):
Cruise Report RV "Sonne" Cruise SO82, 1992

6 (1993) Kulik, Dmitri A.; Harff, Jan:
Physicochemical modeling of the Baltic Sea water-sediment column: I. Reference ion association models of normative seawater and of Baltic brackish waters at salinities 1-40 ‰, 1 bar total pressure and 0 to 30°C temperature
(system Na-Mg-Ca-K-Sr-Li-Rb-Cl-S-C-Br-F-B-N-Si-P-H-O)

7 (1994) Nehring, Dietwart; Matthäus, Wolfgang; Lass, Hans-Ulrich; Nausch, Günther:
Hydrographisch-chemische Zustandseinschätzung der Ostsee 1993

8 (1995) Hagen, Eberhard; John, Hans-Christian:
Hydrographische Schnitte im Ostrandstromsystem vor Portugal und Marokko 1991 - 1992

9 (1995) Nehring, Dietwart; Matthäus,Wolfgang; Lass, Hans Ulrich; Nausch, Günther; Nagel, Klaus:
Hydrographisch-chemische Zustandseinschätzung der Ostsee 1994
Seifert, Torsten; Kayser, Bernd:
A high resolution spherical grid topography of the Baltic Sea

10 (1995) Schmidt, Martin:
Analytical theory and numerical experiments to the forcing of flow at isolated topographic features

11 (1995) Kaiser, Wolfgang; Nehring, Dietwart; Breuel, Günter; Wasmund, Norbert; Siegel, Herbert; Witt, Gesine; Kerstan, Eberhard; Sadkowiak, Birgit:
Zeitreihen hydrographischer, chemischer und biologischer Variablen an der Küstenstation Warnemünde (westliche Ostsee)
Schneider, Bernd; Pohl, Christa:

Spurenmetallkonzentrationen vor der Küste Mecklenburg-Vorpommerns

12 (1996) Schinke, Holger:
Zu den Ursachen von Salzwassereinbrüchen in die Ostsee

13 (1996) Meyer-Harms, Bettina:
Ernährungsstrategie calanoider Copepoden in zwei unterschiedlich trophierten Seegebieten der Ostsee (Pommernbucht, Gotlandsee)

14 (1996) Reckermann, Marcus:
Ultraphytoplankton and protozoan communities and their interactions in different marine pelagic ecosystems (Arabian Sea and Baltic Sea)

15 (1996) Kerstan, Eberhard:
Untersuchung der Verteilungsmuster von Kohlenhydraten in der Ostsee unter Berücksichtigung produktionsbiologischer Meßgrößen

16 (1996) Nehring, Dietwart; Matthäus, Wolfgang; Lass, Hans Ulrich; Nausch, Günther; Nagel, Klaus:
Hydrographisch-chemische Zustandseinschätzung der Ostsee 1995

17 (1996) Brosin, Hans-Jürgen:
Zur Geschichte der Meeresforschung in der DDR

18 (1996) Kube, Jan:
The ecology of macrozoobenthos and sea ducks in the Pomeranian Bay

19 (1996) Hagen, Eberhard (Editor):
GOBEX - Summary Report

20 (1996) Harms, Andreas:
Die bodennahe Trübezone der Mecklenburger Bucht unter besonderer Betrachtung der Stoffdynamik bei Schwermetallen

21 (1997) Zülicke, Christoph; Hagen, Eberhard:
GOBEX Report - Hydrographic Data at IOW

22 (1997) Lindow, Helma:
Experimentelle Simulationen windangeregter dynamischer Muster in hochauflösenden numerischen Modellen

23 (1997) Thomas, Helmuth:
Anorganischer Kohlenstoff im Oberflächenwasser der Ostsee

24 (1997) Matthäus, Wolfgang; Nehring, Dietwart; Lass, Hans Ulrich; Nausch, Günther; Nagel, Klaus; Siegel, Herbert:
Hydrographisch-chemische Zustandseinschätzung der Ostsee 1996

25 (1997) v. Bodungen, Bodo; Hentzsch, Barbara (Herausgeber):
Neue Forschungslandschaften und Perspektiven der Meeresforschung - Reden und Vorträge zum Festakt und Symposium am 3. März 1997.

26 (1997) Lakaschus, Sönke:
Konzentrationen und Depositionen atmosphärischer Spurenmetalle an der Küstenstation Arkona

27 (1997) Löffler, Annekatrin:
Die Bedeutung von Partikeln für die Spurenmetallverteilung in der Ostsee, insbesondere unter dem Einfluß sich ändernder Redoxbedingungen in den zentralen Tiefenbecken

28 (1998) Leipe, Thomas; Eidam, Jürgen; Lampe, Reinhard; Meyer, Hinrich; Neumann, Thomas; Osadczuk, Andrzej; Janke, Wolfgang; Puff, Thomas; Blanz, Thomas; Gingele, Franz Xaver; Dannenberger, Dirk; Witt, Gesine:
Das Oderhaff. Beiträge zur Rekonstruktion der holozänen geologischen Entwicklung und anthropogenen Beeinflussung des Oder-Ästuars.

29 (1998) Matthäus, Wolfgang; Nausch, Günther; Lass, Hans Ulrich; Nagel, Klaus; Siegel, Herbert:
Hydrographisch-chemische Zustandseinschätzung der Ostsee 1997

30 (1998) Fennel, Katja:
Ein gekoppeltes, dreidimensionales Modell der Nährstoff- und Planktondynamik für die westliche Ostsee

31 (1998) Lemke, Wolfram:
Sedimentation und paläogeographische Entwicklung im westlichen Ostseeraum (Mecklenburger Bucht bis Arkonabecken) vom Ende der Weichselvereisung bis zur Litorinatransgression

32 (1998) Wasmund, Norbert; Alheit, Jürgen; Pollehne, Falk; Siegel, Herbert; Zettler, Michael L.:
Ergebnisse des Biologischen Monitorings der Ostsee im Jahre 1997 im Vergleich mit bisherigen Untersuchungen

33 (1998) Mohrholz, Volker:
Transport- und Vermischungsprozesse in der Pommerschen Bucht

34 (1998) Emeis, Kay-Christian; Struck, Ulrich (Editors):
Gotland Basin Experiment (GOBEX) - Status Report on Investigations concerning Benthic Processes, Sediment Formation and Accumulation

35 (1999) Matthäus, Wolfgang; Nausch, Günther; Lass, Hans Ulrich; Nagel, Klaus; Siegel, Herbert:
Hydrographisch-chemische Zustandseinschätzung der Ostsee 1998

36 (1999) Schernewski, Gerald:
Der Stoffhaushalt von Seen: Bedeutung zeitlicher Variabilität und räumlicher Heterogenität von Prozessen sowie des Betrachtungsmaßstabs - eine Analyse am Beispiel eines eutrophen, geschichteten Sees im Einzugsgebiet der Ostsee (Belauer See, Schleswig-Holstein)

37 (1999) Wasmund, Norbert; Alheit, Jürgen; Pollehne, Falk; Siegel, Herbert, Zettler, Michael L.:
Der biologische Zustand der Ostsee im Jahre 1998 auf der Basis von Phytoplankton-, Zooplankton- und Zoobenthosuntersuchungen

38 (2000) Wasmund, Norbert; Nausch, Günther; Postel, Lutz; Witek, Zbigniew; Zalewski, Mariusz; Gromisz, Sławomira; Łysiak-Pastuszak, Elżbieta; Olenina, Irina; Kavolyte, Rima; Jasinskaite, Aldona; Müller-Karulis, Bärbel; Ikauniece, Anda; Andrushaitis, Andris; Ojaveer, Henn; Kallaste, Kalle; Jaanus, Andres:
Trophic status of coastal and open areas of the south-eastern Baltic Sea based on nutrient and phytoplankton data from 1993 - 1997

39 (2000) Matthäus, Wolfgang; Nausch, Günther; Lass, Hans Ulrich; Nagel, Klaus; Siegel, Herbert:
Hydrographisch-chemische Zustandseinschätzung der Ostsee 1999

40 (2000) Schmidt, Martin; Mohrholz, Volker; Schmidt, Thomas; John, H.-Christian; Weinreben, Stefan; Diesterheft, Henry; Iita, Aina; Filipe, Vianda; Sangolay, Bomba-Bazik; Kreiner, Anja; Hashoongo, Victor; da Silva Neto, Domingos:
Data report of R/V "Poseidon" cruise 250 ANDEX'1999

41 (2000) v. Bodungen, Bodo; Dannowski, Ralf; Erbguth, Wilfried; Humborg, Christoph; Mahlburg, Stefan; Müller, Chris; Quast, Joachim; Rudolph, K.-U.; Schernewski, Gerald; Steidl, Jörg; Wallbaum, Volker:
Oder Basin - Baltic Sea Interactions (OBBSI): Endbericht

42 (2000) Zettler, Michael L.; Bönsch, Regine; Gosselck, Fritz:
Verbreitung des Makrozoobenthos in der Mecklenburger Bucht (südliche Ostsee) - rezent und im historischen Vergleich

43 (2000) Wasmund, Norbert; Alheit, Jürgen; Pollehne, Falk; Siegel, Herbert:
Der biologische Zustand der Ostsee im Jahre 1999 auf der Basis von Phytoplankton- und Zooplanktonuntersuchungen

44 (2001) Eichner, Christiane:
Mikrobielle Modifikation der Isotopensignatur des Stickstoffs in marinem partikulärem Material

45 (2001) Matthäus, Wolfgang; Nausch, Günther (Editors):
The hydrographic-hydrochemical state of the western and central Baltic Sea in 1999/2000 and during the 1990s

46 (2001) Wasmund, Norbert; Pollehne, Falk; Postel, Lutz; Siegel, Herbert; Zettler, Michael L.:
Biologische Zustandseinschätzung der Ostsee im Jahre 2000

47 (2001) Lass, Hans Ulrich; Mohrholz, Volker; Nausch, Günther; Pohl, Christa; Postel, Lutz; Rüß, Dietmar; Schmidt, Martin; da Silva, Antonio; Wasmund, Norbert:
Data report of R/V "Meteor" cruise 48/3 ANBEN'2000

48 (2001) Schöner, Anne Charlotte:
Alkenone in Ostseesedimenten, -schwebstoffen und -algen: Indikatoren für das Paläomilieu?

49 (2002) Nausch, Günther; Feistel, Rainer; Lass, Hans Ulrich; Nagel, Klaus;Siegel, Herbert:
Hydrographisch-chemische Zustandseinschätzung der Ostsee 2001
Pohl, Christa; Hennings, Ursula:
Ostsee-Monitoring - Die Schwermetall-Situation in der Ostsee im Jahre 2001

50 (2002) Manasreh, Riyad:
The general circulation and water masses characteristics in the Gulf of Aqaba and northern Red Sea